MASTER OF SCIENCE

A novel role for Sprouty2 in co-ordinating airway and vascular growth of the fetal lung.

Walker, David John

Award date:
2013

MASTER OF SCIENCE

A novel role for Sprouty2 in co-ordinating airway and vascular growth of the fetal lung.

David John Walker

2013

University of Dundee

A novel role for Sprouty2 in co-ordinating airway and vascular growth of the fetal lung.

David John Walker

A dissertation submitted in fulfilment of the requirements for the degree of Master of Science

Division of Cardiovascular and Diabetes Medicine

University of Dundee

May 2013

Contents

List of Figures

List of Tables

Acknowledgements

Firstly, I would like to thank the Wellcome Trust for funding this project and to the University of Dundee for giving me the opportunity to do something that I have a huge passion for and for providing me a platform for a promising career in science.

I would like to thank my principal supervisor (and former boss!), Dr. Stephen Land, who has been extremely supportive during my time in his lab. I couldn't quite dovetail in the 'Nearly Headless Nick' quip into the main body of the thesis, so it gets an honourable mention here. Dems the brakes!

Speaking of honourable mentions, I would also like to thank Dr. Claire Scott for teaching me lots of new techniques and for putting up with my countless questions. I'd also like to thank Kate Wood and Rowan Swan for their help in acquiring some of the data in this thesis. Special thanks also to the lab guru Diane Cassidy, Gordon Watt, Steven Mansell, Dr. Marios Stavridis and Kendra Tosoni for their valuable advice. To the CVDM lab groups: many thanks for all the advice/banter over the relatively short time we have all been together. I guess I should thank the band Nightwish too for their wonderful music which has provided a very apt and compelling soundtrack during the writing of this thesis.

Special final thanks to my family, particularly my wife Allana, for keeping me sane, and my two girls, Louisa and Amelia, for allowing their daddy to devote some of his time to this thesis and for giving me a reason to smile at the end of each day. Finally, I'd like to express my eternal thanks to my Gran, whom I dedicate this thesis to.

Declaration

I hereby declare that I, David John Walker, am the sole author of this thesis. I carried out the experiments and conducted the analyses recorded in this thesis. All references cited herein have been sourced by myself. None of the work in this thesis has been previously accepted for a higher degree.

Signature of Candidate

David John Walker BSc

Supervisors Statement

I certify that David John Walker has fulfilled the conditions of ordinance 39 and of the relevant regulations, such that he is qualified to submit this thesis in application for the higher degree of Master of Science.

Signatures of Supervisors

Dr. Stephen C. Land

Dr. Marios Stavridis

Abbreviations

18S	18S Ribosomal RNA
AKT	Protein Kinase B
APO E	Apolipoprotein E
APS	Ammonium persulphate
ARNT	Aryl Hydrocarbon Receptor Nuclear Translocator
ATI	Alveolar Type I Pneumocytes
ATII	Alveolar Type II Pneumocytes
B2M	$ß_2$ Microglobulin
bHLH	Basic Helix-loop-helix
BNIP3	BCL2/adenovirus E1B 19kDa Protein-interacting 3
BSA	Bovine Serum Albumin
c-Src	c-Src Tyrosine Kinase
C-TAD	C-terminal Transactivation Domain
cCBL	Canonical Casitas B-lineage Lymphoma
CBP/p300	p300-CBP co-activator family
CCND1	G1/S-specific Cyclin-D1
CDK	Cyclin-dependent Kinases
cDNA	Complimentary DNA
CFTR	Cystic Fibrosis Transmembrane Conductance Regulator
ChIP	Chromatin Immunoprecipitation
Cl^-	Chloride Ion
CO_2	Carbon Dioxide
Co-IP	Co-immunoprecipitation
CRD	Cysteine-rich Domain
Ct	Cycle Threshold
ddH_2O	Deionised Water
DMEM/F-12	Dulbecco's Modified Eagle Medium: Nutrient Mixture F-12
dNTPs	Deoxyribonucleic Triphosphates
DT	Dual-tagged
ECL	Enhanced Chemiluminescence

EDTA	Ethlenediaminetetraacetic Acid
EGF	Epidermal Growth Factor
ENaC	Epithelial Sodium Channel
EPO	Erythropoietin
ERK1/2	Extracellular Signal-regulated Kinases 1 & 2
FBS	Fetal Bovine Serum
FDLE	Fetal Distal Lung Epithelial Cells
FGF10	Fibroblast Growth Factor 10
FGFR2b	Fibroblast Growth Factor Receptor 2
FRS2	Fibroblast Growth Factor Receptor Substrate 2
G418	Geneticin
GßL	TOR complex subunit LST8
GAP	GTPase-activating Protein
GDP	Guanosine Diphosphate
GEF	Guanine Nucleotide Exchange Factor
GOI	Gene of Interest
GRB2	Growth Factor Receptor-bound Protein 2
GTP	Guanosine Triphosphate
H3	Histone H3
HAT	Histone Acetyltransferase
HBE	Human Bronchial Epithelial Cells
HCC	Human Hepatocellular Cell Carcinoma
HDAC	Histone Deacetyltransferase
HEK	Human Embryonic Kidney Cells
HELMF	Human Epithelial Mesenchymal Lung Fibroblast Cells
HEPES	4-(2-hydroxyethyl)-1-piperazineethanesulfonic acid
HIF	Hypoxia-inducible Factor
HIF-luc	HIF Luciferase Reporter Gene
HIP1	Huntingtin Interacting Protein
HRE	Hypoxia Response Element
HRP	Horseradish Peroxidase
IHC	Immunohistochemistry

IL	Interleukin
IP	Immunoprecipitation
KRAS	V-Ki-ras2 Kirsten Rat Sarcoma Viral Oncogene Homolog
LADD	Lacrimo-Auriculo-Dento-Digital Syndrome
LAR II	Luciferase Assay Reagent II
$MeCP_2$	Methyl CpG Binding Protein 2
MEK	Mitogen-activated Protein Kinase Kinase
mSIN1	Mammalian Stress-activated Protein Kinase Interacting Protein 1
mTOR	Mammalian Target of Rapamycin
mTORC1	mTOR Complex 1
mTORC2	mTOR Complex 2
NEB	New England Biolabs
NP-40	Nonidet P-40
NSCLC	Non-Small-Cell Lung Carcinoma
NT	Non-target
ODDD	Oxygen Dependent Degradation Domain
PBS	Phosphate Buffered Saline
PCR	Polymerase Chain Reaction
PH	Pleckstrin Homology Domain
PHD	Prolyl Hydroxylase Domain
PI3K	Phosphoinositide-3-Kinase
PIP_3	Phosphatidylinositol (3, 4, 5)-trisphosphate
PM	Peripheral Mesenchyme
PMA	Phorbol 12-myristate 13-acetate
PNEC	Pulmonary Neuroendocrine Epithelial Cells
pO_2	Partial Pressure of Oxygen
PP2A	Protein Phosphatase 2
PPAR- γ	Peroxisome Proliferator-activated Receptor-γ
pRb	Retinoblastoma Protein
pRL	Renilla
PTC1	Patched-1

PTEN	Phosphatase and Tensin Homolog
pVHL	Von Hippel-Lindau tumour suppressor
RAC1	Ras-related C3 Botulinum Toxin Substrate 1
RAF	Proto-oncogene Serine/threonine-protein Kinase
RAG	Recombination Activating Genes
RanBP2	Ran-binding Protein 2 Zinc Finger Domain
RAPTOR	Regulatory-associated Protein of mTOR
Rheb	Ras Homolog Enriched in Brain
RICTOR	Rapamycin-insensitive Companion of mTOR
RTK	Receptor Tyrosine Kinase
S6K	Ribosomal Protein S6 Kinase Beta-1 (P70-S6 Kinase 1)
SDS	Sodium dodecyl sulphate
SDS-PAGE	SDS Polyacrylamide Gel Electrophoresis
SEM	Standard Error of the Mean
SH3	SRC Homology 3 Domain
SH3BP4	SH3 Domain-binding Protein 4
SHH	Sonic Hedgehog
shRNA	Small Hairpin RNA
SHP2	Protein Tyrosine Phosphatase
SIAH2	Seven in Absentia Homolog 2
SOS	Son of Sevenless
Sp1/3	Specificity Protein 1/3
SPRY2	Sprouty2
STAT3	Signal Transducer and Activator of Transcription 3
TAE	Tris-acetate-EDTA Buffer
TBS	Tris Buffered Saline
TCA	Tricarboxylic Acid
TEMED	N, N, N', N' –tetramethylethylenediamine
TGFß	Transforming Growth Factor Beta
Thr	Threonine
TK	Thymidine Kinase
TKB	Tyrosine Kinase Binding Domain

TOS	TOR Signalling Motif
TSC1/2	Tuberous Sclerosis Complex (Hamartin/Tuberin)
Tyr	Tyrosine
VE-cadherin	Vascular Endothelial Cadherin
VEGF-A	Vascular Endothelial Growth Factor A
VEGFR1/2	VEGF Receptor 1 (FLT1) / 2 (FLK1/KDR)
WT	Wild-type
Y55	Tyrosine 55
Y55F	Y55 Null Mutant
ZnF	Zinc Finger

Summary

Airway branching and vascular growth in the developing lung are intimately co-ordinated processes which involve cross-talk between the primary inducer of airway tube elongation, Fibroblast Growth Factor 10 (FGF10) and the pro-vasculogenic transcription factor, Hypoxia Inducible Factor 1α (HIF-1α). The FGF receptor antagonist, Sprouty2 (SPRY2), influences the duration of this signalling activity and thus governs periodical airway and vascular branching. However, the mechanism behind this coordination is unknown. The aim of this thesis was to establish if SPRY2 acts as a key co-ordinator of airway and vascular development in the fetal lung and to explore the implications of this role for vasculogenic signalling from the endodermal epithelium.

SPRY2 is present in the nucleus in both rat Fetal Distal Lung Epithelial (FDLE) and Human Bronchial Epithelial (HBE) cells where its FGF10-induced loss correlates with an increase in Histone 3 (H3) phospho-acetylation. Chromatin Immunoprecipitation (ChIP) assays revealed a dominant interaction between SPRY2 and GC-rich regions of the Vascular Endothelial Growth Factor (VEGF-A) promoter. Mutation of SPRY2 at tyrosine 55 (Y55) and SH3 motifs induced HIF-1α transcriptional activity while by contrast; cysteine mutation suppressed this activity and abolished SPRY2 interaction with the VEGF-A promoter. Knockdown of SPRY2 by shRNA induced phosphorylation of Extracellular Signal-regulated Kinases 1 & 2 (ERK1/2) and Mammalian Target of Rapamycin Complex 1 (mTORC1) while also amplifying VEGF-A gene expression. Knockdown of SPRY2 amplified HIF-1α transcriptional activity approximately 3.5 fold at normoxia and this was reflected in ChIP assays showing increased association of HIF-1α with the VEGF-A promoter.

Taken as a whole, this data supports the hypothesis that SPRY2 is potentially the 'missing link' responsible for co-ordinated airway and vascular growth of the lung epithelium. It achieves this by regulating vascular gene expression by binding to methylation sites of the VEGF-A promoter, coupled with the potential for SPRY2 to bind G-proteins to its SH3 binding domain in order to silence airway and potentially vascular signalling cues from the epithelium.

Chapter 1 - General Introduction

The mammalian lung

Every living organism requires energy to survive and this energy is principally derived from food intake and the inhalation of oxygen required for respiration and metabolic processes. For air-breathing animals, the lung is the essential respiring organ which transports atmospheric oxygen into the bloodstream in concurrence with the expulsion of carbon dioxide produced by cells back into the atmosphere. Inhaled air is breathed in through the nasal or oral passage and passes down into the trachea which branches into single left and right bronchi. Each bronchus enters each lung lobe itself and further partitions into bronchioles which supply air into millions of tiny air sacs called the alveoli, a group of specialised cells surrounded by an extensive capillary network. The vast number of alveoli in the lungs provides an ideal huge surface area for gas exchange to occur. Gas exchange between the air and the blood occurs across the thin walls of the alveoli; the blood-air barrier. Oxygen diffuses through this barrier into the blood coupled with the transport of carbon dioxide produced by the cells back into the alveoli before exhalation. The maintenance of this diffusion is kept in stasis by continuous breathing of fresh air into the lungs. However, this mechanism also requires energy through the means of muscular contraction of the external intercostal muscles and the diaphragm. The unique structure of the lungs and the complexity of the mammalian respiratory system arises from a series of co-ordinated biochemical, biophysical and molecular events, which stem from early embryonic development (McMurty, 2002).

Development of the mammalian lung

Lung development occurs under surprisingly extreme conditions. *In utero*, the lung grows at hypoxia, a partial pressure (pO_2) akin to the summit of Mount Everest (3% O_2, ~23mmHg). Development must be sustained to allow gas exchange to incorporate normoxic conditions upon birth (21% O_2, ~100mmHg). Adult human beings only experience hypoxia through scaling high altitudes, but there are several instances where the lung has experienced localised or global hypoxia physiologically or pathologically (Shimoda & Semenza, 2011).

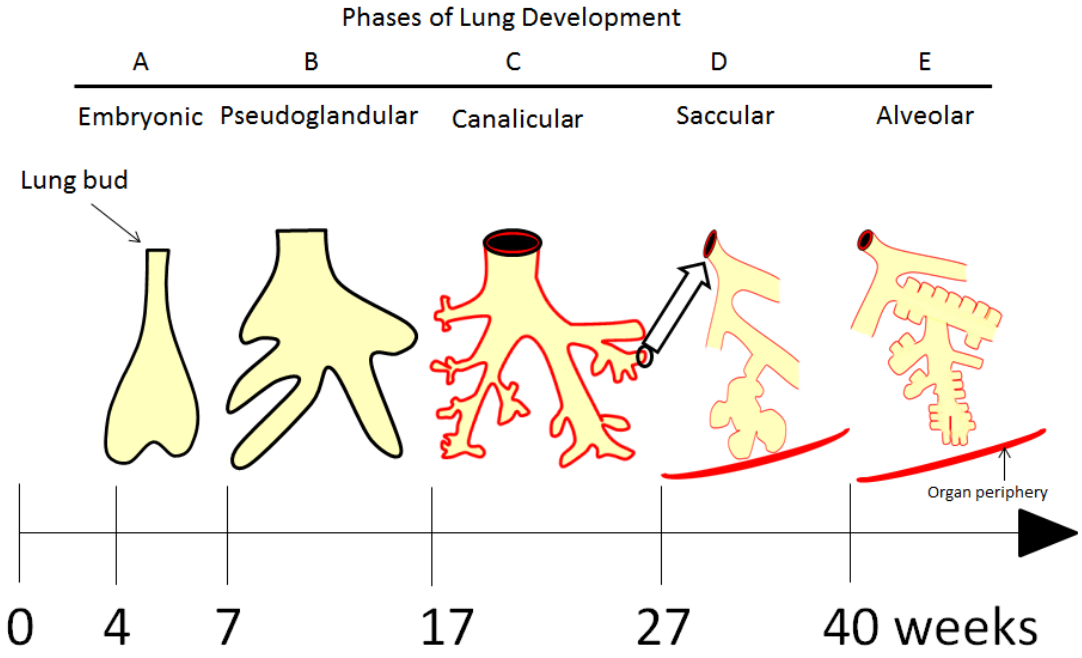

Figure 1.1. The stages of lung development. See text for details (diagram adapted from Resp!Rare, 2012).

Development of the human embryonic lung (Figure 1.1) commences around 3-7 weeks of gestation with the emergence of a primitive lung bud (Figure 1.1A), the laryngo-tracheal groove, which is derived from the foregut endoderm (Del Moral *et al.*, 2006). This groove rapidly induces the formation of the trachea and another

primitive lung bud, which then elongates and divides into two main bronchi (Mailleux *et al*., 2001). Around the age of 4.5 weeks, five tiny saccules are visible; two on the left-hand side and three on the right, which will ultimately form the lobar bronchi and corresponding lung lobes. These primitive lung buds are also lined with epithelium derived from differentiated endodermal cells, which coat the conducting respiratory airways (Ten Have-Opbroek, 1991). Smooth muscle and early blood vessel formation also occurs, which is induced by mesenchymal cells surrounding the developing airway (Deutsch & Pinar, 2002).

The pseudoglandular phase (7-16 weeks; Figure 1.1B) is a critical stage in the formation of the airway. This is where branching morphogenesis occurs, in which the acinar tubules are formed from rapid dichotomous branching of the lung's peripheral bud network (Finney *et al.,* 2008). This dichotomous growth is of a fractal nature and continues to branch into the mesenchyme of the visceral pleura (Weibel, 2009) for approximately 10 weeks. This phase is also defined by the appearance of differentiated columnar epithelial cells, which line the bronchiole tubules. The airways and major blood vessels also become coated with smooth muscle (Bucher & Reid, 1961) and a series of pulmonary vessels sprout from the pulmonary artery to line the branching epithelium and extend into the surrounding mesenchyme. Epithelial morphogenesis of the airway branch network is sustained by an intraluminal pressure, which is also linked in determining the rate of vascular development of the lung (Unbekandt *et al*., 2008).

The canalicular phase (16-26 weeks; Figure 1.1C) is characterised by intense vascular development (highlighted by the red outline of the airways in Figure 1.1C) and the differentiation of the epithelium surrounding the alveolar ducts. In this phase, the alveolar type I and II pneumocytes (ATI, ATII) are first observed, formed from differentiation of the cuboidal epithelial cells (Deutsch & Pinar, 2002). The growth of major blood vessels and differentiation of the pulmonary epithelium also occurs leading to the formation of the air-blood barrier, providing the capability for gas exchange (Burri & Moschopulos, 1992). Several studies have shown that throughout mid-gestation, the airway epithelium is in close proximation with the endothelium, whose cells comprise the air-blood barrier (Hislop, 2002).

In the saccular phase (28-35 weeks; Figure 1.1D), the epithelium continues to differentiate giving rise to the alveolar epithelial cells, a group of specialised ATI and ATII cells. In doing so they become the most populated group of epithelial cells in the fetal lung (Deutsch & Pinar, 2002), comprising 99% of the lung's surface area. Smooth-walled sacculi appear at the terminus of each respiratory tract forming a matrix with the neighbouring septa, which permits further growth and differentiation of the epithelium (Rannels & Rannels, 1989).

The final stage of lung development is the alveolar phase (36 weeks up through infancy; Figure 1.1E) where by this point approximately 23 generations of airway branching has occurred (Weibel, 2009), along with the formation of approximately 150 million alveoli, which is between a third and a half of those found in the adult lung (Hislop *et al*., 1986). This allows oxygen to be supplied upon birth while alveolar

development continues for at least 2-3 years after birth in humans and matures over the first seven years of life. The pulmonary vasculature is radically transformed at birth upon first breath and postnatally continues to develop exponentially, closely matching the rate of alveolarisation (Gebb & Torday, 2008).

The formation and role of the pulmonary epithelium in regulating normal lung function.

Upon normal branching morphogenesis, a vast network of hollow tubes form, which are comprised of a variety of endothelial and epithelial cell types (Metzger & Krasnow, 1999). A layer of pseudostratified epithelium coats the trachea and bronchi and the proximal airways themselves are composed of columnar epithelium. This is defined as the pulmonary epithelium, which is composed of a number of specialised epithelial cells that serve to maintain proper lung function by regulating lung fluid balance, gas exchange, ion transport and acting as barriers to foreign agents (Hermans & Bernard, 1999).

Pulmonary Neuroendocrine Cells (PNEC)

PNECs are one of the earliest epithelial phenotypes observed in lung development (~E13.5) (Shan *et al*., 2007) and their formation in the proximal airways is thought to be regulated by Notch signalling (Rock & Hogan, 2011). Their function in fetal development is to supply prospective airways with a series of peptides to aid signalling of branching morphogenesis (Sunday, 1996). Little is known of the long-term function of PNEC's but it is thought that they play a role in mediating epithelial

cell turnover via paracrine mechanisms, as well as a playing a chemosensory role in detecting hypoxia (Cutz, 1982).

Ciliated cells

Ciliated cells possess a columnar morphology and coat the tracheal and bronchial regions of the lung. Their function is to secrete a mucosal layer which surrounds the pulmonary epithelium that serves as a barrier to infection. In tandem with the goblet cells, the sweeping action of the cilia propels away any particulate matter adhered to the mucosal layer. It is also suggested that ciliated cells play a role in restoring airway tissue damage (Lawson *et al*., 2002).

Goblet cells

Goblet cells are a group of specialised ciliated columnar epithelial cells which secrete mucous glycoproteins into the bronchial lumen allowing the surface fluid to trap particulate matter and thus protecting the epithelial membrane (Chang *et al*., 2008). However, in many lung-associated diseases, such as asthma, goblet cell proliferation (hyperplasia) results in a build-up of mucous secretion around airway ducts and thus can compromise airway function (Chang *et al*., 2008)

Clara cells

Clara cells are non-ciliated columnar cells which are localised in the conducting airways and bronchioles in large mammals (Chang *et al*., 2008). Their main function is to express surfactant proteins which are responsible for reducing surface tension throughout the lung and thus prevent lung collapse. An additional function of these

cells is to eradicate toxins dissolved in the airway lumen (Widdicombe, 2002). Clara cells also have unique stem cell capabilities (Bishop, 2004) and have been reported to be involved in the regeneration of the lung structure (Rawlins *et al*., 2009). As such, clara cells have long been regarded to act as progenitors of cells for the terminal bronchioles (Bishop, 2004).

Alveolar Type I and II Pneumocytes

The large, flat morphology of the ATI cells serve to provide a large surface area suitable for gas exchange (Williams, 2003). By contrast, ATII cells are cuboidal in appearance and are responsible for the recruitment of surfactant molecules and proteins to their lamellar bodies in order to aid host defence from infections (Whitsett *et al*., 2010), as well assist fluid and ion transport across the airway epithelium (Kemp & Oliver, 1996). In contrast to their ATII counterpart, relatively little is known regarding the function of ATI cells as they have proven to be difficult to isolate *in vitro* (Berthiaume *et al*., 2006). One function for ATI cells postulated by Chen *et al*., (2006), suggests that they protect the alveolar epithelium from oxidative stress by secreting antioxidant proteins such as Apolipoprotein E (Apo E) and Transferrin. Interestingly, ATI cells are unique in that they do not undergo mitotic division and depend upon mitosis and differentiation of their ATII counterpart (Evans *et al*., 1975).

Development of the pulmonary vasculature.

The majority of studies on branching morphogenesis have focused specifically on the formation of the bronchial tree. However, there is evidence to suggest that the airway tree formation is co-ordinated with development of the vascular tree via pulmonary circulation (Glenny, 2010). The lung becomes vascularised as early as the pseudoglandular phase with the vascularisation of the primitive lung bud through the ingrowth of a vascular plexus form the heart/aortic sac and dorsal aorta (Jones & Capen, 2011). This primitive aorta and pulmonary trunk gives rise to the circulatory mechanism that exists between the heart and the lung capillary plexus (Gao & Raj, 2010). At this point, a mesenchymal capillary plexus forms resulting in the emergence of pulmonary macrovascular (arteries and veins) and microvascular (capillaries) structures (Hall *et al*., 2002; deMello *et al*., 1997). The mesenchyme is derived from the lateral plate mesoderm and introduces a raft of vascular progenitor cells, such as smooth muscle and endothelial cells (Hislop, 2005). This forms a vascular network in the mesenchyme which surrounds the tips of the branching airways that are in close proximation with the major pulmonary blood vessels (Weibel, 2009), resulting in a network of blood vessels that interweave with the proximal airway. This establishes an efficient surface for gas exchange, which is further enhanced by the close association between the capillary network and the epithelial airway lining (Weibel, 2009). After 23 generations of airway branching, the pulmonary vasculature undergoes an additional 5 generations of branching, culminating in the formation of a vast capillary network and the appearance of micro-vascular structures around each alveolus (Land, 2011).

The lung vasculature is thought to form concurrently by two processes; angiogenesis and vasculogenesis. Angiogenesis is the process by which blood vessels form from progenitor endothelial cells, which extend from existing blood vessels from the cardiac tissue (Cardoso & Lü, 2006). On the other hand, vasculogenesis is defined as the formation of new blood vessels, derived from differentiated endothelial cells coupled by a *de novo* production of angioblasts that form a primitive vascular network (Vailhé *et al*., 2001). Vasculogenesis involves the formation of blood vessels that are in close proximity to the developing airway epithelium. This results in the formation of a large capillary network that unites blood vessels, leading to the complete vascularisation of the lung. However, how angiogenesis and vasculogenesis co-ordinate with each other is unknown. One school of thought is that these two processes converge and 'fuse' during mid-late gestation (deMello *et al*, 1997), while other studies suggest that both angiogenesis and vasculogenesis occur independently of one another (Hall *et al*, 2002). In order to avoid this ambiguity, this thesis will simply refer to vascular development of the lung as 'vascular growth'.

Organisation of the vascular tree.

The tightly co-ordinated development between the airway and pulmonary vasculature culminates in the formation of a system of three closely related branching trees that comprise the adult lung (Weibel, 2009). These three interwoven tubular structure consist of the airway, pulmonary artery/venal and the bronchial artery/venal systems (Figure 1.2), which are all packed into the chest cavity

at a compressed volume of 6 litres (Land, 2011). The pulmonary arteries branch in parallel with the airways and the bronchial tubules, presumably so that the exchange of deoxygenated blood to the alveoli can occur with each generation of branching. On the other hand, the pulmonary veins position themselves between the broncho-arterial units (Weibel, 2009) and mediate the transport of oxygenated blood from the lung to the left atrium of the heart. The bronchial circulatory system forms a dense vascular plexus in the airway wall, where the arteries are responsible for supplying deoxygenated blood and nutrients to the airway and other lung structures (Charan *et al*., 1984). The bronchial arteries are derived from the thoracic aorta and are distributed around the bronchial glands and coat the walls of the larger bronchial tubes and pulmonary vessels (Gray, 1918). The bronchial vein is established at the root of the lung where it forms part of the venous drainage system of the lung, which is responsible for supplying part of the deoxygenated blood to the azygos vein (right bronchi) and the left superior intercostal vein (left bronchi), while the remaining blood is returned to the heart via the pulmonary veins (Charan *et al*., 2007). Embedded within the vascular tree is a complex pulmonary lymphatic system, which is an important part of the body's immune system. The lymphatic system acts to keep the lungs dry, regulates lung fluid level and acts to eliminate foreign agents that can penetrate the epithelium (Schraufnagel, 2010). It achieves this through the circulation of lymph in the lymphatic vessels, which is derived from the interstitial fluid. The lymph is circulated around through lymph vessels and lymph nodes before emptying into to the subclavian veins, which return this recycled blood plasma back to the heart. The structure of the lymphatic system in the lung is

of a tubular and saccular nature, allowing them to interweave with surrounding blood vessels and the airway itself (Schraufnagel, 2010). .

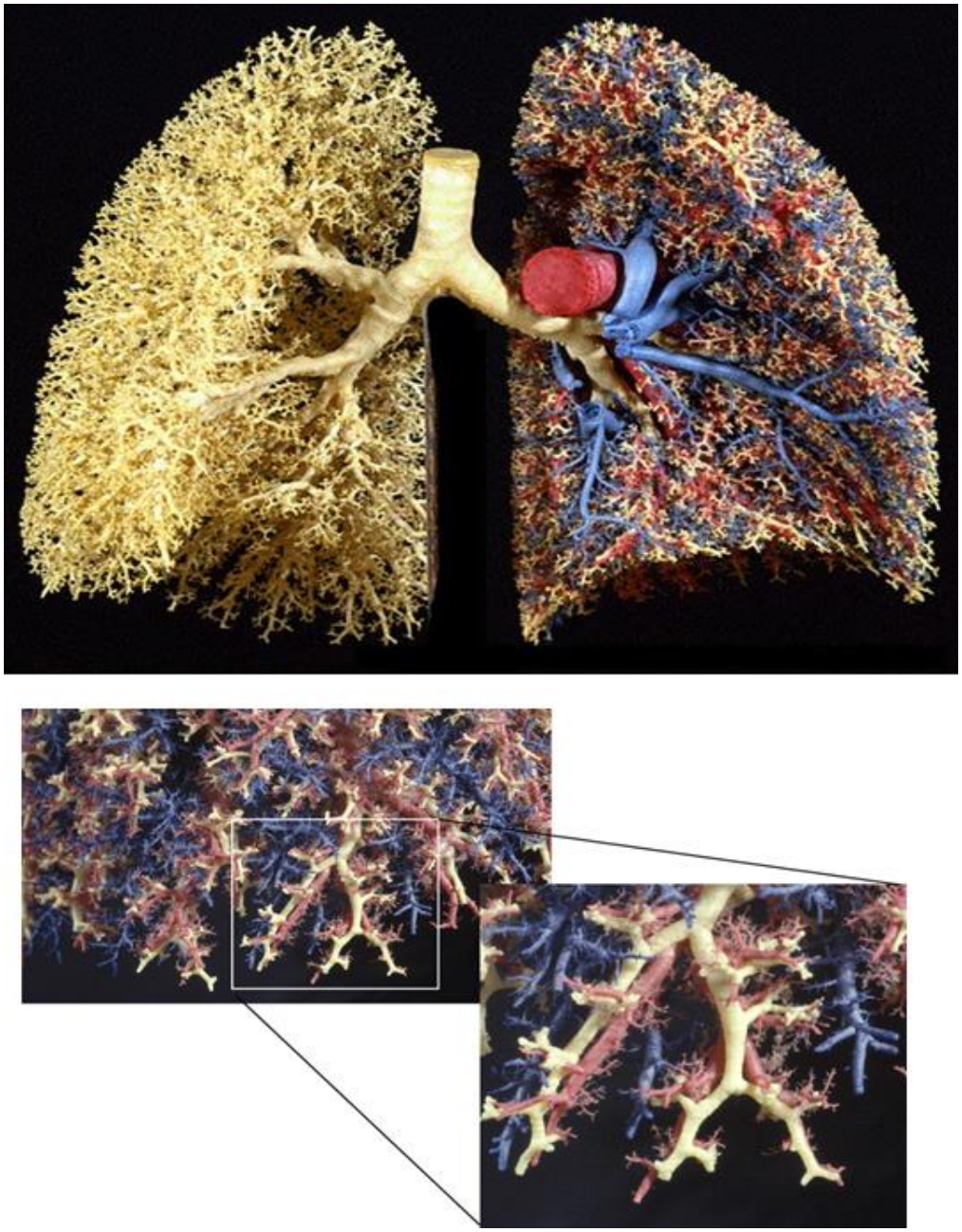

Figure 1.2. A resin cast of the lung vasculature. This interwoven branching network consists of the airway (yellow) and the pulmonary arteries (red) and veins (blue). Magnified image illustrates the extent of branching and close association between the airway and the pulmonary vasculature. Model and figure originally constructed by Weibel (2009).

Vascular endothelial growth factor (VEGF); the hallmark of lung vasculogenic signalling.

VEGF is a key regulator of vascular growth during embryonic development and its significance has been extensively researched. Originally described for its permeability properties (Senger *et al*., 1983), VEGF acts as a specific endothelial cell mitogen. In mammals, five ligands of VEGF have been identified, of which VEGF-A is the best described (referred to henceforth in this thesis). The primary function of VEGF in lung development is to direct growth of the lung vasculature; secretion of VEGF from the lung epithelium signals the production of precursor endothelial cells (Acarregui *et al*., 1997; Brown *et al*., 2001), which are responsible for blood vessel formation. VEGF also acts as a growth factor in mediating the development of ATII cells, therefore linking the vascular role of VEGF with that of epithelial differentiation. VEGF has long standing implications in the maintenance of adult lung function as it induces the formation of blood vessels upon injury and during poor blood circulation in response to oxidative stress achieved through exercise and disease.

VEGF is highly expressed in the airway epithelium of the developing lung but is initially expressed in the lung mesenchyme and epithelium around E12.5-14.5 and then becomes increasingly confined to the epithelium later on during development (Gebb & Shannon, 2000). Vascular signalling occurs through binding of VEGF to its specific Receptor Tyrosine Kinases (RTK) on the cell surface, VEGF receptor 1 (VEGFR-1/FLT1) and VEGF receptor 2 (VEGFR-2/FLK1/KDR). Upon dimerisation and activation of these receptors, signalling induces the upregulation of genes

responsible for encoding endothelial proliferation and migration to differentiate into vascular tissue (Scott *et al*., 2010). Specifically, activation of VEGFR-2 results in the activation of the ERK pathway and association with Vascular-Endothelial Cadherin (VE-cadherin) (Voelkel *et al*., 2006). This association releases phosphorylated β-catenin to translocate to the nucleus to induce epigenetic up-regulation of the VEGF gene and subsequently, protein expression (Skurk *et al*., 2005). However, VEGFR-1 and -2 both differ in their signalling properties (Ferrara *et al*., 2003). It is thought that VEGFR-2 mediates almost all the known cellular responses to VEGF (Holmes *et al*., 2007), whereas VEGFR-1 has been shown to transduce different VEGF-dependent cellular events, which have proven difficult to elucidate (Voelkel *et al*., 2006). This could be explained by the possibility that VEGFR-1 only becomes active when it is heterodimerically bound to VEGFR-2 (Waltenberger *et al*., 2000).

The importance of VEGF in regulating lung development cannot be understated. VEGF gene splicing of mRNA in humans and mice has given rise to several isoforms all with varying biological activities (Voelkel *et al*., 2006). In mice, the loss of a just a single VEGF allele results in lethality around embryonic day 11.5 (E 11.5) (Del Moral *et al*., 2006) and knockouts of both VEGFR-1 and -2 also result in lethality, prior to development of the lung capillary plexus (Gebb & Shannon, 2000). Conversely, overexpression of VEGF in lung epithelium causes lung dysplasia, thus indicating that regulation of VEGF is vital for normal lung development and function (Zeng *et al*., 1998).

Hypoxia Inducible factors and the regulation of VEGF-A gene expression.

Hypoxia inducible factors (HIFs) are a family of transcription factors that are susceptible to changes in oxygen in the cellular environment (Smith *et al*., 2008) and are responsible for the expression of >70 genes required for metabolism and apoptosis/survival (Land & Tee, 2007). There are three HIF isoforms that are expressed in the fetal lung (HIF-1, HIF-2 and HIF-3). Under hypoxic conditions, HIF-1 was originally discovered bound to the hypoxia response element (HRE) of the Erythropoietin (EPO) gene, which regulates red blood cell production (Semenza & Wang, 1992). HIF-1 is highly conserved and its acitvity is tightly governed by oxygen homeostasis. It has a heterodimeric structure, consisting of its α and ß subunit and low oxygen enhances HIF activity through stabilisation of the α subunit (Land & Tee, 2007). The oxygen-sensing component of HIF-1α is a Prolyl Hydroxylase Domain (PHD), which exists within the Oxygen Dependent Degradation Domain (ODDD) of the HIF-1α protein (Figure 1.3A). Upon oxygenation, HIF is highly unstable and the hydroxylated prolines on the HIF protein become ubiquitylated by the Von Hippel-Lindau (VHL) E3 ubiquitin ligase derived from the VHL tumour suppressor, which results in the complete degradation of the HIF-1α protein. VHL syndrome is a rare genetically inherited disease which is caused by a mutation in the VHL tumour suppressor gene on chromosome 3p25.3 (Wong *et al*., 2007). VHL is characterised by symptoms such as renal cell carcinoma and angiomatosis, which accounts for 37.2% of patients presenting with VHL (Wong *et al*., 2007).

As discussed earlier, fetal lung development occurs in hypoxic conditions, where the PHD remains inactive and HIF is stabilised due to the fact that hydroxylases and VHL proteins are both inhibited in the absence of oxygen (Ziello *et al*., 2007). At this point, the HIF-1β subunit can bind to the α-subunit at the N-terminal basic helix-loop-helix (bHLH) and PAS motifs (Crews, 1998) and this newly formed heterodimer rapidly translocates to the nucleus (Figure 1.3A, B). The HIF-1β subunit is an Aryl-hydrocarbon Receptor Nuclear Translocator (ARNT) that is universally expressed by almost all cells, whereas HIF-1α is very lowly expressed under normoxic conditions (Shimoda & Semenza, 2011). Upon nuclear translocation, the HIF dimer binds to DNA sequences on the HRE of an associated target gene, such as VEGF-A and transcription is sequentially activated through the interaction between the C-terminal Transcriptional Activation domain (C-TAD) of HIF-1α and the histone acetyltransferase, CBP/p300 (Land & Tee, 2007) (Figure 1.3C). Upon stabilisation at low oxygen, HIF ultimately induces the expression of oxygen-independent cellular responses and notably the upregulation of the VEGF-A gene. In the fetal lung, HIF-1α expression is localised to the branching airway epithelium (Groenman *et al*., 2007), where its depletion correlates with reduced lung branching moprhogeneis and vascular growth (van Tuyl *et al*., 2005) and its geneteic knockout is embryonic lethal at embryonic day (E) 10.5 (Kotch *et al*., 1999).

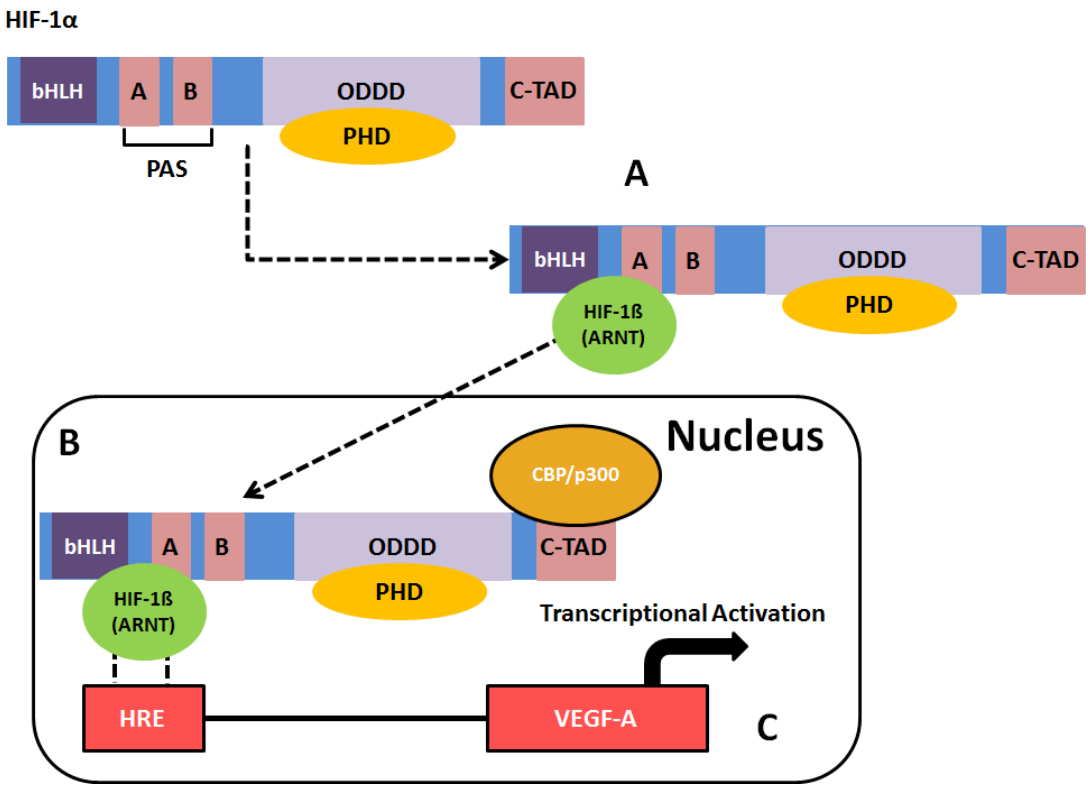

Figure 1.3. Nuclear translocation and activation of HIF-mediated VEGF-A gene expression. HIF-1α translocates to the nucleus upon dimerisation with HIF-1ß (A) and binds to the HRE of the VEGF-A promoter (B). This interaction is coupled activity of the histone acetyltransferase CBP/p300 on the C-TAD domain of HIF-1α, which permits expression of the VEGF-A gene (C).

HIF-2α is also expressed in the airway epithelium and has been reported to serve important functions during lung development. HIF-2α displays the same structural affinities as HIF-1α and can also translocate to the nucleus upon dimerisation with HIF-1β. Where HIF-2α varies from its isomeric counterpart is in its pattern of expression. HIF-2α is only expressed in certain tissues (Wiesener *et al*., 2003) unlike HIF-1α, which is widely expressed. HIF-1α and HIF-2α are closely related and are both involved in the transcriptional activity of HRE-dependent genes (Wenger, 2002), although the preferential regulation of VEGF by either isoform appears to be

dependent on individual cell types (Rankin *et al*, 2008). Furthermore, phenotypic studies of HIF-1α and HIF-2α knockout mice have indicated that both isoforms have different functional roles (Holmquist-Mengelbier *et al*., 2006). This is further indicated by, Eubank *et al*., (2011), who speculates that HIF-1α and HIF-2α play opposing roles in regulating VEGF, whereby HIF-2α acts as an antagonist of VEGFR-1 function, opposing HIF-1α pro-angiogenic signalling of VEGF secretion. In the lung specifically, HIF-2α expression is strongly associated with the development of vascular structures (Groenman *et al.,* 2007) and has also been reported to regulate the expression of certain VEGF isoforms in the developing lung (Voelkel *et al*., 2006). However, unlike HIF-1α, it does not regulate VEGF-A in the fetal system as it is only expressed in the lung during late embryonic stages (Ahlbrecht *et al*., 2008). This was established by studies from Compernolle *et al*., (2002), who demonstrated that knockout of HIF-2α caused vascular defects during alveolar septation, which marks the transition from the saccular to alveolar phase of lung development at which point VEGF-A expression is reported to decline (Levy *et al*., 2005; Remesal *et al*., 2009).

The final known isoform of HIF is HIF-3α. It differs in the structural features of its isomeric counterparts as it lacks the C-TAD required for transcriptional initiation (Hara *et al*., 2001). Its expression and function are poorly understood but it is postulated that it acts as a repressor of HIF-regulated gene expression (Hara *et al*., 2001).

The molecular cues that signal airway and vascular growth.

In spite of the ambiguity surrounding development of the lung vasculature, it is certain that this process is heavily influenced by cellular and molecular cues (Gebb & Torday, 2008), which involve cross-talk between the mesenchyme, airway epithelium and the vascular network. The early phases of lung development rely on the activation of angiogenic growth factors and their associated receptors (Han & Stewart, 2006), which contribute to the stereotypical fractal patterning of the airway. The maintenance of the mesenchymal-epithelial-vascular bed axis is crucial as it dictates the fractal patterning that is diagnostic for normal lung development. It is also necessary for patterning blood vessel growth and differentiation of many cell types as well as smooth muscle and cartilage formation (Unbekandt *et al*., 2008). This axis can be severely compromised if disrupted; for example, if there is no mesenchymal tissue present, then there are no cellular cues present to induce branching of the nearby epithelium (Gebb & Torday, 2008). Conversely, in the absence of epithelium, the mesenchymal cells will die and consequently, the vascular networks will perish (Demayo *et al.*, 2002). This close intimacy is vital for complete lung development and also for the sustainment of normal lung function (Demayo *et al.*, 2002). A number of signalling proteins have been shown to putatively influence branching morphogenesis as demonstrated by gene studies in *Drosophila* (Metzger & Krasnow, 1999). However, there are a number of known key players that regulate the close association between airway and vascular development.

FGF10 is a key inducer of airway outgrowth of the lung epithelium.

Fibroblast Growth Factors are vital in organogenesis as they induce the activity of RTKs leading to the proliferation and differentiation of several cell types (Glienke *et al.*, 2000) and have been reported to be specifically involved in the formation of the epithelium and the vascular system throughout all phases of lung development (Sutherland *et al.*, 1996). In the early phases, FGF1 and 7 both induce airway epithelial proliferation (Lebeche *et al*., 1999) whereas FGF3 and 4 are important in mediating post-natal development of the alveoli (Weinstein *et al*., 1998). FGF10 in particular plays a vital role in lung morphogenesis (Ornitz & Itoh, 2001) and is known to play a chemotactic role in epithelial structuring which determines branch patterning (Unbekandt *et al*., 2008). Originally discovered to be localised in the mesenchyme of E14 rat lungs (Yamasaki *et al*., 1996), several studies have demonstrated that FGF10 is closely associated with lung bud formation (Bellusci *et al*., 1997a). The known role of FGF10 is to determine the length of airway tubules and the location of subsequent branch generations which results in primary bud formation. This function appears to share homology with the *branchless* gene observed in *Drosophila* (Sutherland *et al*., 1996). However, FGF10 has also been reported to induce secondary budding of lung lobes upon interaction with other growth factors which will be discussed later in this chapter. During development, FGF10 is secreted from the mesenchyme and binds to the epithelial-bound receptor, Fibroblast Growth Factor Receptor 2 (FGFR2b). Upon activation and dimerisation of FGFR2b, FGF10 induces structural changes to the adjacent epithelial cells (Mailleux *et al*., 2001), accompanied with signalling of RTK pathways, promoting proliferation

and the outward movement of the endoderm. This culminates in the elongation of the airway towards the FGF10 source (Menshykau *et al*., 2012; Scott *et al*., 2010). Conversely, inactivation of FGFR2b leads to disruption of this diagnostic bifurcation of the airway and the emergence of small epithelial outgrowths which arise arbitrarily along the main bronchi (Alber *et al*., 2009). The FGF10/FGFR2b mechanism has only been demonstrated *in vitro* (Warburton *et al*., 2003) but some *in vivo* models have shown that without the FGF10/FGFR2b association, lung development would cease (De Moerlooze *et al*., 2000) and in developmental diseases such as LADD (lacrimo-ariculo-dento-digital) syndrome, which is caused by mutations that modify the 'b' isoform of FGFR2b, the chemotactic influence of FGF10 is severely compromised (Rohmann *et al*., 2006). The role of FGF10 in mediating vascular development is unknown although it has been speculated that VEGF-A induction may be directly regulated by the FGF10 signalling (Del Moral *et al*., 2006).

Sonic Hedgehog (SHH) and Bone Morphogenetic Protein 4 (BMP4) control the spatial expression of FGF10.

In addition to FGF10, Sonic Hedgehog (SHH) is thought to play an important role in branching morphogenesis, particularly in determining the bifurcating pattern of the developing airway epithelium (Menshykau *et al*., 2012). Upon induction of FGF10, SHH protein is highly expressed in the foregut endoderm from where branching morphogenesis commences and it acts as a positive regulator of cell proliferation (Bellusci *et al*., 1997b). During development, SHH is secreted by the epithelium in the distal tips of the airways (Pepicelli *et al*., 1998). Its mode of action is to reversibly signal to the mesenchyme and bind to its receptor, a transmembrane

protein known as Patched 1 (PTC1). Activation of PTC1 triggers signalling to several target genes associated with SHH, which ultimately leads to the repression of FGF10 signalling. The resulting repression 'splits' the FGF10 signal to promote the next round of branching. This 'inhibition' is reversed through the activation of Hedgehog Interacting Protein 1 (HIP1) in the mesenchyme, which represses epithelial SHH signalling, thus allowing FGF10 expression to induce airway elongation (Chuang & McMahon, 2003). An illustrative depiction of the SHH signalling mechanism is described in Figure 1.4. Much like FGF10, SHH shares a distinct homology with its corresponding hedgehog gene in *Drosophila* (Miller *et al*., 2001) and both proteins interact with each other indirectly and are essential in facilitating normal airway development. *In vivo* models of SHH null mutants have been shown to cause severe defects in branching morphogenesis and overexpression of SHH reduces FGF10 expression and the magnitude of distal branching (Menshykau *et al*., 2012).

Bone morphogenetic protein 4 (BMP4) is another secondary gene induced by FGF10 expression. BMP4 is a member of the Transforming Growth Factor β (TGFβ) superfamily of proteins whose function has been highly conserved throughout evolution (Weaver *et al*., 1999) and is expressed in both the mesenchyme and the distal tips of the airway epithelium. Much like SHH, BMP4 signalling is regulated through expression of a specific antagonist, in this case, Noggin, which is transiently expressed in the mesenchyme (Weaver *et al.*, 1999). However, the mechanism by which BMP4 regulates lung development remains difficult to elucidate. Its proposed function is to negatively regulate FGF10 thus inhibiting epithelial cell proliferation and disturbing branch extension (Hogan, 1999). While this theory has been

demonstrated with *in vitro* models (Menshykau *et al*., 2012), Bragg *et al*., (2001), showed that adding BMP4 to lung organ cultures promoted branching morphogenesis and epithelial budding, Examinations of BMP4 expression in early lung development have highlighted a potential role for BMP4 in determining the structuring of the early lung (Weaver *et al*., 2000). Regardless of this ambiguity, BMP4 signalling draws several parallels with that of SHH signalling in that they both influence FGF10 expression.

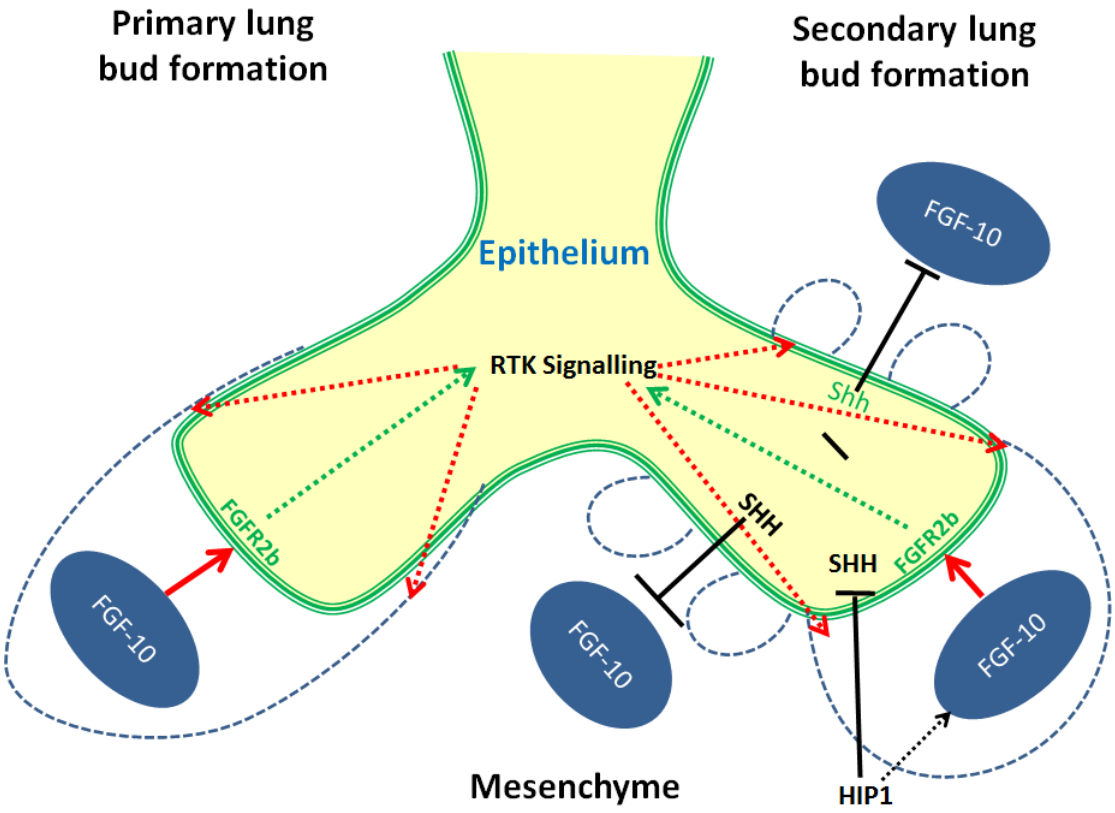

Figure 1.4. FG10 and SHH signalling branching morphogenesis in the fetal lung. The left hand-side exhibits the stereotypical FGF10-FGFR2b signalling cascade resulting in the elongation of the airway buds. The right-hand side demonstrates secondary budding initiated by SHH regulation of FGF10 signalling through interaction with HIP1. This results in reduced SHH signalling and increased FGF10 expression in the immediately adjacent regions, allowing secondary budding to occur (Cardoso & Lü, 2006).

FGFR2b activation induces airway growth through the MAPK pathway.

Signalling of the Mitogen-activated Protein Kinase (MAPK) pathway governs cell growth, differentiation and apoptosis (Qiu *et al*., 2000) and its activity is well-established in the developing lung. Upon activation of FGFR2b at the epithelial membrane, a complex consisting of the lipid-docking protein, Fibroblast Growth Factor Receptor Substrate 2 (FRS2), Growth Factor Receptor-bound Protein 2 (GRB2) and Son of Sevenless (SOS) forms (Warburton *et al*., 2003). In addition to this, FGFR2b also binds a positive tyrosine phosphatase regulator, Src-homology 2 Domain-containing Phosphatase 2 (SHP2) to FRS2, which is required to fully potentiate MAPK activity (Hadari *et al*., 1998). The formation of this complex results in the catalysis of RAS from its Guanine Diphosphate (GDP) to the Guanine Triphosphate (GTP) active form, which enables the RAF serine/threonine kinase to induce the Mitogen-activated Protein Kinase Kinase-1 (MEK-1) activation of ERK1/2 (Land, 2011) (Figure 1.4). The outcome of this growth-factor mediated signalling cascade is potentiated outward growth of the lung airway epithelium towards the FGF10 source.

The PI3K/AKT and mTOR pathways drive vascular signalling of the fetal lung.

Much like the MAPK signalling cascade, Phosphatidylinositol 3-kinase (PI3K) regulates cell growth, differentiation and survival but is also a key regulator of protein synthesis (Taniguchi *et al*., 2006). Similarly, activation of PI3K is known to occur upon FGR2b dimerisation and interaction with FRS2 (Eswarakumar *et al*., 2005). However, PI3K activity can also be stimulated independently of RTK activity

by means of G-protein coupled-receptors and a number of other stimuli (Goncharova *et al*., 2002). PI3K activation induces the production of 3-phosphoinositide lipids (PIP_3), whose phosphorylation can be reversed by Phosphatase and Tensin Homolog Deleted on Chromosome 10 (PTEN) activity, thereby counteracting PI3K activity (LoPiccolo *et al*., 2008). This process is of significance as PTEN has been found to be mutated in a number of cancers. Upon its phosphorylation, PIP_3 acts as a plasma membrane docking site for proteins that contain Pleckstrin-homology (PH) domains (Castellano & Downward, 2011). One such PH-containing protein is the serine/threonine kinase, AKT, also known as protein kinase B (PKB). AKT is an established regulator of cell growth, proliferation, metabolism and survival (Manning & Cantley, 2007). Little is known of a role for the PI3K/AKT signalling cascade in regulating fetal lung development but recent evidence suggests that a loss of AKT has detrimental effects on normal lung epithelial development (Alphonse *et al*., 2011).

In terms of cell growth, a key downstream target of AKT is the serine/threonine protein kinase, the Mammalian Target of Rapamycin (mTOR). mTOR integrates the input from upstream signalling pathways and as such regulates cell growth, motility, survival, protein synthesis and transcription (Hay & Sonenberg, 2004). Activity of mTOR itself is sensitive to nutrients, energy metabolism and growth factor signalling and disruption of these upstream regulators can have severe implications for the role of mTOR in metabolic diseases and cancer (Hay & Sonenberg, 2004). mTOR exists as two distinct complexes; mTORC1 and mTORC2. mTORC1 is a downstream target of PI3K/AKT that is comprised of a Regulatory Associated Protein of mTOR

(RAPTOR) and a mammalian LST8/G-protein ß-subunit-like protein (Villanueva *et al*., 2008). mTORC1 acts as a regulator of cell growth through activation of Ribosomal Protein S6 Kinase Beta-1 (S6K) where phosphorylation at threonine 389 (Thr^{389}) is used as an assay to measure mTORC1 activity (Pullen & Thomas, 1997). On the other hand, mTORC2 is composed of a Rapamycin-insensitive Companion of mTOR (RICTOR), a TOR complex subunit LST8 (GßL) (Sarbassov *et al*., 2004) and Mammalian Stress-activated Protein Kinase Interacting protein 1 (mSIN1) (Frias *et al*., 2006), where it functions as a key regulator of the cytoskeleton (Sarbassov *et al*., 2004).

In the context of fetal lung development, the PI3K pathway is essential for up-regulation of VEGF-A in epithelial cells (Rak *et al*., 2000), while mTORC1 is thought to be the key component that drives vascular signalling as mTORC2 is basally insensitive to rapamycin (Land, 2011). Furthermore, high levels of S6K phosphorylation at Thr^{389} have been observed in the epithelium within the airway bud (Scott *et al*., 2010). This was confirmed by Land & Tee (2007) who identified an mTOR signalling motif (TOS) between amino acids 99 and 104 of HIF-1α. This motif was shown to bind to the RAPTOR component of mTORC1, which can complex with HIF-1ß to induce nuclear translocation (as shown in Figure 1.3). Upon shuttling to the nucleus, HIF-1α can then interact with its transcriptional co-activator CBP/p300 to initiate transcriptional activation of VEGF-A (Land, 2011). While there is evidence to suggest that mTORC1 may act to link the FGF10 induced airway and vascular signalling cues, there is another potential key player in this development.

SPRY2 antagonises FGF10/FGFR2b signalling in the lung epithelium.

Sprouty is a protein that was originally discovered in the *Drosophila* genome and was shown to antagonise Epidermal Growth Factor (EGF) and FGF signalling in the developing trachea (Hacohen *et al.*, 1998). Four isoforms of mammalian Sprouty have been reported (SPRY1, -2, -3, -4). The expression of SPRY1, -2 and -4 is widespread in embryonic and adult cells while the expression of SPRY3 is thought to be more restrictive (Cabrita & Christofori, 2008). Each Sprouty protein carries a highly conserved cysteine-rich domain on the C-terminus and a tyrosine-containing sequence on the N-terminus of the gene (Satoh *et al*., 2010), which is phosphorylated upon FGF signalling (Cabrita & Christofori, 2008). The cysteine-rich domain is the most conserved domain between species (Glienke *et al*., 2000) and mutation of this domain in *Drosophila* was shown to drastically alter SPRY2 membrane association (Glienke *et al*., 2000), thus confirming the importance of these functional domains. In addition to the findings of Sprouty proteins acting to restrict growth-factor signalling, they also act as tumour suppressors in a variety of cancers (Lito *et al*., 2009). For example, in mouse lung epithelium, Minowada and Miller (2009) demonstrated that overexpressing the SPRY2 isoform inhibited the development of tumours. This indicates that Sprouty proteins may be of clinical significance in the treatment of cancers.

In the mammalian lung, SPRY2 is expressed in the epithelial tips of the developing airways, where it is has been widely reported to function as a negative feedback regulator of FGF receptor signalling (Unbekandt *et al*., 2008) by specifically inhibiting the MAPK pathway (Guy *et al*., 2009) resulting in a repression of lung epithelial

migration and proliferation (Cardoso & Lü, 2006). Additionally, knockout studies of SPRY2 report an increase in the extent of epithelial tube branching (Mailleux *et al*., 2001) and alteration of airway diameter (Metzger *et al*., 2008), thus implying SPRY2 as a key regulator of airway branching. The mechanism by which SPRY2 achieves this negative regulation is complex (Figure 1.5A). Upon activation of FGFR2b, the tyrosine 55 (Y55) residue located on the N terminus of the Spry2 protein, becomes phosphorylated by a c-Src Tyrosine Kinase (c-Src) (Guy *et al*., 2009). The Y55 residue also binds Protein Phosphatase 2A (PP2A), a widely expressed phosphorylation regulator in mammalian cells (Lao *et al*., 2007). Src-phosphorylation of the Y55 domain activates PP2A, which causes dephosphorylation of the serine-rich domain, thereby promoting the inhibitory hold SPRY2 has over ERK phosphorylation (Guy *et al*., 2009). Both the c-Src and PP2A phosphorylation events permit the proline-rich *PXXPXR* SRC Homology 3 Domain (SH3) to become exposed on the C terminus. PP2A specifically induces changes in the structure of the serine-rich domain in order to facilitate canonical SH3 binding of adapter proteins. One such adapter protein is GRB2, which becomes silenced upon recruitment by the SH3 binding-motif of SPRY2, resulting in the inhibition of ERK (Guy *et al*., 2009) and subsequently limiting development of the airway. SPRY2 has been reported to also act as an adapter protein for the E3 ubiquitin ligase, Canonical Casitas B-lymphoma (cCBL), which is also a known inhibitor of the ERK pathway. The cCBL tyrosine kinase-binding (TKB) motif is conserved between species and all proteins of the Sprouty family, indicating its interaction with SPRY2 is important in regulating SPRY2 activation on RTK signalling. Upon Y55 phosphorylation, cCBL binds to the TKB domain of SPRY2 and directs ubiquitylation and subsequent destruction of SPRY2 (Guy *et al*., 2009).

However, Lao *et al.,* (2007) showed that cCBL and PP2A compete for binding to the Y55 domain of SPRY2 in human embryonic kidney cells (HEK), leading to the presumption that both bind to different pools of SPRY2 in the cell. Another hypothesis postulated by Land (2011) suggests that SPRY2 acts as an adaptor protein by binding proteins to its SH3 domain before presenting them to cCBL for subsequent degradation (Figure 1.5B).

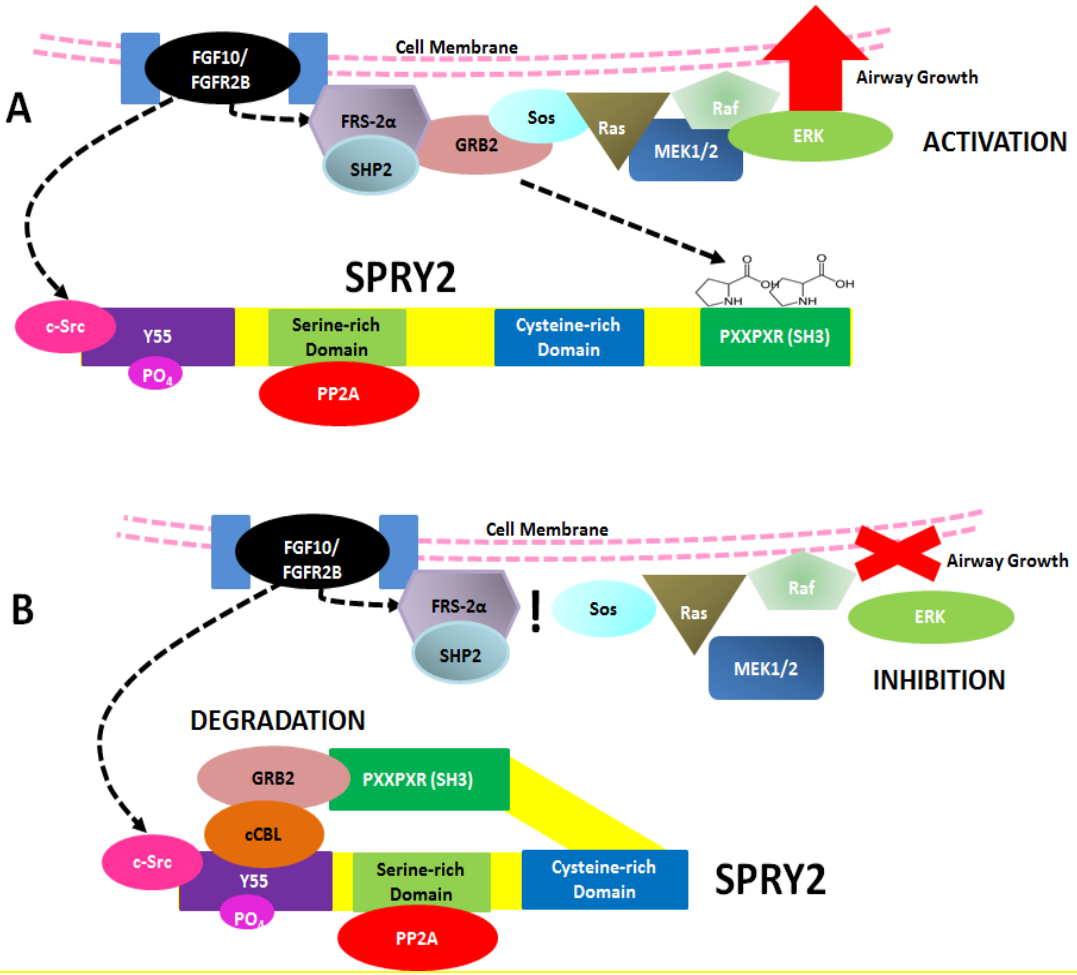

Figure 1.5. Negative feedback regulation of FGF10/FGFR2b-induced ERK activation by SPRY2. A. FGFR2b stimulation at the cell membrane signals downstream activation of ERK through the MAPK signalling cascade, whilst simultaneously activating c-Src kinase, which induces phosphorylation of the SPRY2 Y55 motif. This allows the C-terminal *PXXPXR* (SH3) motif to become exposed. B. SPRY2 recruits the SH3 domain-containing protein, GRB2, to its SH3 binding motif from the MAPK signalling cascade and presents it to cCBL on its Y55 domain as described by Land (2011). See text for further details.

.

Is there a missing link between airway and vascular growth of the fetal lung?

While the structure of the lung is vast and complex, it is hard to imagine that a structure of such great magnitude can be packed into such a small space in the body, yet is still capable of allowing gas exchange to occur. To get around this, each lung branching structure is arranged into a fractal tubular network that persists with each generation of branching during fetal development. This fractal pattern of branching follows geometric principles originally established by Weibel & Gomez (1962) and the growth of the fractal airway and vascular trees require strict organisation of the molecular signals which regulate the magnitude of tree development. If these structures are to develop relative to one another, there must be a mechanism that co-ordinates growth of both the airway and vascular trees.

The negative feedback mechanism by which SPRY2 regulates FGF10 signalling has been well documented. Furthermore, it has been recently established that the FGF10/FGFR2b/SPRY2 model facilitates airway growth in a time-dependent matter (Scott *et al*., 2010). This has led to the premise that an airway branching periodicity clock exists, which determines the fractal nature of airway branching observed in the adult lung. However, how this process is linked to vascular growth of the developing lung remains unknown. Scott *et al*., (2010) expanded on the 'molecular clock' hypothesis by demonstrating a possible mechanism linking the role of SPRY2-mediated FGF10 signalling to its potential to induce secretion of VEGF-A from the epithelium (Figure 1.6). This mechanism involves silencing of the Tuberous Sclerosis Complex (TSC1/2; Hamartin/Tuberin), which is induced through interaction between

SPRY2 at Y55 and cCBL, which ultimately results in the downstream activation of mTORC1. TSC2 contains a GTPase-activating protein (GAP) domain that stimulates activation of the small G-protein Ras Homolog Enriched in Brain (Rheb), which is a potent activator of mTORC1 (Huang & Manning, 2009). Upon silencing of TSC1/2 by the SPRY2-cCBL scaffold, inactive Rheb-GDP can be converted to an active GTP state, thereby catalysing the activation of mTORC1. This allows mTOR to bind to the TOS motif on stable HIF-1α protein, enabling VEGF-A gene expression and vascular growth to occur. Given that FGF10 regulation is dependent upon phosphorylation of the Y55 residue on the SPRY2 protein, resulting in the sequestration of cCBL and silencing of the TSC1/2 complex, this potentially allows SPRY2 to play a pivotal role in directing vascular signalling directed through activation of mTORC1 and subsequent VEGF-A expression.

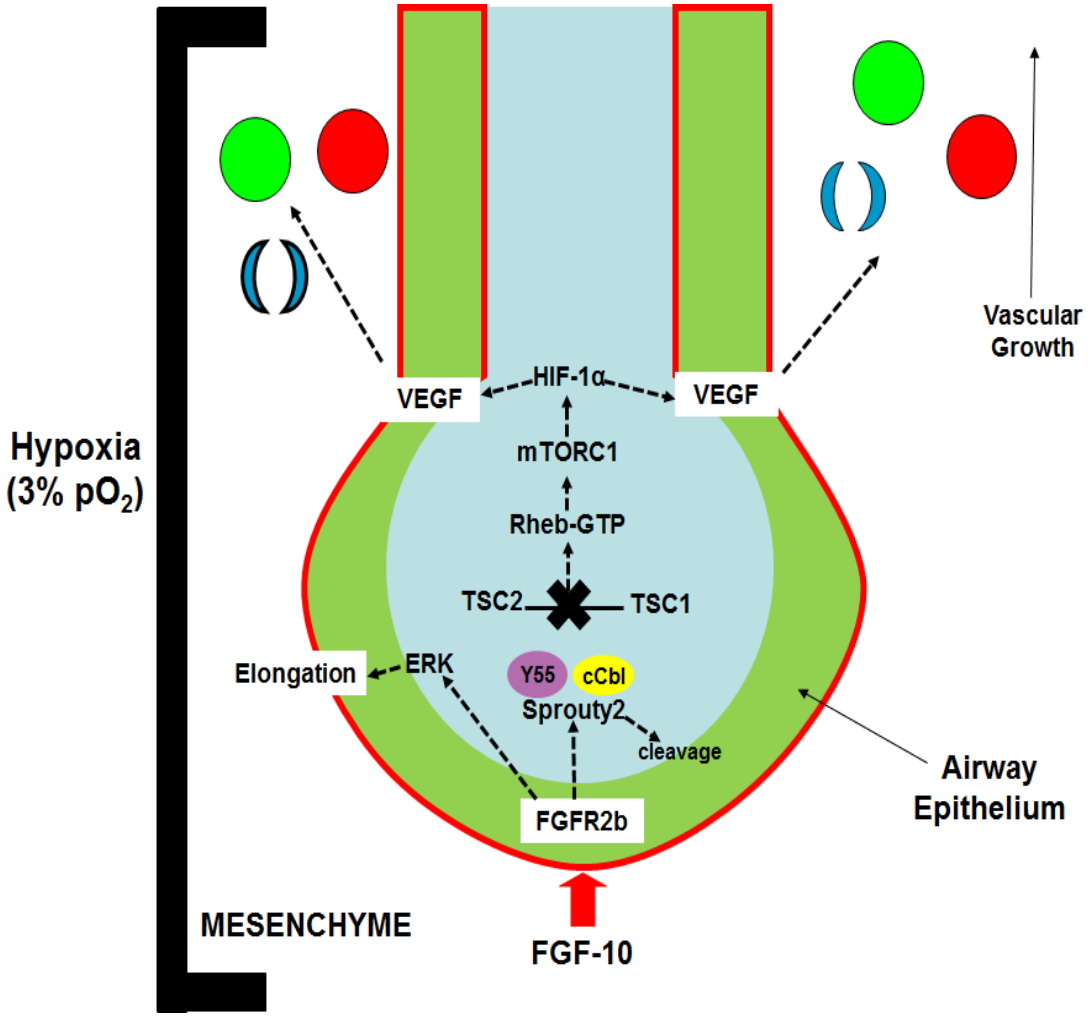

Figure 1.6. Proposed mechanism integrating airway growth and vasculogenesis in the fetal lung originally described by Scott *et al.*, (2010). FGF10 expression in the mesenchyme induces 'cleavage' of SPRY2 in the distal epithelium. This 'cleavage' event is accompanied by formation of a complex between Spry2, cCBL and TSC2. This interaction silences the TSC1/2 complex permitting catalysis of Rheb-GTP and downstream activation of mTORC1, which then binds to the TOS motif of HIF-1α. Subsequent transcriptional expression of VEGF is then induced by HIF-1α translocation to the nucleus and CBP/p300 interaction (see Figure 1.3), resulting in the appearance of vascular structures behind the growing tip of the airway, as indicated by the circular structures.

Aims and hypothesis

Considering that the development of the lung airway and pulmonary vasculature is tightly co-ordinated, it is surprising to learn that the majority of studies of fetal lung development are largely confined to examining the signalling cues responsible for directing epithelial outgrowth of the airway branching tree. As a consequence, relatively little is known regarding the signalling molecules that trigger development of the lung vasculature. Furthermore, there is little evidence present that establishes a candidate responsible for regulating co-ordinated development of both the airway and vascular trees.

One possible candidate that could link airway and vascular growth of the fetal lung is SPRY2. SPRY2 is expressed in fetal lung epithelium throughout development and is capable of trafficking to plasma and intracellular membranes upon FGF10 stimulation (Jesudason *et al*., 2010). Scott *et al*., (2010) established that an increase in SPRY2 activity correlated with the inhibition of airway signalling (ERK1/2) and activation of mTORC1 in response to FGF10, implying a role for SPRY2 in directing the portioning of kinase signals that cue airway and vascular growth of the epithelium. Furthermore, SPRY2 is known to interact with a wide range of proteins, including those that are critical for signalling airway and vascular growth (e.g. GRB2/TSC2). This evidence highlights SPRY2 as a potential key orchestrator of co-ordinated airway and vascular development of the fetal lung.

Therefore, the aim of this thesis is to test the hypothesis that SPRY2 acts as the 'missing link' that governs co-ordinated development of the airway and vascular trees in the fetal lung. In order to achieve this aim, SPRY2 expression was examined

in *ex vivo* rat FDLE and *in vitro* HBE cell models in response to FGF10 stimulation. The effect of modifying SPRY2 function via overexpression and mutation was examined with particular emphasis placed on the effect this had on ERK1/2, mTORC1, HIF-1α and VEGF-A expression. Finally, considering SPRY2 is capable of shuttling from one cellular compartment to another, experiments were carried out to ascertain if SPRY2 directs vascular growth through the epigenetic regulation of vascular genes.

Chapter 2 - Materials & Methods

Antibodies

Tables 2.1 and 2.2 below list both primary and secondary antibodies used for experiments described in this chapter.

Primary Antibody	Species	Supplier	Dilution Factor/Concentration	Molecular Weight (kDa)
ß-Actin	Rabbit	NEB (4970)	1:5000 (WB)	45
C-myc	Mouse	Life Technologies (46-0603)	1µg (ChIP)	36 (fused to C-terminal SPRY2)
CBP/p300	Mouse	Abcam (ab14984)	1:1000 (WB)/2µg (ChIP)	300
HDAC1	Mouse	Abcam (ab46985)	1:1000 (WB)	~55-57
HDAC2	Rabbit	Abcam (ab32117)	1:100 (WB)	~55-60
HIF-1α	Rabbit	Abcam	1:1000 (WB)/2µg (ChIP)	120
HIF-3α	Rabbit	Abcam (ab2165)	1:1000 (WB)	~72-80
Histone H3 Total	Rabbit	NEB (2650)	1:5000 (WB)/1µg (ChIP)	17
MAPK (ERK1/2)	Rabbit	NEB (9102)	1:1000 (WB)	Doublet at 42 and 44
P84 Nuclear Matrix	Mouse	Abcam (ab487)	1:2000 (WB)	84
p70 S6 Kinase	Rabbit	NEB (9202)	1:1000 (WB)	70
phospho (Ser10)-acetyl (Lys14)-	Rabbit	Millipore (07-081)	1:1000 (WB)	17
Phospho MAPK (ERK1/2) (Thr202/Tyr204)	Mouse	NEB (9106)	1:1000 (WB)	Doublet at 42 and 44
Phospho p70 S6 Kinase (Thr^{389})	Mouse	NEB (9206)	1:1000 (WB)	70
Sprouty 2	Rabbit	Abcam (ab50317)	1:1000/2000 (IHC/WB), 2µg (ChIP), 1µg (Co-IP)	Doublet at 39 and 35

Table 2.1. A list of primary antibodies used in this study. Information provided includes the species from which each antibody was derived, the supplier, concentration/dilution used for each application and the molecular weight(s) of the detected protein. Acronyms: WB (Western blot), IHC (Immunohistochemistry), ChIP (Chromatin Immunoprecipitation), IP (Immunoprecipitation), NEB (New England Biolabs).

Secondary Antibody	Supplier	Dilution Factor/Concentration
Alexa Fluor 555 Donkey Anti-Rabbit	Life Technologies (A31572)	1:2000 (IHC)
Anti-Biotin, HRP-linked	NEB (7075S)	1:1000 (WB)
Anti-Mouse IgG, HRP-linked	NEB (7076S)	1:1000 (WB)
Anti-Rabbit IgG, HRP-linked	NEB (7074S)	1:1000 (WB)

Table 2.2. A list of secondary antibodies used in this study. HRP-linked refers to the secondary antibodies being conjugated with the enzyme horseradish peroxidase (HRP), to allow for detection of protein by Enhanced Chemiluminescence (ECL).

Chemicals and reagents.

All Chemicals were obtained from Sigma Aldrich and were made up in deionised water (ddH_2O) unless otherwise stated.

Plasmids

The HIF-1α luciferase (HIF-luc) reporter gene was generated as described in Land & Tee (2007). Renilla (pRL) luciferase control reporter vector was obtained from Promega (#E2241). PXJ40-FLAG-human(h) SPRY2, PXJ40-FLAG-SPRY2(Y55F), -ve2000 (non-target [NT]) and SPRY2 small hairpin RNA (shRNA) constructs were kindly provided by P. Yusoff and G. Guy (Proteos, Singapore). Dual-tagged (DT) plasmids of wild-type SPRY2 ($SPRY2^{WT}$), $SPRY2^{C218A}$ and $SPRY2^{C221A}$ were created by and obtained from Dr. Claire Scott (University of Dundee). In order to create a mutant form of the cryptic *PXXPXR* SH3 domain, three prolines at amino acids 304, 307 and 308 (*PTVPPR*) were substituted for phenylalanines. This was achieved by amplifying a single of transcript of SPRY2 from HBE cells and using the restriction enzyme, *Dpn1*,

to target and destroy methyl groups allowing the mutant to be distinguished from the wild-type (WT) counterpart. Plasmids were transformed into the *Escherichia coli* (E. COLI) vector and a single colony was selected for plasmid purification. DNA was isolated from the plasmid using a Mini-prep kit (Life Technologies; K2100-10) and DNA was sequenced against the T7 promoter sequence to establish successful mutation.

HBE cell culture.

Immortalised HBE (16HBE14o-; Cozens *et al*., 1994) were obtained from Dr. D Gruenert, California Pacific Medical Center, San Francisco, CA. All cells were cultured in Dulbecco's Eagle Minimal Essential Medium supplemented with Ham's F-12 nutrient mix (DMEM/F-12) (Life Technologies; #31331-093), 10% (v:v) Fetal Bovine Serum (FBS; #F9665) and 50mg.ml^{-1} Primocin (Source Bioscience; #ant-pm-1). All cultures were maintained at 37°C in a humidified atmosphere containing 21% O_2 and 5% CO_2. Fresh stocks of HBE were brought up to replace those that had been in culture for up to 12 weeks (12 passages) and frozen stocks of each cell line were created every 2 weeks. Upon confluency, HBE were washed twice with sterile PBS and were digested using Trypsin/EDTA (Life Technologies; #25300054) and once detached, the cells were resuspended in 10ml DMEM. 10µl of cell suspension was dispensed into a cell haemocytometer (Immune systems; #BVS100) and cells were counted 4 times within 4x4 grids, with the average number of cells counted as Xx10^{4}cell.ml^{-1}. HBE cells were routinely seeded out at a calculated density of 3x10^{5}cells.ml^{-1} and would become confluent within 7 days. Cultures of HBE expressing shRNA and/or overexpressed/mutated variants were cultured similarly.

Prior to experimentation, HBE cells were supplemented with DMEM containing 2% charcoal-stripped serum (#F6765) and 50mg.ml^{-1} Primocin. All cells were cultured in a MACS VA500 Microaerophilic Workstation (Don Whitley Scientific, Shipley, West Yorkshire, UK) equilibrated at fetal pO_2 (3%) and 37°C unless otherwise stated

Creation of stable SPRY2 HBE cell lines.

DNA was purified using a plasmid midi-prep kit (Qiagen; #12145) according to the manufacturer's instructions. HBE cells were seeded out in a 25cm^2 sterile culture flask and 10µg of each DNA construct was transfected into the cells using Lipofectamine 2000 (Life Technologies; #11668019) according to the manufacturer's instructions. The transfection mixture was left on for 4 hours before the media was replaced with 2% charcoal-stripped DMEM. Approximately 24 hours after the transfection mix was applied, the cells were supplemented with DMEM/F-12 containing 10% (v:v) FBS, and 50mg.ml^{-1} Primocin. For the shRNA and SPRY2 cysteine mutant constructs, the media was supplemented 1µg.ml^{-1} of Puromycin (Life Technologies; #A11138-03) and 500µg.ml^{-1} Geneticin (G418; #A1720) respectively. Cells were allowed to grow to form isolated colonies at which point they were digested with Trypsin EDTA and each colony was separately seeded into 75cm^2 sterile culture flasks and allowed to grow to confluency. Cells were routinely supplemented with puromycin/G418 coated DMEM/F-12 medium every two days and split once per week. The extent of SPRY2 shRNA/overexpression/mutation was assessed by protein and gene expression analysis.

Isolation and primary culture of rat FDLE cells.

The preparation and isolation of rat FDLE cells in this study was adapted from a method originally described by Dobbs (1990). Time-mated pregnant female Sprague Dawley rats were purchased from Charles River and were housed in the animal care facility at Ninewells Hospital. At gestation day 19 (which resembles the late pseudoglandular/early saccular phase of fetal lung development), rats were killed by cervical dislocation according to Home Office Legislation under The Humane Killing of Animals under Schedule 1 to the Animals (Scientific Procedures) Act 1986. The fetuses were removed by caesarean section and decapitated immediately. The lungs were then excised from each fetus and placed in ice-cold sterile Ca^{2+} and Mg^{2+} free Hank's Balanced Salt Solution (HBSS; *5*.4mM KCl, 0.44mM KH_2PO_4, 137mM NaCl, 4.2mM $NaHCO_3$, 0.34mM Na_2HPO_4 and 5.5mM Glucose, pH 7.4 with 1M NaOH).

The lungs from each fetus were dissected, finely chopped and washed in HBSS to remove excess blood and cardiovascular tissue. The cleaned tissue was then resuspended and digested in 15ml of pre-warmed D/T solution (0.012% [w:v] DNase I {#DN25} and 0.02% [w:v] Trypsin {T4126} dissolved in 1x HBSS) supplemented with 10-12 drops of pre-warmed SSDNase (3mg.ml^{-1} DNase I [w:v] dissolved in 1x HBSS) and was rotated for 20 minutes at 37°C. The tissue was pelleted at 100 x g for 2 minutes and digestion was repeated a further time. The digested tissue was resuspended in collagenase (0.012% [w:v] DNase I and 0.1% collagenase {CO130} in 1x HBSS) and was rotated for 15 minutes at 37°C. After brief centrifugation, the supernatant was transferred to a fresh centrifuge tube and the proteolytic acitvity

was neutralized by the addition of an equal volume of DMEM (supplemented with 10% [vol:vol] FBS) and 50mg.ml^{-1} Primocin. The supernatant and remaining digested tissue were passed through a 100µm sterile cell strainer with trituration through the use of a sterile pastuer pipette. The filtrate was pelleted and the supernatant removed leaving two layers of epithelial and non-epithelial lung tissue. The proteolytic activity of the tissue was again neutralised through resuspension of the pellet in DMEM and pelleted at 420 x g for 5 minutes. The pellet was resuspended and added to a sterile 75cm^2 cell culture flask and was incubated at 37°C, 5% CO_2 for 30 minutes to allow attachment of the lung fibroblast cells. The supernatant was then collected and pelleted to preserve unattached cells (FDLE) and the procedure of fibroblast isolation was repeated a further time. After fibroblast tack-down, the unattached cells were collected through centrifugation and the pellet was resuspended in serum-free DMEM (-FBS) and briefly spun (130 x g for 2 minutes) to remove excess fibroblasts, blood and non-epithelial material. This resuspension was repeated until the medium was clear and an epithelial layer was visible.

FDLE cells were quantified and calculated by weight: volume ratio and were seeded out at 5mg.ml^{-1} and 2.5mg.ml^{-1} in sterile 6-well plates for nuclear protein and RNA analysis respectively. FDLE were cultured at 37°C in a humidified atmosphere containing 5% CO_2. After 24 hours, FDLE cultures were supplemented with DMEM containing 2% charcoal-stripped serum and 50mg.ml^{-1} Primocin before being cultured at in a MACS VA500 Microaerophilic Workstation at 3% oxygen to simulate hypoxia.

FGF10 treatment

FGF10 was purchased from Source Bioscience (#ABC144) as a 25µg lyophilised powder and was reconstituted in 0.1% Bovine Serum Albumin (BSA) in 1x PBS and 50 $\mu g.ml^{-1}$ FGF10 aliquots were stored at -80°C. Both FDLE and HBE unless otherwise stated were treated with a dose-response range of FGF-10 concentrations consisting of 0, 0.01, 0.03, 0.1, 0.3 and 1$\mu g.ml^{-1}$ in 2% charcoal-stripped serum. Cells were incubated with FGF10 for 6 hours prior to cell lysis.

Whole cell lysis

Cell lysis buffer was obtained from Cell Signaling (#9803S) and diluted down from 10x stock to 1x with ddH_20. A protease inhibitor tablet (Roche; 11697498001) was added per 15ml. All cells seeded in 6-well culture dishes were lysed in 150µl and sheared 10-20 times using a 200µl pipette. Lysates were then pelleted at 14,000rpm for 10 minutes in a pre-chilled centrifuge.

Nuclear lysis

Cell medium was aspirated and cells were twice washed with ice-cold 1x PBS before being scraped into 1x PBS containing 10µM MG132 (MERCK; #474790) and pelleted at top speed for 5 minutes. The cell pellet was resuspended in 200µl Cytosolic Lysis Buffer (25mM HEPES, 5mM KCl and 0.5mM $MgCl_2$) containing 10µM MG132 and sheared 10-20 times before being agitated for 10 minutes in an eppendorf shaker. 10µl of 10% Nonidet P-40 (NP-40) was added to each lysate to rupture the nuclear membrane. The lysates were shaken for a further 5 minutes before pelleting at top speed for 3 minutes. The supernatant containing the cytosolic fraction was

transferred to a separate eppendorf. The remaining pellet was then resuspended in 100µl of Nuclear Lysis Buffer (25mM HEPES, 10% [w:v] Sucrose, 350mM NaCl and 0.01% [v/v] NP-40) containing 10µM MG132, sheared 10-20 times and then sonicated for two 10 second bursts at an amplitude of 6 microns. The lysate was then pelleted at top speed for 10 minutes and the supernatant containing the nuclear fraction was transferred to a separate eppendorf.

Bradford Assay

The Bradford Assay is a colorimetric assay that is used to quantify the concentration of a protein in a solution at an absorbance of 595nm when the protein binds to the acidic solution of Coomassie Brilliant Blue (Bradford, 1976). Each cell lysate was diluted 1:100 in ddH_2O and a standard curve was generated by preparing a concentration gradient from 10mg.ml^{-1} BSA, which was used as background concentration for the protein lysates. 20µl of Bradford Reagent (Biorad; #500-0006) was loaded into each well of a 96-well plate and 180µl of each standard and diluted cell lysate was added in duplicate and mixed thoroughly by pipetting. The absorbance at 595nm for each sample was measured using a microplate reader. The absorbance of each BSA standard was plotted linearly and a line of best fit generated a 'y = mx + c' equation, where the absorbance at 595nm is y, x is the protein concentration and c is the y-intercept coordinate generated by the equation. Protein concentration of each lysate was calculated using the following equation:

$$X\ [mg.ml^{-1}] = [(Y-C)/M] \times \text{Dilution Factor}$$

The volume required to analyse 30µg of protein by western blot was calculated and added to 10µl of protein loading dye (32mM Tris-HCl pH 6.8, 12.5% glycerol, 1% SDS, 0.05% bromophenol blue) containing 10% β-2-mercaptoethanol.

Western blotting

Whole cell and nuclear lysates were analysed by SDS Polyacrylamide Gel Electrophoresis (SDS-PAGE) using 10% and 12% resolving gels respectively (373mM Tris-HCl [pH 8.8], 10% or 12% Acrylamide Bis [Biorad; #161-0158], 65.6mM APS, 3.45mM SDS and 0.12% TEMED) and a 3% stacking gel (123mM Tris-HCl [pH 6.6], 4% Acrylamide Bis, 65.6mM APS, 3.45mM SDS and 0.12% TEMED). Nuclear lysates were run on a 12% resolving gel in order to resolve lower molecular weight proteins. Prior to loading, lysates were boiled at 95-100°C prior to loading on the gel. All lysates were run with a Precision Plus Protein Kaleidoscope Standard (Biorad; #161-0375) and a Biotinylated marker (NEB; #7727) as an additional indicator of protein molecular weights. All gels were run in 1x Running Buffer (190mM Glycine, 24.8mM Trizma Base, 173µM SDS) at 150V and were stopped after the blue dye front began to run off the bottom of the resolving gel. Gels were carefully removed and were placed in a module in contact with a nitrocellulose membrane. The transfer module was filled with ice-cold 1x transfer buffer (186mM Glycine, 24.8mM Trizma Base, 20% methanol) and the proteins were transferred onto the membrane for 1-2 hours at 100V. Blots were stained with Ponceau S Solution (#P7170) to identify even transfer and loading of proteins across the membrane. Ponceau was washed with 1x

Tris Buffered Saline with Tween (TBS-T; 20mM Trizma Base, 137mM NaCl, [pH 7.6] and 0.1% Tween 20) before being blocked in blocking solution (2.5% non-fat skimmed milk; Tesco) in TBS-T for 1 hour. Blots were incubated in primary antibody against the protein of interest overnight. The next day blots were washed 4 times in 20ml TBS-T for 5 minutes before being incubated for an hour in blocking solution containing the corresponding secondary and an anti-biotin antibody required for exposure of the biotinylated marker. Blots were washed 4 times in 20ml TBS-T for 5 minutes before being exposed onto film using Luminata Classico HRP substrate (Millipore; #WBLUC0500) for detection by ECL. Exposures for every blot were carried out at time intervals of; Immediate, 10 seconds, 30 seconds, 1 minute and upward in extreme cases. If required, blots were stripped using 20ml of acid stripping buffer (400mM Glycine, 6.94mM SDS, 2% Tween 20, [pH 2.2]) twice for 30 minutes. Blots were then washed 3 times with 20ml 1x PBS for 5 minutes and once with 20ml TBS-T before being blocked for 1 hour and then reprobed with a primary antibody targeting the protein of interest.

Reporter gene assays.

Cells were seeded out at $3x10^5$cells.ml^{-1} per well of a 6 well plate and were allowed to achieve 60-80% confluency. DNA was transfected into the cells using Lipofectamine 2000 according to the manufacturer's instructions. The HIF luciferase reporter vector (pGL2-TK-HRE) used in this study contains four copies of the HRE (5'-GTGACTACGTGCTGCCTAG- 3') derived from hVEGF-A ahead of a Thymidine Kinase (TK) promoter complex, which binds RNA polymerase (Figure 2.1). In tandem, these two domains are responsible for regulating the production of firefly luciferase

(*Phontius pyralis*). On the other hand, the luciferase control reporter vector, pRL (Figure 2.1), lacks the HRE and contains a luciferase gene from a different species (Sea pansy: *Renilla reniformis*). However, it does contain the TK promoter complex required for luciferase activity, thus allowing it to be used as a control for transfection efficiency. Each transfection mixture contained a total of 4µgDNA.well^{-1}, consisting of 0.5µgDNA.well^{-1} pRL and either 1 or 3.5µgDNA.well^{-1} HIF-luc used for transient SPRY2 construct transfections and for stable cell lines respectively. Transfection medium was left on the cells for 4 hours. The medium was replaced with 2% charcoal-stripped medium and cells were placed at either 3% or 21% pO_2 and left for 18 hours. Cells were lysed and 10µl duplicates of each sample were added to a 96-well plate and run on a Fluostar Optima plate reader (BMG Labtech) using the Dual-luciferase® Reporter Assay System (Promega, #E1910), which allows the activities of firefly and *Renilla* luciferase activities to be measured simultaneously. The activity of firefly luciferase is measured first for approximately one minute upon application of Luciferase Assay Reagent II (LAR II). The reaction is then quenched and the *Renilla* luciferase activity is measured after addition of Stop & Glo® Reagent to the same sample. For data analysis, means were taken of each duplicate and the means generated for firefly luciferase activity were divided by those of *Renilla* luciferase activity.

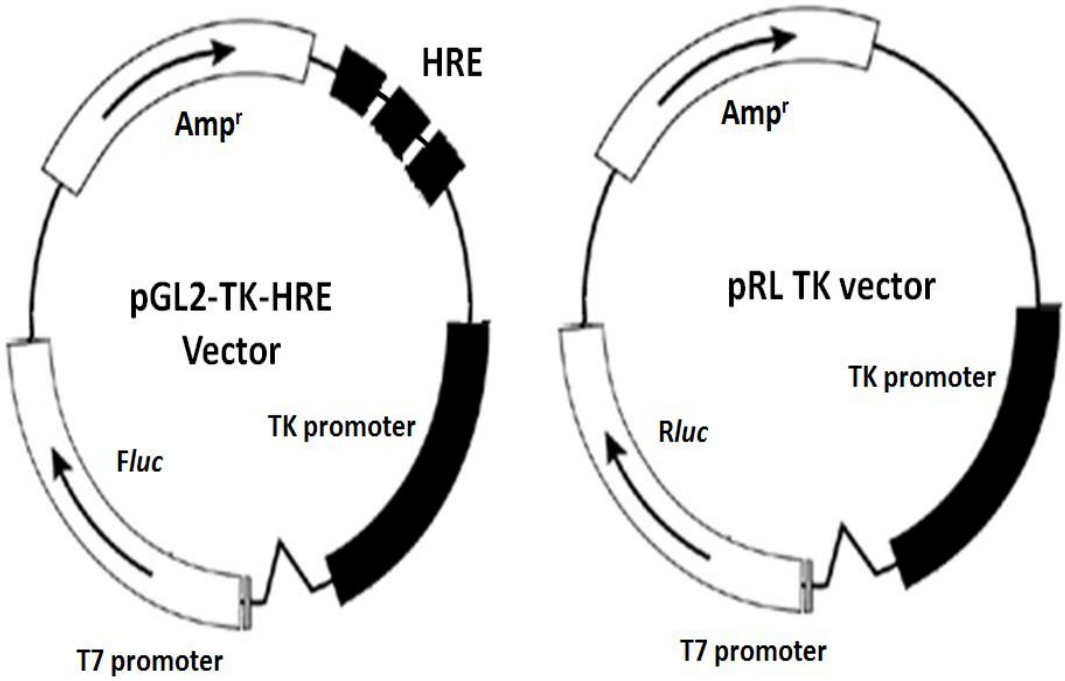

Figure 2.1. Plasmid maps of the HIF-luc and pRL-luc vectors. See text for details. Acronyms: F*luc* (Firefly luciferase), R*luc* (Renilla luciferase), Amp^r (Ampicillin resistant marker domain).

RNA isolation and quantification.

RNA was lysed from cells using a Nucleospin RNA II Kit (Macherey-Nagel; #740955) according to the manufacturer's instructions. 5µl of RNA was diluted in 495µl of nuclease-free H_20 in a cuvette and the light absorption of the diluent was measured at 260nm and 280nm spectrophotometer. The concentration of RNA was calculated using the following equation.

$$\text{Total RNA } (ng.\mu l^{-1}) = A260 \times \text{dilution factor} \times 40^*$$

*A260 = 1, corresponds to 40 $ng.\mu l^{-1}$ of single stranded DNA or RNA.

RNA was routinely checked for DNA and/or protein contamination by measuring the ratio of A260 to A280. A ratio of ≥1.9 was indicative of pure RNA and was deemed viable for use in subsequent analyses.

cDNA synthesis and quantitative real-time polymerase chain reaction (qPCR).

1µg of RNA was reverse-transcribed into complimentary DNA (cDNA) using a Quantitect Reverse Transcriptase Kit (Qiagen; #205311) according to the manufacturer's instructions. For the qPCR reactions qPCR was performed on Rotor-Gene Q cycler using a Rotor-Gene SYBR Green PCR Kit (Qiagen; #204074). All cDNA samples were diluted 50-fold for use in the qPCR assay. A standard curve was generated form serial dilutions of a designated sample defined as the calibrator, to which each sample's relative gene expression is measured against. This sample is generally an untreated control. The concentrations of the standard curve consisted of 30ng.µl^{-1}, 15ng.µl^{-1}, 7.5ng.µl^{-1}, 3.75ng.µl^{-1} and 1.875ng.µl^{-1}. Quantitect Primer Assays were purchased from Qiagen for use in the qPCR assay and were diluted from 10x stock to 1x aliquots. A list of these primers is provided in Table 2.4.

Gene	Primer Assay Catalogue #
Hs_B2M	QT00088935
Rn_B2M	QT00176295
Hs_BNIP3	QT00024178
Hs_CCND1	QT00495285
Hs_SPRY2	QT00005495
Hs_VEGF-A	QT01682072
Rn_VEGF-A	QT00198954

Table 2.3. List of Quantitect Primer Assays used in the qPCR analysis. Hs and Rn denote primers against Human and Rat species respectively.

A master mix consisting of 12.5µl of 2x Rotor-Gene SYBR Green RT-PCR Master Mix (1x) and 2.5µl of Primer was prepared per sample. 15µl of this mixture was dispensed into Rotor-Gene PCR tubes and 10µl of standard curve samples and cDNA dilutions was added per tube to create a final reaction volume of 25µl. PCR reaction conditions were as follows: 95°C for 10 minutes, 95°C for 7 seconds, 60°C for 14 seconds, followed by an a temperature ramp from 57-95°C where the temperature increased by 1°C every 5 seconds. All samples were run in duplicate. The 'housekeeping' or normalising gene used for each assay was Beta-2 Microglobulin (B2M), which served as an endogenous reference gene as its expression tends to not vary between treatments. The relative expression of the gene of interest (GOI) in relation to the 'housekeeping' gene was calculated using the 'delta delta C_t' (ΔΔCt) method, which is derived from the following series of equations (Pfaffl, 2001):

$$R = 2^{[Ct\ sample - Ct\ control]}$$

$$R = 2^{\Delta Ct}$$

$$R = 2^{-[\Delta Ct\ sample - \Delta Ct\ control]}$$

$$R = 2^{-\Delta\Delta Ct}$$

Where R is the relative expression ratio of the GOI and Ct (Cycle threshold) is the cycle number at which point the cDNA is exponentially amplified. ΔCt is given as the difference between the GOI and the housekeeper gene and ΔΔCt is the difference between the ΔCt of the control sample and the ΔCt of the GOI.

The fidelity of each run was assessed by the efficiency (e) of the corresponding PCR assay, which was calculated according to the equation $E = 10^{[-1/slope]}$ (Rasmussen, 2001), where efficiency values close to '1' corresponded to 'perfect efficiency'. The fidelity of each assay was also assessed by the correlation coefficient (R^2) obtained from the standard curve serial dilutions. This was used to evaluate the linearity of each test sample by measuring it against the regression line generated by the standard curve and in doing so, provides an indication of the variability between each sample. A value of >0.98 was considered desirable for each qPCR reaction.

Immunohistochemistry

FDLE were treated with 0.02 and 0.1μg.ml^{-1} FGF-10 along with an untreated control and were left for 2 hours in hypoxia. Cells were fixed with 4% paraformaldehyde (in 1x PBS) for 20 minutes at room temperature and were then washed 3 times with ice-cold 1x PBS. Cells were blocked for 1 hour in blocking buffer (5% FBS and 0.3% Triton X-100 in 1x PBS) were then incubated overnight in antibody dilution buffer (1% BSA,

0.3% Triton X-100 in 1x PBS) containing primary antibody against SPRY2 at a 1:1000 dilution. To control for non-specific fluorescent staining, identically treated FDLE were incubated overnight in blocking buffer containing non-immunospecific FBS immunoglobulins. Cells were treated with the secondary antibody at a 1:2000 dilution for 1 hour in the dark at room temperature. Cells were viewed on under oil immersion at x 40 objective on a Zeiss Axiovert confocal fluorescent microscope and images were obtained using Improvision 5 software.

Co-immunoprecipitation (Co-IP)

Cells were plated at a density of 5 x 10^6 cells.ml^{-1} in 10cm sterile petri dishes and were placed overnight at 3% pO_2 upon full confluency. Cells were lysed in 500µl of TETN-250 Buffer (25mM Tris-HCl [pH 7.5], 5 mM EDTA, 250 mM NaCl and 1% Triton X-100) and were sheared 10-20 times ensure complete lysis. The lysates were then centrifuged at top speed and protein content was quantified by Bradford assay. 40µg of cell lysate was placed in a fresh eppendorf to be used as a total cell lysate representative (TCL). 500µg of the remaining lysate was diluted up to a total volume of 300µl with TETN 250 buffer and 50µl of pre-cleared Protein-A-Sepharose beads (P3391-1G) were added to each lysate and were incubated at 4°C for 1 hour with rotation. The bead/lysate mixture was then pelleted by centrifugation and the supernatant was transferred to a fresh tube. 1µg of SPRY2 primary antibody was added to each lysate, which were subsequently incubated at 4°C for overnight with rotation.

The next days, 50µl of pre-cleared Protein-A-Sepharose beads were added to each sample and were incubated for a further 3 hours at 4°C with rotation. The

bead/lysate fraction was then spun down by centrifugation and the supernatant was discarded. Each bead pellet was washed for 5 minutes; twice with 1ml of TETN-250 buffer and twice with 1ml TE Buffer at 4°C with rotation. After the final wash, the beads were resuspended in 50µl of protein loading dye, which was subsequently boiled at 95°C for 5 minutes prior to loading on SDS-PAGE gels.

Chromatin immunoprecipitation assay (ChIP)

Tables 2.5 and 2.6 provide a list of the primers used for ChIP DNA analysis of the rat and human VEGF-A promoter respectively. Fragments listed are upstream of the transcriptional start site.

Rat VEGF-A promoter fragment	Forward Sequence (5' to 3')	Reverse Sequence (5' to 3')	Base pair size
-944 to -633bp	TCTGCCAGACTCCACAGTG (19bp)	GCAGGCTTTGACTTCCCAAATAG (23bp)	311
-661 to -384bp	GTTTCCGAGGTCAAACAAGC (20bp)	CACACTATACCCAGACACAC (20bp)	277
-403 to -124bp	GTGTGTCTGGGTATAGTGTG (20bp)	GCCACTACTGCGAAATAGAAA (21bp)	279

Table 2.4. A list of primers used to analyse regions of the rat VEGF-A promoter.

Human VEGF-A promoter fragment	Forward Sequence (5' to 3')	Reverse Sequence (5' to 3')	Base pair size
-1079 to -882bp	CCTCAGTTCCCTGGCAACATCTG	GGCACCAAGTTTGTGGAGCTGAG	197

Table 2.5. Primers used to analyse regions of the human VEGF-A promoter.

The ChIP assay method in this study largely adopts the protocol provided by Millipore with modifications. Cells were washed twice in ice-cold 1x PBS and then were cross-linked by adding 500µl of 1x formaldehyde for 10 minutes. The

formaldehyde was washed off twice with ice-cold 1x PBS and the cells were then scraped into 1x PBS containing a protease inhibitor tablet. Cells were pelleted at top speed for 5 minutes and the supernatant wad discarded. Pellets were resuspended in 200µl SDS Lysis buffer (50mM Tris-HCl pH 8.1, 10mM EDTA and 1% SDS, one protease inhibitor tablet was added per 15ml), and were left on ice for 10 minutes to allow the cells to swell. Each lysate was sonicated ten times at amplitude of 10 microns with 15 second bursts and 45 second rest periods to prevent overheating and DNA denaturation. This sonication protocol had been verified beforehand for use in this study. The lysates were then pelleted at top speed for 10 minutes and the supernatant was placed in a fresh, sterile 2ml eppendorf.

Lysates were the diluted 10-fold in ChIP Dilution Buffer (16.7mM Tris-HCl pH 8.1, 167mM NaCl, 1.2mM EDTA, 0.01% SDS and 1.1% Triton X-100). 20µl of the diluted cell supernatant from one of the lysates was kept to run as a control (input) in the subsequent PCR assay. Lysates were then pre-cleared with 75µl of Salmon Sperm DNA/Protein A Agarose-50% Slurry (Millipore; #16-157C) for 30 minutes at 4°C with rotation to remove non-specific background. Agarose was gently pelleted at 1000rpm for 1 minute and the supernatant was collected and divided into 500µl fractions in fresh sterile 1.5ml eppendorfs. 1-2µg of immunoprecipitating antibody was added to the designated fraction and was incubated overnight at 4°C with rotation. For a negative and positive control, 1µg of non-immune murine IgG and H3 antibody were used respectively.

The following morning, 60µl of Salmon Sperm DNA/Protein A Agarose Slurry was added to each fraction and the fractions were incubated for 1 hour at 4°C with rotation to collect the antibody/histone complex. Agarose was pelleted gently at 1000rpm for 1 minute and the supernatant was carefully removed by aspiration. The protein A Agarose/antibody/histone complex was then washed for 5 minutes at 4°C with rotation in 1ml of the following buffers in the order listed; one wash in Low Salt Immune Complex Wash Buffer (20mM Tris-HCl [pH 8.1], 150mM NaCl, 2mM EDTA, 0.1% SDS and 1% Triton X-100), one wash in High Salt Immune Complex Wash Buffer (20mM Tris-HCl [pH 8.1], 500mM NaCl, 2mM EDTA, 0.1% SDS and 1% Triton X-100), one wash in LiCl Immune Complex Wash Buffer (10mM Tris-HCl [pH 8.1], 1mM EDTA, 0.25M LiCl, 1% IGEPAL-CA630 and 1% deoxycholic acid) and finally, two washes in TE buffer (10mM Tris-HCl and 1mM EDTA, pH 8.0). 250µl of ChIP Elution Buffer (0.1M $NaHCO_3$ and 1% SDS) was added to the pelleted protein A Agarose/antibody/histone complex, vortexed briefly and then incubated at room temperature with rotation in order to elute the histone complex from the antibody. The agarose was spun down at top speed for 1 minute and the supernatant was collected in a fresh 1.5ml eppendorf. This step was repeated a further time to produce a final combined eluate volume of ~500µl. 20µl of 5M NaCl was added to each of the combined eluates. 1µl of 5M NaCl was added to the 'input' sample too. All samples were incubated at 65°C overnight to reverse the histone-DNA crosslinks.

The following morning, 10µl 0.5M EDTA, 20µl Tris-HCl (pH 6.5) and 2µl of 10mg.ml^{-1} Proteinase K was added to each eluate and the samples were incubated for one hour at 55°C. Samples were then boiled at 95-100°C for 10 minutes to denature the

Proteinase K. DNA was extracted from each eluate using a Nucleospin Gel and PCR clean-up kit (Macherey-Nagel; #740609) according to the manufacturer's instrcutions. Binding Buffer NTB (Macherey-Nagel; #740595), which is specifically designed to bind SDS-containing lysates to the columns, was used to prevent precipitation of SDS in the extraction procedure. DNA was eluted in a final volume of 50µl of 5mM Tris-HCl (pH 8.5).

PCR analysis was performed on a Rotor-Gene Q cycler. 5µl of template ChIP DNA was run in a 25µl reaction mixture containing 15µl of 2x Rotor-Gene SYBR Green PCR Master Mix and 5µl of 10µM primer. Reaction conditions were identical to the qPCR conditions described earlier in this chapter except for the annealing temperature of the rat primers (58°C). PCR reactions were run on a 1% agarose gel with a 100bp DNA ladder and gels were viewed under a UV transilluminator.

Statistical analysis

All values are expressed as means ± standard error (SEM) unless otherwise stated in the figure legend. 'n' is the term used to describe the number of independent experiments were the number is defined by the number of repeats. A student's t-test was used to analyse paired single treatments. For multiple comparisons, normally-distributed data were analysed by one-way analysis of variance (ANOVA) with a Bonferroni's *post-hoc* test to allow for comparisons between individual treatments. A P value of < 0.05 was the threshold value for statistical significance.

Chapter 3 - Characterisation of SPRY2 and its epigenetic role in fetal lung epithelium.

Introduction

FGF10 as an inducer of airway and vascular signalling.

FGF10 is widely regarded as an inducer of airway branching morphogenesis, whose signalling is antagonised by SPRY2 expression. Scott *et al*., (2010) also established that in FDLE, FGF10 amplified HIF-1α activity through the induction of mTORC1 expression and this signalling cascade was mediated by SPRY2 expression. This augmented VEGF-A gene expression and acted as an effective link between airway and vascular growth. This was supported by studies in fetal lung explants from mice bearing the lacZ gene under the control of the angiopoietin promoter, Tie2 (Tie2-lacZ), that showed discrete induction of vascular genes occurred around regions of the explants that had been implanted with FGF10 soaked beads (Figure 3.1).

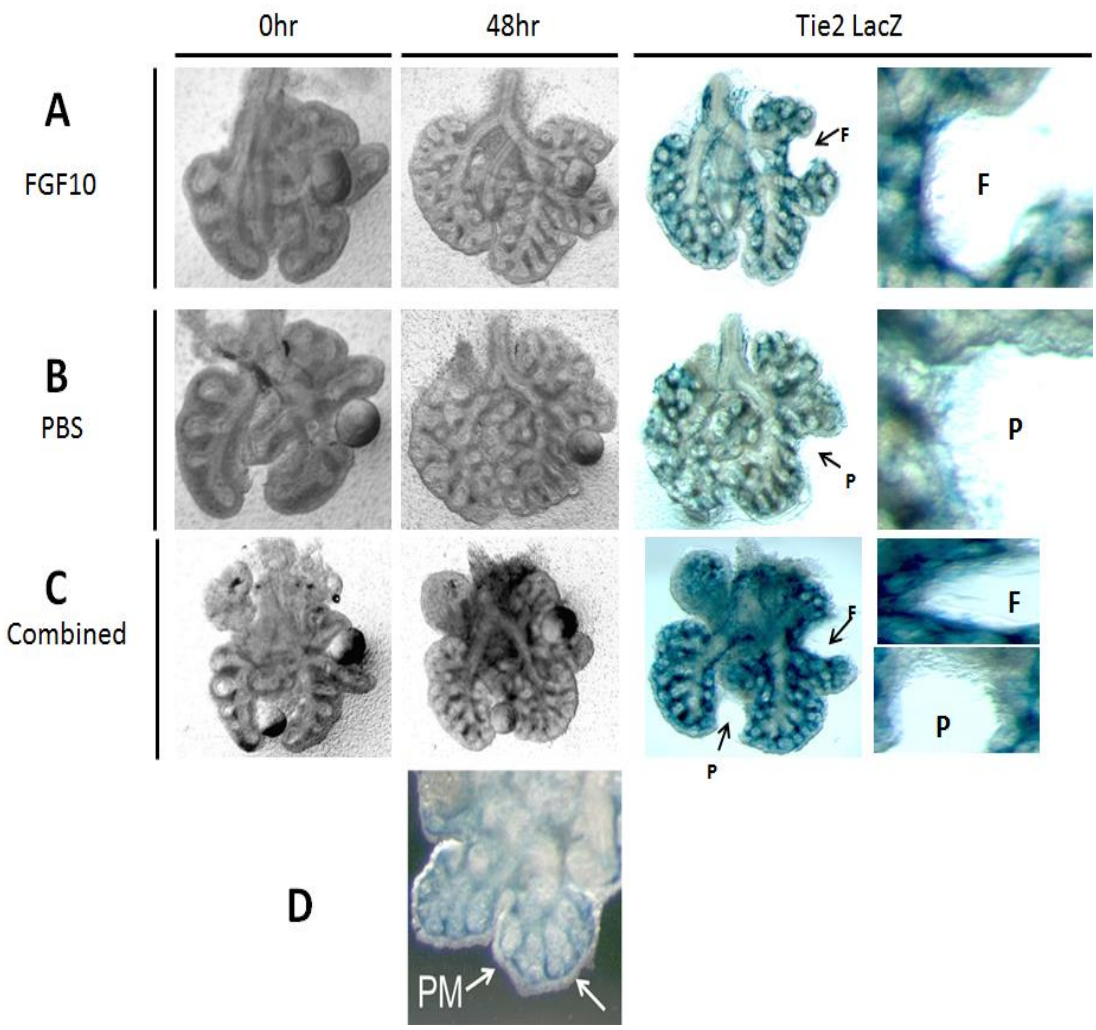

Figure 3.1. E12 fetal lung explants from Tie2-lacZ mice ±FGF10 stimulation stained for lacZ reporter expression. The degree of Tie2-lacZ expression is indicated by regions of blue staining on the explants. The greyscale images on the left show bead localisation and morphogenesis over the course of the 48 hours. The diagrams shown on the right are those same explants after subsequent lacZ staining and removal of beads. The higher magnification images show detail of intense staining upon FGF10/PBS stimulation. The positions of the beads in these explants are given as F (FGF10) and P (PBS). The peripheral mesenchyme (PM) is highlighted (D) in order to differentiate it from the epithelium. Note the lack of blue staining and thus Tie2-lacZ gene expression in the Peripheral Mesenchyme (PM) which demonstrates that vasculogenesis is strictly confined to the epithelium in these explants. Data originally published in Scott *et al*., (2010).

VEGF-A expression as a measure of vascular growth.

Little is known about the biology of VEGF-A in fetal lung epithelium. There is a wealth of evidence to suggest that the expression of HIF isoforms and oxygen concentration are key regulators of VEGF-A expression (Acarregui *et al*., 1999, Rajatapiti *et al*., 2010). As discussed in chapter 1, HIF-1α is expressed throughout fetal development and its genetic knockout causes severe vascular defects (Kotch *et al*., 1999). On the other hand, knockout of HIF-2α does not effect vascular development until late alveologenesis (Compernolle *et al*., 2002). Taking this into account, and the fact that little is known of the function of HIF-3α, HIF-1α is considered the major regulator that drives early vascular development and as such VEGF-A can be used as an assay for quantifying HIF-1α activity. The major finding of Scott *et al*., (2010) showed that the expression of VEGF-A, which is driven by HIF-1α induction in the fetal lung, may be linked to the FGF10 airway outgrowth signal by SPRY2. This suggests that SPRY2 is of central importance to the process of vascular growth in the lung and may act as a functional link between FGF10 and VEGF-A expression. This chapter aims to establish the basis for this interaction by deteremining if SPRY2 is directly involved in the genetic regulation of VEGF.

Fetal distal lung epithelium as a cellular model of the fetal lung.

Rat FDLE were used in this study to represent the fetal lung *ex vivo*/*in vitro*. Their phase of development is within the late pseudoglandular/early saccular stage of lung development, where epithelial proliferation is at its maximal level. Several studies have used the FDLE model to study epithelial cell biology. A publication by Jassal *et*

al., (1991) revealed that FDLE grow and divide readily in culture. Prior to their experiments, FDLE cultures were supplemented with low-serum which this study has also replicated, due to the complications in quantifying growth factor signalling attributed to normal serum exposure. Jassal *et al*., (1991) also stated that FDLE growth conditions favoured 3% oxygen, akin to fetal pO_2, which is once again replicated in this study. Subsequent studies have examined FDLE cells in the context of epithelial ion transport. This phenomenom has been observed in primary cultures of FDLE (Matalon & O'Brodovich, 1999) and a further study by Land and Collett (2001), demonstrated the presence of a chloride ion (Cl^-) gradient in FDLE. During development, chloride ion Cl^- secretion across the lung epithelium osmotically drives liquid into the lumen (Olver & Strang, 1974), which provides the distending pressure required for normal development of the lung. At the time of birth, this fluid must be reabsorbed and this process is driven by Na^+ transport through the epithelial Na^+ channel (ENaC) (Baines *et al*., 2001). These findings are significant as they provide strong evidence for the FDLE cell model as a phenotype representative of the fetal lung. While the majority of research based on the FDLE cell model has focused on epithelial ion transport, a recent publication examined the significance of airway branching morphogenesis using the FDLE model (Scott *et al*., 2010). However, there have been no studies investigating vascular signalling of the epithelium in the fetal lung using the FDLE model. This chapter aims to identify vascular events which may be regulated by interaction between FGF10 and the repressor of airway growth, SPRY2.

Results

Sprouty2 exists in the nucleus of FDLE and HBE cells.

Initial characterisation of SPRY2 expression in FDLE was observed in Figure 3.2, which shows the epithelial distribution of SPRY2 ±FGF10 stimulation. SPRY2 is shown to be expressed in the cell membrane and endosomal compartments but is also strongly observed in the nuclei of these cells.

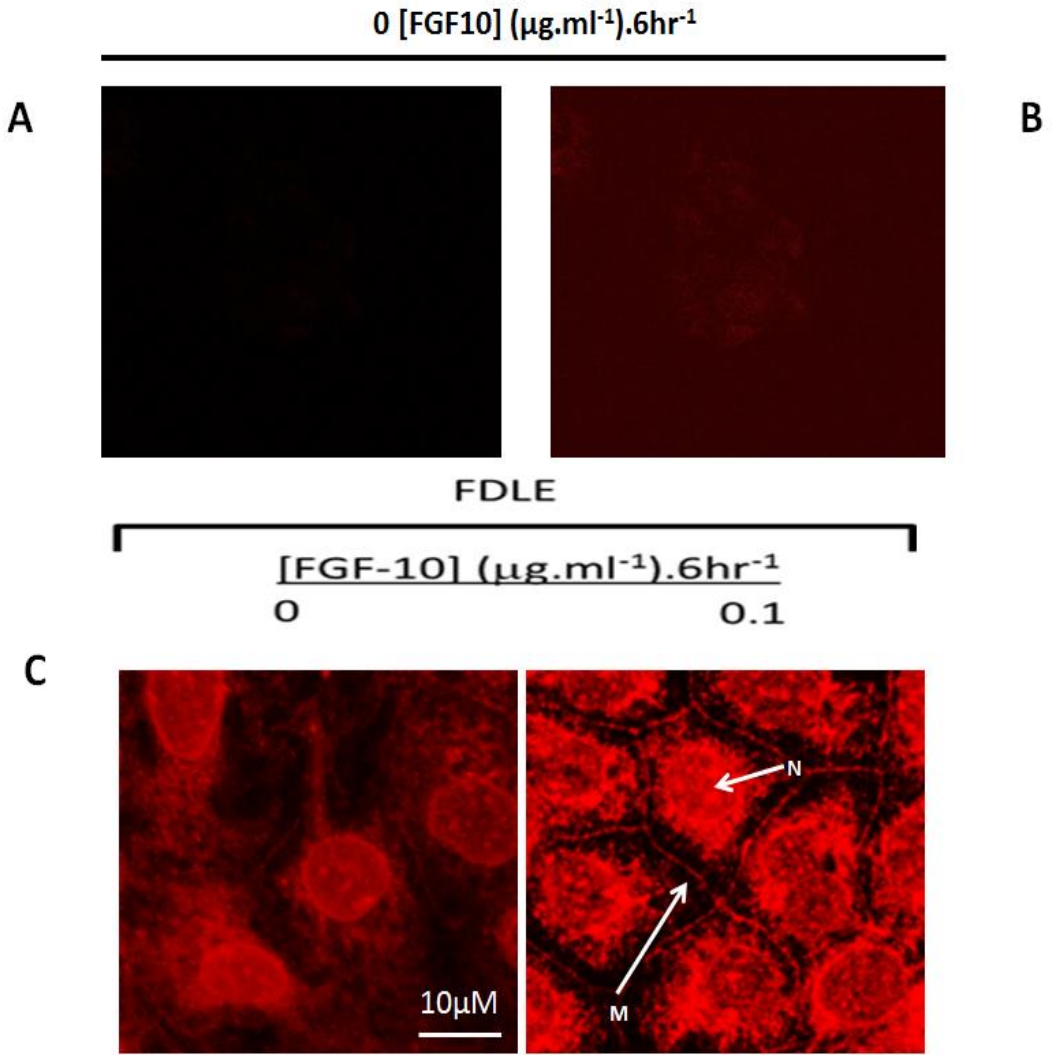

Figure 3.2. Immunofluorescent staining of SPRY2 in FDLE cells. Images of cells in top panel showing background fluorescence (A) and high brightness contrast setting (B) respectively, were probed with non-immunospecific FBS immunoglobulins. C. SPRY2 staining at the cell membrane (M) and the nucleus (N). Confocal images taken at x800 magnification stained with the amino-terminal antibody to SPRY2. Images in bottom panel (C) were taken with the same settings as image A. Images shown are representative of 3 independent experiments.

Further confirmation of the nuclear localisation of SPRY2 is displayed in Figure 3.3, which displays endogenous Spry2 protein abundance in both FDLE and HBE. SPRY2 protein was resolved as a double band with molecular weights of approximately 35.4+/-0.5kDa and 39.3+/-0.6kDa (n = 18), using the same aminoterminal antibody used in the immunofluorescene experiments (Figure 3.3A). Densitometric analysis showed that nuclear SPRY2 (nSPRY2) abundance in FDLE was approximately double the abundance levels observed in the HBE cell line (Figure 3.3B). H3 protein expression (17kDa) was run as a loading control and as an independent confirmation of nuclear fractionation of the lysates blotted.

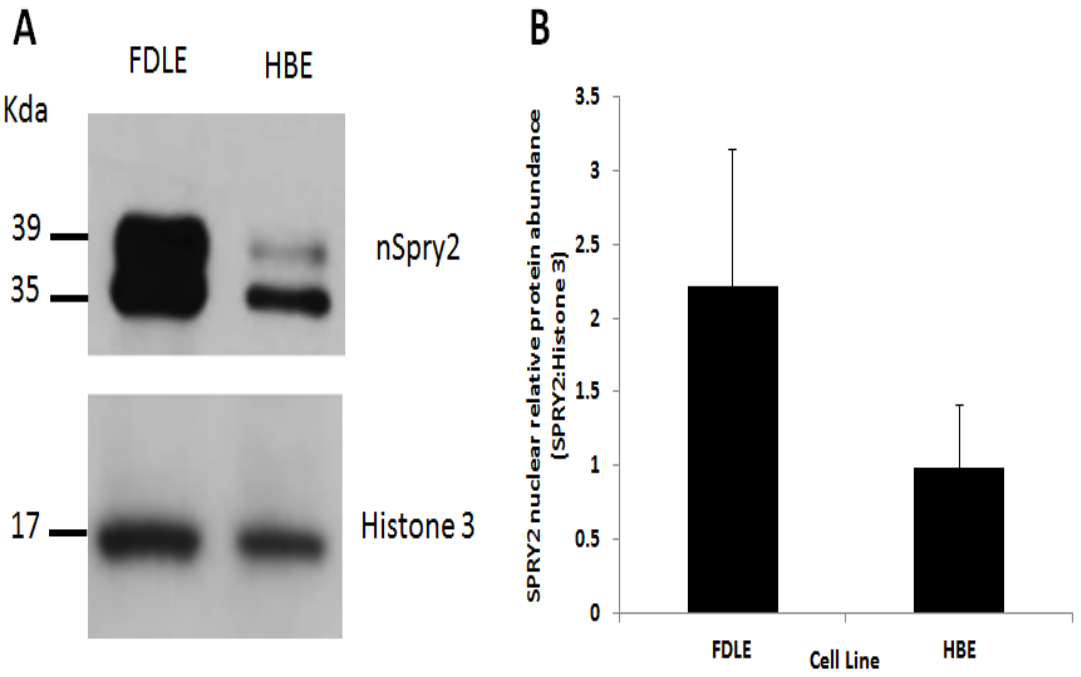

Figure 3.3. Endogenous nuclear protein expression of SPRY2 in FDLE and HBE cell lines. Cells were maintained at fetal pO_2 prior to nuclear lysis and western blot analysis. Blots are representative of 4 independent experiments where error bars are $\bar{x} \pm$ SEM (n = 4).

FGF10 induces clearance of the higher molecular weight form of nSPRY2 at both fetal and normoxic pO_2.

Western blot analysis was carried out to determine the effect of FGF10 stimulation on SPRY2 protein expression. Figure 3.4 shows the effect of increasing concentrations of FGF10 on cytosolic and nuclear SPRY2 protein abundance observed in FDLE. FGF10 induced a concentration dependent decline in the 39kDa form of SPRY2 in both fractions, with no apparent change in 35kDa abundance. This observation was also independent of pO_2. ß-Actin and H3 were blotted as loading controls for the cytosolic and nuclear fractions respectively.

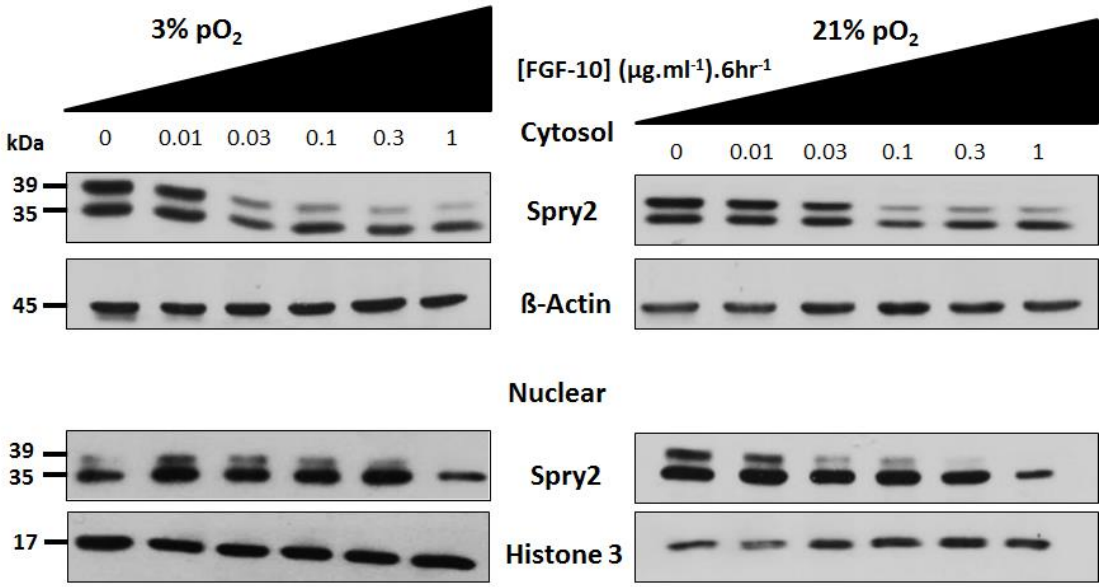

Figure 3.4. Effect of increasing FGF10 stimulation upon SPRY2 protein abundance. Cells were maintained and FGF10 treated at both fetal and normoxic pO_2 prior to subsequent lysis and analysis by western blot. Blots are representative of a minimum of 5 independent experiments.

Densitometric analysis of the effect of FGF10 on the ratio of nSPRY2 39:35 kDa protein abundance is shown in Figure 3.5. The FGF10-induced loss of the 39kDa form of nSPRY2 was shown to be of very high statistical significance.

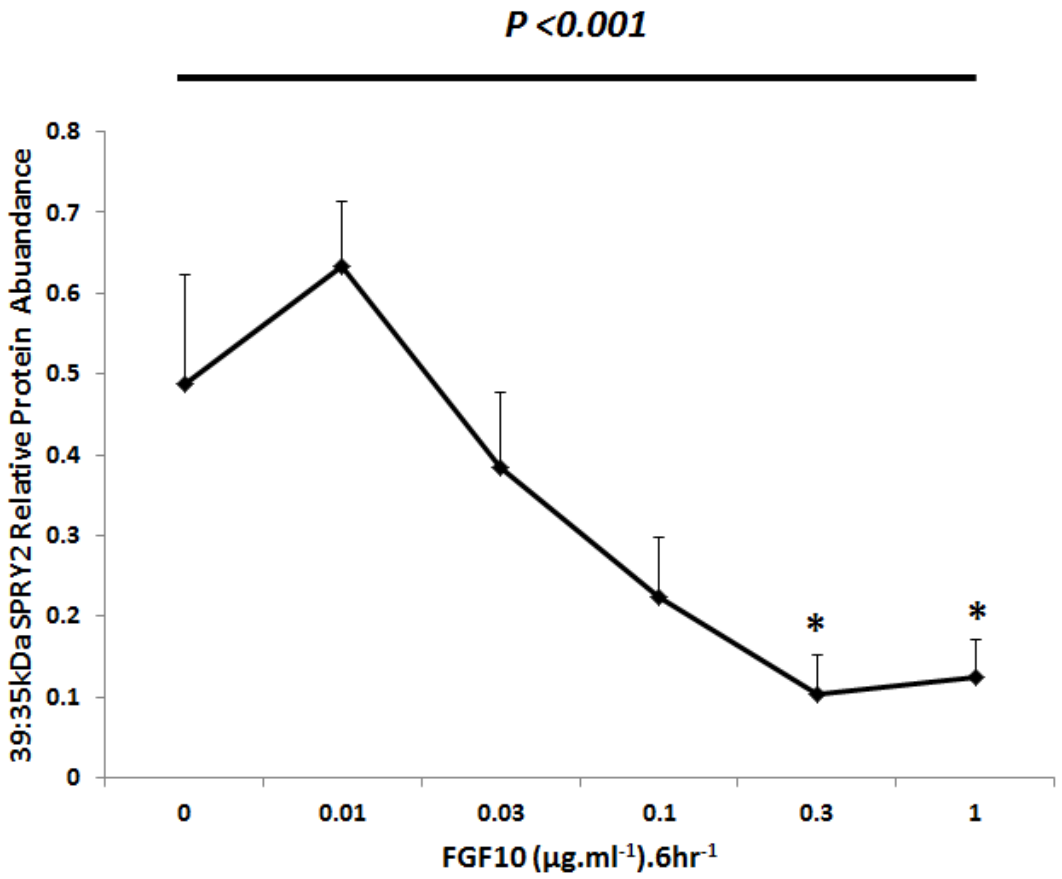

Figure 3.5. Ratio of nSPRY2 protein abundance in response to increasing FGF10 concentration. Asterisks denote statistical significance ($P < 0.05$; ANOVA, Bonferroni *post-hoc* test) when compared with the untreated control (0µg.ml^{-1} FGF10). Error bars are $\bar{x} \pm$ SEM (n = 4).

FGF10 evoked clearance of nSPRY2^{39kDa} correlates with H3 phospho-acetylation.

Figures 3.2 and 3.3 established the nuclear localisation of SPRY2, with the latter figure demonstrating co-expression with H3. Therefore, further investigations into the role of SPRY2 as a potential regulator of gene expression were undertaken. For the purposes of this study, the serine 10 (S10) and lysine 14 (K14) residues of H3 were selected as these residues are known to respond to growth factor stimulation (Mahadevan *et al*., 1991) and are both involved in permitting transcription and cell division (Prignet & Dimitrov, 2003; Nowak & Corces, 2004). HDAC1 and HDAC2 activity was also examined as their functions are linked to transcription (Miller *et al*., 2010) and should also serve as a reverse measurement of S10 phosphorylation and K14 acetylation. Figure 3.6 shows the effect of increasing FGF10 concentration on H3 phospho-acetylation and HDAC activity represented by both HDAC1 and 2 expression. Increasing FGF10 concentration induced an increase in phosphorylation and acetylation of the Serine 10 and Lysine 14 residues of Histone H3 respectively. This also correlated with a decline in HDAC1 and HDAC2 protein abundance upon increasing FGF10 titration, coupled with the complete loss of nSPRY2^{39kDa}.

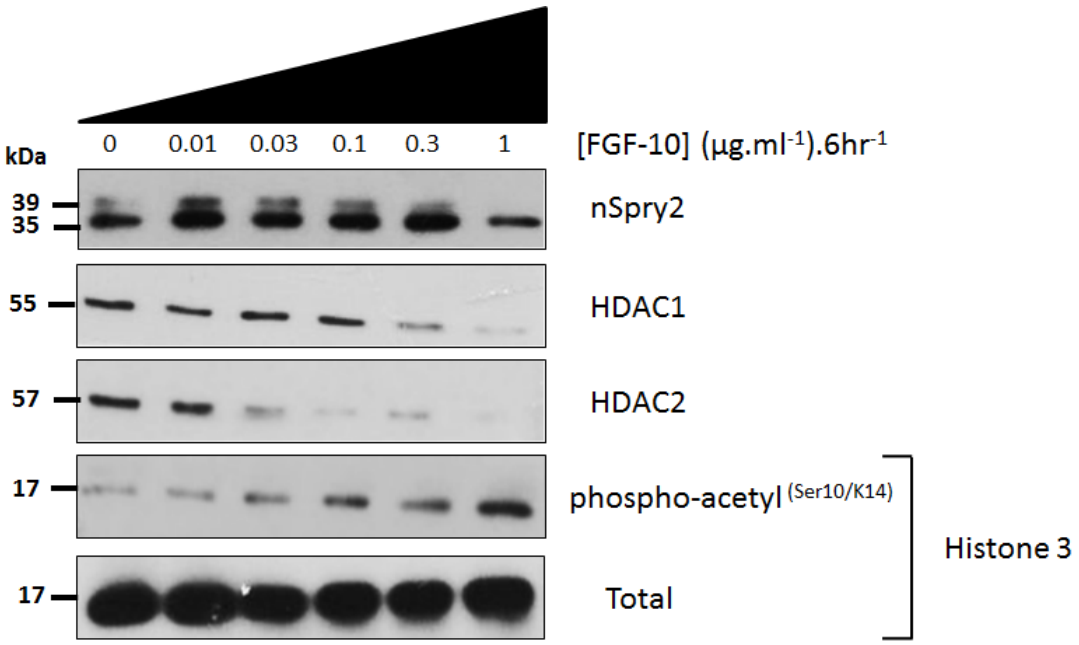

Figure 3.6. Effect of FGF10 concentration on H3 phosphorylation and acetylation in FDLE cells. Cells were treated as described in Figure 3.4. Blots are representative of 4 independent experiments.

Figure 3.7 shows densitometric analysis illustrating the increase in H3 phospho-acetylation with increasing FGF10 concentration (Figure 3.7A) and the negative association between H3 phospho-acetylation and with nSPRY2$^{39kDa:35kDa}$ abundance (Figure 3.7B). There is an increased trend in H3 phospho-acetylation with increasing FGF10 stimulation. Although this association is not statistically significant (P = 0.101; ANOVA) across treatments, there is statistical significance observed between the highest FGF10 dosage and the untreated control (Figure 3.7A). The loss of nSPRY2^{39kDa} is associated with an increase in FGF10 concentration and H3 phospho-acetylation (Figure 3.7B).

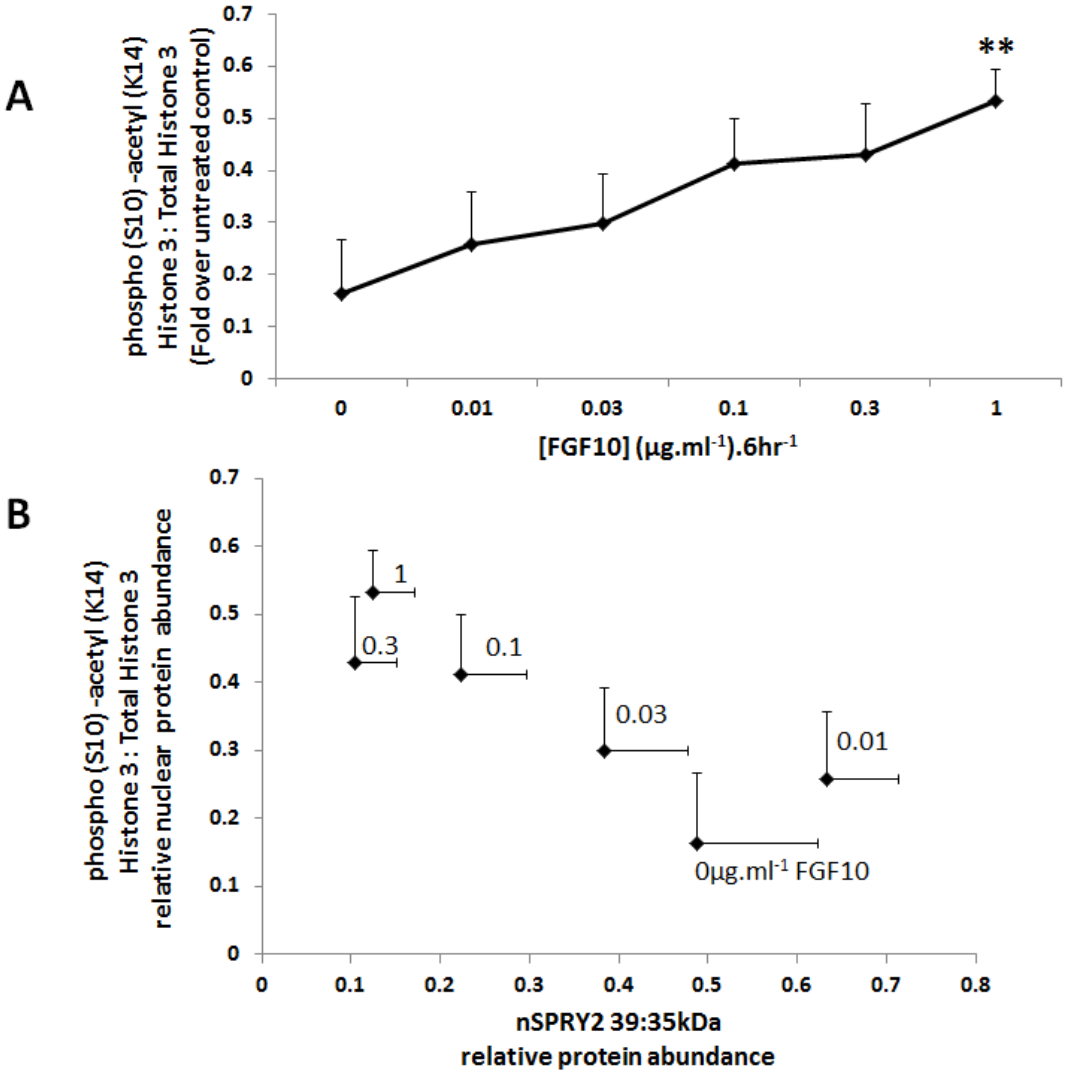

Figure 3.7. Densitometric analysis of the relationship between Histone H3 phospho-acetylation and nSPRY2$^{39:35kDa}$ upon increasing FGF10 concentration. A. Asterisks denote statistical significance ($P < 0.01$; student's t-test) relative to the untreated control (0µg.ml^{-1} FGF10). B. Association between H3 phospho-acetylation: total H3 and nSPRY2$^{39:35kDa}$ protein abundance. Values above each plot represent the FGF10 concentration (µg.ml^{-1}). Measurements are $\bar{x}$ ±SEM (n = 4).

FGF10 induces a trend towards increased SPRY2 and VEGF-A gene expression.

Having established the response of nSPRY2 to FGF10, qPCR assays were performed to assess the effect of FGF10 concentration on gene expression levels of SPRY2 and the major regulated gene product of HIF-1α , VEGF-A. Figure 3.8 shows the outcome of increasing FGF10 concentration upon SPRY2 and VEGF-A gene expression in FDLE. Both SPRY2 and VEGF-A mRNA tended to increase with mid-range concentrations of FGF10 but failed to reach statistical significance.

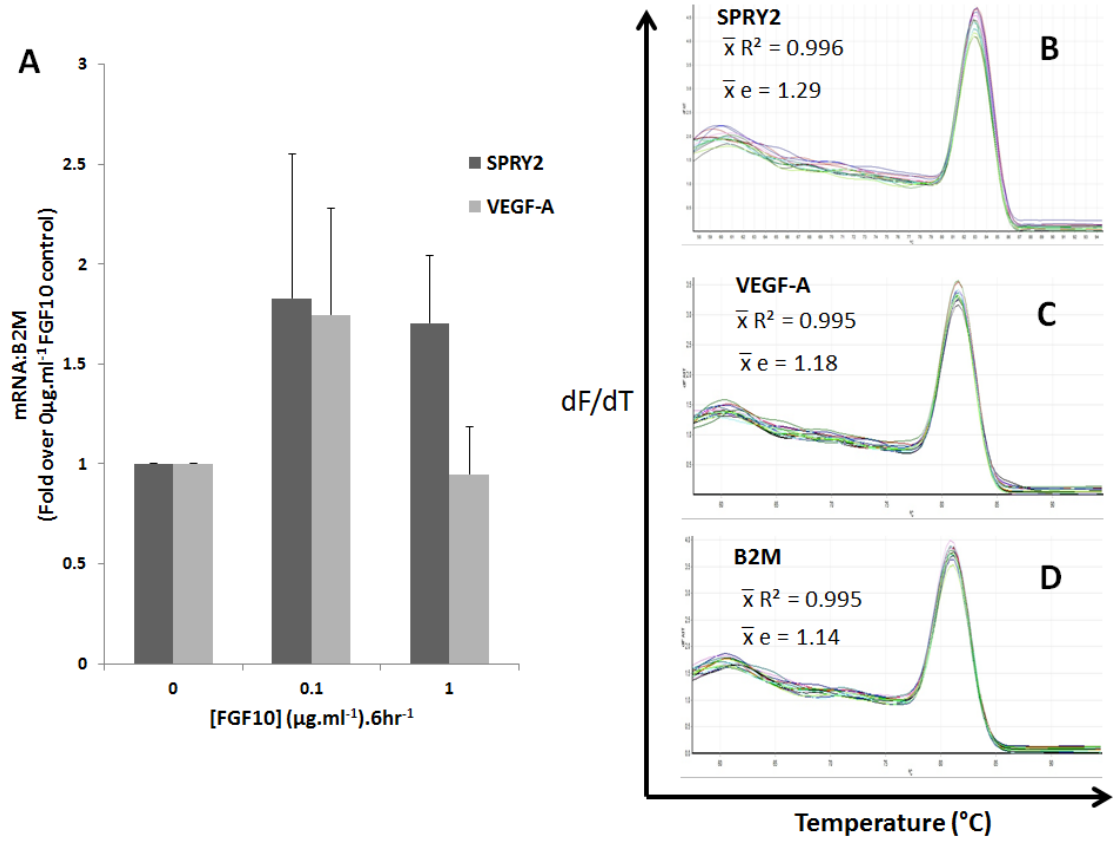

Figure 3.8. FDLE gene expression levels of SPRY2 and VEGF-A in response to increasing FGF10 concentration. FDLE cells were seeded out at 2.5mg.ml^{-1} per well of a 6 well plate and were used for RNA. A. Values generated were measured over B2M expression levels and represent fold change over the 0µg.ml^{-1} FGF10 response. Error bars are ±SEM of fold change (n = 4). Melt curve representatives for the SPRY2 (B), VEGF-A (C) and B2M (D) gene are provided where dF/dT is the measure of the rate of change of fluorescence. Each line of the melt curve represents cDNA template of each sample and also the standard curve generated for the qPCR assay. Melt curves each provide a single peak indicating amplification of the desired gene. Average efficiency and R^2 values for each gene analysed are provided with the corresponding melt curve (n = 4).

SPRY2 and CBP/p300 bind to distal regions of the VEGF-A promoter that contain GC-Rich domains.

Figures 3.6 and 3.7 established a correlation between the loss of nSPRY2^{39kDa} and an increase in phosphorylation and acetylation of H3. Following on from this observation, ChIP assays were performed to assess potential role for SPRY2 in facilitating gene expression. To link this to the hypothesised role of SPRY2 in regulating vascular growth, regions of the VEGF-A promoter were assessed for the affinity of SPRY2, HIF1-α and its co-activator CBP/p300 to bind to these regions. A schematic of the rat VEGF-A promoter is shown in Figure 3.9 listing the key binding domains that were selected for analysis. A list of the primers that flank these regions and their corresponding molecular weights are provided in Table 2.1.

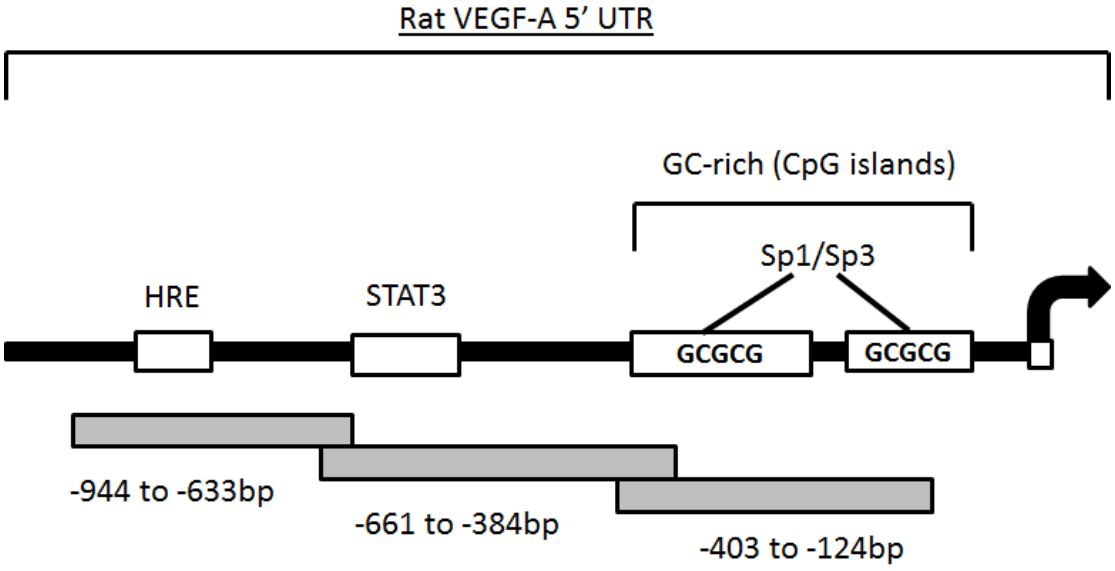

Figure 3.9. Schematic of the rat VEGF-A promoter displaying the key regulatory domains assessed for binding affinity in the ChIP assays. Amplified regions upstream of the transcriptional start site (arrow) are shown in grey.

The regions of the VEGF-A promoter that were selected included HRE, a Signal Transducer and Activator of Transcription 3 (STAT3) binding domain and a heavily GC-rich domain further downstream on the promoter. As stated earlier, HIF-1α and CBP/p300 form a complex within the nucleus that facilitates gene expression during fetal lung development. Therefore, this experiment looked to determine if nSPRY2 was capable of interacting with the VEGF-A promoter and if this altered HIF-1α and CBP/p300 binding. The affinity for SPRY2 (A), HIF-1α (B) and CBP/p300 (C) to bind to regions of the VEGF-A promoter in response to increasing FGF10 concentration is shown in Figure 3.10. SPRY2 predominantly bound to regions of the VEGF-A promoter which contain GC-rich elements (Figure 3.10A). The affinity for SPRY2 to bind at these regions appeared to be independent of FGF-10. A weak interaction was also observed with the region of the promoter containing the HRE. HIF-1α surprisingly showed very weak binding affinity to the HRE on the promoter but this could be FGF10 regulated as a band was observed in the 0.1μg.ml^{-1} lane (Figure 3.10B). HIF-1α appeared to bind more strongly downstream of the HRE in a region known to contain a functional STAT3 binding site. The histone acetyltransferase and the HIF transcriptional co-activator, CBP/p300, was also found to bind strongly to this same region with increasing FGF10 concentration. (Figure 3.10C) No observation was made of CBP/p300 binding to the HIF consensus site (data not shown). Histone H3 ChIP samples were run with all test samples and primer sets as a positive control for the assay to demonstrate the fidelity of the ChIP assay technique) and binding was observed at all regions of the VEGF-A promoter.

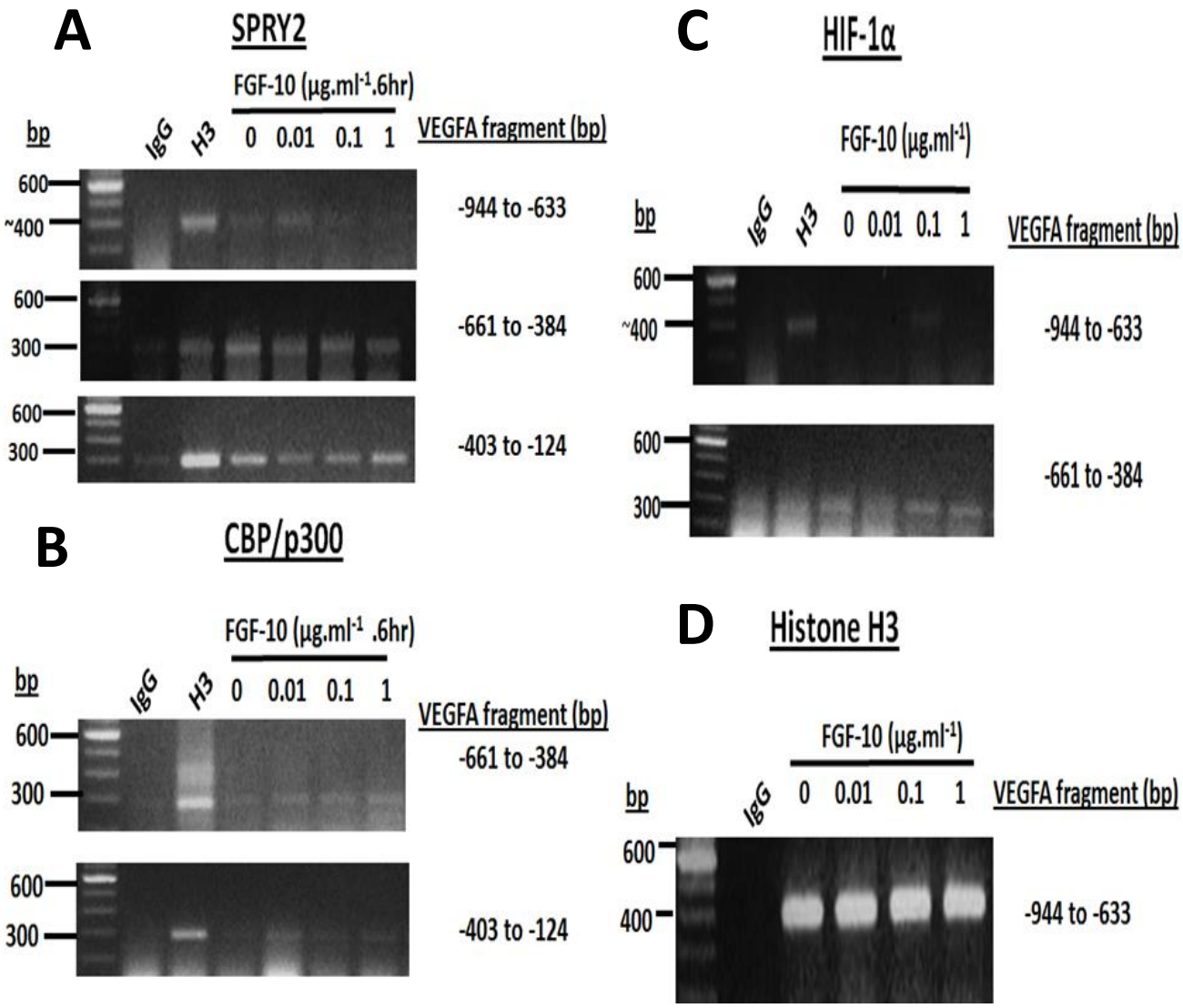

Figure 3.10. ChIP assays showing SPRY2, HIF-1α, CBP/p300 and Histone H3 interacting with distal regions of the VEGF-A promoter. SPRY2 was shown to bind strongly to the GC-rich domain of the VEGF-A promoter (A), accompanied by binding of CBP/p300 to this same region (B). Binding of HIF1α to the HRE of the VEGF-A promoter was weakly observed (C). Non-immune murine IgG and H3 chipped DNA (D) were run as negative and positive controls for all primer sets respectively in the qPCR reaction. qPCR reactions were run on 1% agarose gel and were stained with ethidium bromide. Molecular weights of bands observed are 311bp (-944 to -633bp), 277bp (-661 to -384bp) and 279bp (-403 to -124bp). Results shown are representative of 4 independent experiments.

Discussion

Previous studies of the cellular distribution of SPRY2 in fetal and adult lung epithelium describe it as being exclusively in the endosome, where it migrates to the plasma membrane in response to RTK activation by growth factors (Lim *et al*., 2000, 2002), such as FGF10. This chapter provides evidence that SPRY2 exists in the nucleus of both fetal and adult lung epithelial cells as shown in Figure 3.2 and subsequent figures of nuclear protein abundance. This corroborates with two other observations of nSPRY2 in developing neural tissue (Aranda *et al*., 2008; Hausott *et al*., 2012). Moreover, the major regulator of SPRY2 function in the fetal lung, FGF10, induced vascular signalling in intact fetal lungs as demonstrated in Figure 3.1, suggesting interplay between FGF10, SPRY2 and vascular development.

SPRY2 protein was resolved as two distinct double bands by SDS-PAGE and this is in accordance with previous studies (Chandramouli *et al*., 2008; Medina *et al*., 2011). However, other studies have observed multiple bands of SPRY2 occurring (Lao *et al*., 2006; Edwin *et al*., 2009), while another study recorded only a single 35kDa band (Fritzsche *et al*., 2006). Surprisingly, the majority of these studies fail to acknowledge the exact molecular weights of both these bands. In this study, SPRY2 was resolved at molecular weights of approximately 39 and 35kDa, where the 39kDa form was cleared upon increasing FGF10 stimulation and the 35kDa was unaffected. This is acknowledged by Lao *et al*., (2006), who stated that FGF stimulation favours the faster migrating band. However the mechanism by which the loss of the higher molecular weight form of SPRY2 occurs is currently unknown.

Scott *et al*., (2010) postulated that this mechanism may be 'proteasomal cleavage' after conducting experiments using the protease inhibitor MG132, through which they found that MG132 stabilised the SPRY2 doublet in the presence of FGF10. Furthermore, there is presently no function tied to either of the two forms of SPRY2, although a number of post-translational modifications are implicated. Impagnatiello *et al*., (2001) postulated that the presence of the higher molecular weight form of SPRY2 is the result of phosphorylation as it disappears with phosphatase treatment. Although the data for this is not shown, this observation allowed Lao *et al*., (2007) to speculate that the higher molecular weight form is related to the serine-rich domain, which is known to become dephosphorylated upon binding of PP2A, a protein phosphatase. Lao *et al*., (2007) also established that SPRY2 was predominantly phosphorylated on specific serine residues which are dephosphorylated upon FGF stimulation.

Another post-translational modification that may mechanistically facilitate the FGF10-induced loss of $SPRY2^{39kDa}$ is palmitoylation; a process that regulates subcellular trafficking of proteins to the cell membrane and other cellular compartments upon recruitment of fatty acids (e.g. palmitate) via a liable thioester bond to the cysteine residues on proteins (Salaun *et al*., 2010). SPRY2 itself contains an unusually large number of cysteine residues making it a likely candidate for palmitoylation and experiments conducted by Impagnatiello *et al*., (2001) established that SPRY2 is indeed anchored to the membrane by palmitoylation. However, this study does not factor in which form of SPRY2 is palmitoylated, nor the

fact that growth factor signalling also plays a role in promoting membrane trafficking of SPRY2 (Lim *et al*., 2000).

The results presented here show that nSPRY2^{39kDa} form is sensitive to FGF10 stimulation and that its loss is accompanied by an increase in H3 phospho-acetylation and thus gene expression. This would suggest that the 'full-length' form of SPRY2 acts to repress gene expression and this effect is relieved by FGF10 stimulation. Taking into account the various post-translational modifications SPRY2 has been suggested to undergo, it is known that FGF10 induces c-Src phosphorylation of SPRY2 at its Y55 domain (Li *et al*., 2004; Scott *et al*., 2010). In doing so, this initially activates SPRY2, which may explain the initial induction in SPRY2 protein abundance observed at 0.01μg.ml^{-1} FGF10 (Figure 3.5). As FGF10 concentration increases, this causes the 39kDa form of SPRY2 to translocate to the cell membrane, possibly in accompaniment with palmitoylation of the unusually large number of cysteine residues. This permits phosphorylation and acetylation of H3 and the unwinding of DNA leading to the expression of genes. This hypothesis appears to be supported by the evidence presented in Figures 3.6 and 3.7, which both show that H3 phosphorylation and acetylation were significantly induced with increasing FGF10 concentration. This was matched by a decline in the loss of HDAC1, HDAC2 and also the clearance of SPRY2^{39kDa}. Interestingly, the expression of the 35kDa form of SPRY2 persists in the nucleus and is unaffected by FGF10 stimulation, suggesting that this form of SPRY2 may function in the nucleus in some way.

Gene expression occurs in the nucleus through the catalysis of histone proteins, which promote unwinding of DNA. Histones are arranged into octomeric structures known as nucleosomes. The nucleosomes are tightly compacted into chromatin fibres which restrict the interaction of proteins with the packaged genomic DNA, leading to implications on cellular processes such as transcription and cell division (Hans & Dimitrov, 2001). Each histone contains an N-terminal tail domain which protrudes from the nucleosomal surface and is subject to a raft of post-translational modifications such as acetylation, methylation, phosphorylation and ubiquitylation (Hans & Dimitrov, 2001). Specifically, phosphorylation of the serine 10 (S10) residue on H3 has been extensively described as a key inducer of transcriptional activation and chromosomal condensation (Lo *et al*., 2000). Its activity is also known to dramatically increase upon stimulation of the MAPK pathway (Clayton & Mahadevan, 2003), whose signalling is induced by FGF10 expression. Interestingly, the S10 and lysine 14 (K14) residues are in close proximation on the H3 tail (Lo *et al*., 2000) and it has been reported that S10 phosphorylation favours K14 acetylation as it abolishes acetylation and methylation of the lysine 9 residue of H3 (Bazer *et al*., 2012). Histone acetyltransferases (HAT) are enzymes that specifically target the lysine residues on the amino-terminal tail of histones. They function to neutralise the positively charged histones thereby reducing the interaction of the N termini on the histone tails with the negatively charged phosphate backbone of DNA. Acetylation of histones promotes gene expression; recombination and DNA damage repair (Wang *et al*., 2012a). Acetylation however, can be counteracted by Histone deacteyltransferase (HDAC) activity. HDAC enzymes function to restore the positive charge to the histones, thereby strengthening the interaction between the histones

and the DNA, thus conserving the condensed structure of chromatin. HDAC1 and HDAC2 belong to the Class I HDACs which are expressed ubiquitously in a variety of repressor complexes and have been extensively used in tumourigenic studies (Wilting *et al*., 2010). In lung development specifically, the loss of HDAC1/HDAC2 has been shown to correlate with reduced airway development (Morrisey, 2012). The correlation observed in Figures 3.6 and 3.7 suggests that activation of SPRY2 by FGF10 is required for phosphorylation and acetylation of H3 to catalyse the unwinding of DNA from the nucleosome, and like SPRY2, the extent of unwinding appears to be affected by FGF10 concentration. Similarly FGF10 appears to down-regulate HDAC1 and HDAC2 expression as it amplifies phospho-acetylation of H3 and induces putative membrane translocation of $SPRY2^{39kDa}$. However, the expression of $nSPRY2^{35kDa}$ is sustained thus implicating a potential role in regulating transcriptional activation of genes.

FGF10 appears to induce vascular signalling (Figure 3.1, Scott *et al*., 2010) and has been reported to do so through mTORC1 activation (Scott *et al*., 2010). However, FGF10 stimulation only induced an increased trend towards increased VEGF-A and SPRY2 gene expression before a decline in expression is observed at $1\mu g.ml^{-1}$ FGF10 (Figure 3.8). These observations are in agreement with Acosta *et al*., (2001) and Scott *et al*., (2010), who showed that FGF10 induced SPRY2 mRNA expression and VEGF-A secretion in the fetal lung respectively. It should also be noted that there were difficulties in measuring gene expression due to the variability in housekeeper gene expression. The housekeeper gene used for this experiment was B2M, where levels of expression were found vary between samples and the lack of statistical

significance in the data may have arisen through difficulties in quantifying corrective gene expression levels. To quality control this, 18S ribosomal RNA (18S) was used as a replacement housekeeper gene. However expression levels of this gene similarly fluctuated between samples and independent experiments. This observation requires further investigation in order to select a viable housekeeper gene with which to quantify gene expression in FDLE, if indeed, it is possible.

The anatomical evidence presented by Scott *et al*., (2010) in Figure 3.1 also indicates that FGF10 is a pro-vasculogenic growth factor of fetal lung development. FGF10 localisation appears to induce vascular differentiation of the peripheral mesenchyme in addition to the epithelium. Studies from Bellusci *et al*., (1997a) demonstrated a technique whereby the endodermal layer surrounding the mesenchyme was removed using a trypsin/pancreatin solution. This allowed closer observation of morphological changes of the airway bud and had this technique been applied to the experiment in Figure 3.1, then there would be a potential to closely observe the morphology of the epithelium in response to localised signalling of FGF10.

The ChIP assays conducted in Figure 3.10 show that CBP/p300, HIF-1α and SPRY2 are capable of interacting with the VEGF-A promoter. CBP/p300 and SPRY2 bind strongly to the GC-rich regions of the VEGF-A promoter suggesting that there may be a key functional domain at these GC-rich regions of the promoter. Given its close proximity to the transcriptional start site, it is possible that SPRY2 and CBP/p300 could act upon the transcriptional start site on the gene, where SPRY2 would act to antagonise the catalytic function of CBP/p300 to initiate gene expression. These

'CpG' islands are also susceptible to methylation and as a consequence, the promoter can be held silent and gene expression is inhibited. (Bird, 2002). Within the GC-rich domains themselves reside the binding sites for the Specificity Protein 1 and 3 (Sp1, Sp3) transcription factors (Pagès & Pouysségur, 2005). Sp1 and its repressor Sp3 have both been reported to regulate VEGF and consequently angiogenic signalling (Pagès & Pouysségur, 2005). Given the ability of SPRY2 to interact with other proteins as alluded to in Chapter 1, it could be possible that SPRY2 may be involved in regulating the recruitment of transcription factors, such as Sp1/3, to bind to the VEGF-A promoter.

Conclusions

The data presented here demonstrates the unique observation that SPRY2 is present in the nucleus of the developing lung epithelium where it acts to regulate gene expression. In the nucleus, FGF10 induces the loss of the nSPRY239^{kDa} and this is accompanied by an increase in H3 phospho-acetylation, which catalyses the unwinding of the DNA from its histone core, thus promoting gene expression. The data also shows SPRY2 interacts with CpG-rich domains of the VEGF-A promoter. Given its close proximity to the transcriptional start site, nSPRY239^{kDa} may act to antagonise the transcriptional activation of VEGF-A, which is relieved by FGF10-evoked clearance of 'full-length' SPRY2. This stimulation can then permit growth of the vasculature as observed in the fetal mouse lung explants, which is also indicated by an increased trend in VEGF-A gene expression. Therefore, this study suggets a novel role for SPRY2 in the nucleus of fetal lung epithelium where it functions within the VEGF-A promoter to regulate events that promote vasculogenic gene expression.

Chapter 4 - The effect of modifying SPRY2 protein function on airway and vascular signalling in HBE cells.

Introduction

Regulation of SPRY2 function – the Y55 domain.

Chapter 3 demonstrated that SPRY2 is present in the nucleus and is capable of interacting with the VEGF-A promoter and so links the FGF10 stimulus to vascular signalling. As discussed in Chapter 1, FGF10 activates SPRY2 by inducing phosphorylation of its Y55 residue via c-Src kinase activity (Li *et al*., 2004; Guy *et al*., 2009). Src-phosphorylation of Y55 also promotes PP2A-induced dephoshorylation of two serine residues within the serine-rich domain (Ser^{115} and Ser^{118}), which exposes the cryptic proline-rich SH3-binding motif (Lao *et al*., 2007) at the C-terminal end. Many studies have demonstrated that activation of the Y55 phosphorylation residue is vital for SPRY2 to function (Fong *et al*., 2003; Chitra *et al*., 2010), as it is capable of binding the E3 ubiquitin ligase, cCBL, which is thought to regulate levels of SPRY2 in the cell (Hall *et al*., 2003). Thus, it would appear that the Y55 residue is clearly rate-limiting for SPRY2 activation. Mason *et al*., (2004), demonstrated that c-Src failed to induce tyrosine phosphoryaltion of SPRY2 upon mutation of the Y55 residue, which also subsequently abolished interaction of SPRY2 with cCBL. Y55 mutation was also shown to reduce the capability of SPRY2 to interact with other molecules and ultimately hinder its characteristic function of inhibiting RTK signalling (Chitra *et al*., 2010).

The cysteine-rich domain.

In contrast to the Y55 tyrosine kinase phosphorylation domain, little is known of the function of the Cysteine-rich Domain (CRD) located near the C-terminus on SPRY2. One function assigned to this region is Cys-palmitoylation and subsequent membrane translocation of SPRY2 (Impagnatiello *et al*., 2001). Lim *et al*., (2002), expanded on this hypothesis by demonstrating that a mutant of SPRY2 (R242D) resulted in its failure to translocate to the membrane, coupled with its failure inhibit ERK signalling. Subsequent studies have continued to demonstrate the compromised ability of SPRY2 to interact with other proteins and its failure to inhibit ERK upon mutation of the CRD (Nonami *et al*., 2005; Cabrita *et al*., 2006). However, the true role of the CRD with respect to SPRY2 function remains ambiguious, a fact acknoweldged by the in-depth review of SPRY2 from Guy *et al*., (2009).

Recent bioinformatic analysis from collaborators of our lab has unveiled two cysteines within the CRD of SPRY2 (C218 and C221), which were shown to be highly conserved among the SPRY isoforms and across species with homology observed as far back as the *Drosophila* lineage (Figure 4.1). These cysteines have also been shown to share partial homology with the Ran-binding protein Zinc finger domain (RanBP2). This homology was discovered by entering the SPRY2 amino acid sequence into the protein database program PROSITE (http://prostieexpasy.org/), which identifies domains of unrelated proteins that share a similar amino acid sequence with that of the input protein. The program provides a value which is used to calculate a similarity score for any alignment between the input protein sequence and that of an unrelated protein sequence. In this case, the value generated by the

program gave a score of 6.514 for Zinc finger RanBP2 relative to the the amino acid sequence of SPRY2 (Figure 4.1A), albeit with a low confidence level rating and low hit level.

The term 'zinc finger' (ZnF) was used to describe a 30-amino acid sequence motif originally discovered in the transcription factor TFIIIA from *Xenopus laevis.* This motif was found to form an independent DNA-binding mini-domain folded around a centralised zinc ion, with a tetrahedral arrangement of cysteine and histidine metal ligands (Miller *et al*., 1985). The arrangement of this domain is such that, a series of adjacent ZnFs protrude and 'grip' the DNA and other interacting particles (hence the term finger) and they have subsequently been discovered in many eukaryotic DNA binding proteins (Klug & Schwabe, 1995). ZnFs themselves are structurally diverse and are classified as a series of fold groups, based on the strucutral properties around the zinc-binding site. The best studied of these fold groups are the Cys_2-His_2 ZnF, which is commonly found in mammalian transcription factors (Krishna *et al*., 2003) and the zinc ribbon fold.

Ran-binding proteins (RanBP) themselves are involved in regulating receptor-mediated transport between the nucleus and the cytoplasm (Steggerda & Paschal, 2002), where the ZnF protrusions act to bind DNA, RNA, proteins and other small molecules. The ZnF of RanBP were first identified in the nuclear export protein RanBP2. The ZnF are arranged by the zinc ribbon fold configuration, whereby ZnF fold into a structure composed of two ß-hairpin strands, which sandwhich a zinc ion (Gamsjaeger *et al*., 2007). The partially-shared cysteine homology that exists between RanBP2 and SPRY2, suggests that the CRD of SPRY2 may also harbour a

potential ZnF DNA-binding domain, thus providing further evidence that SPRY2 functions in the nucleus as described in Chapter 3.

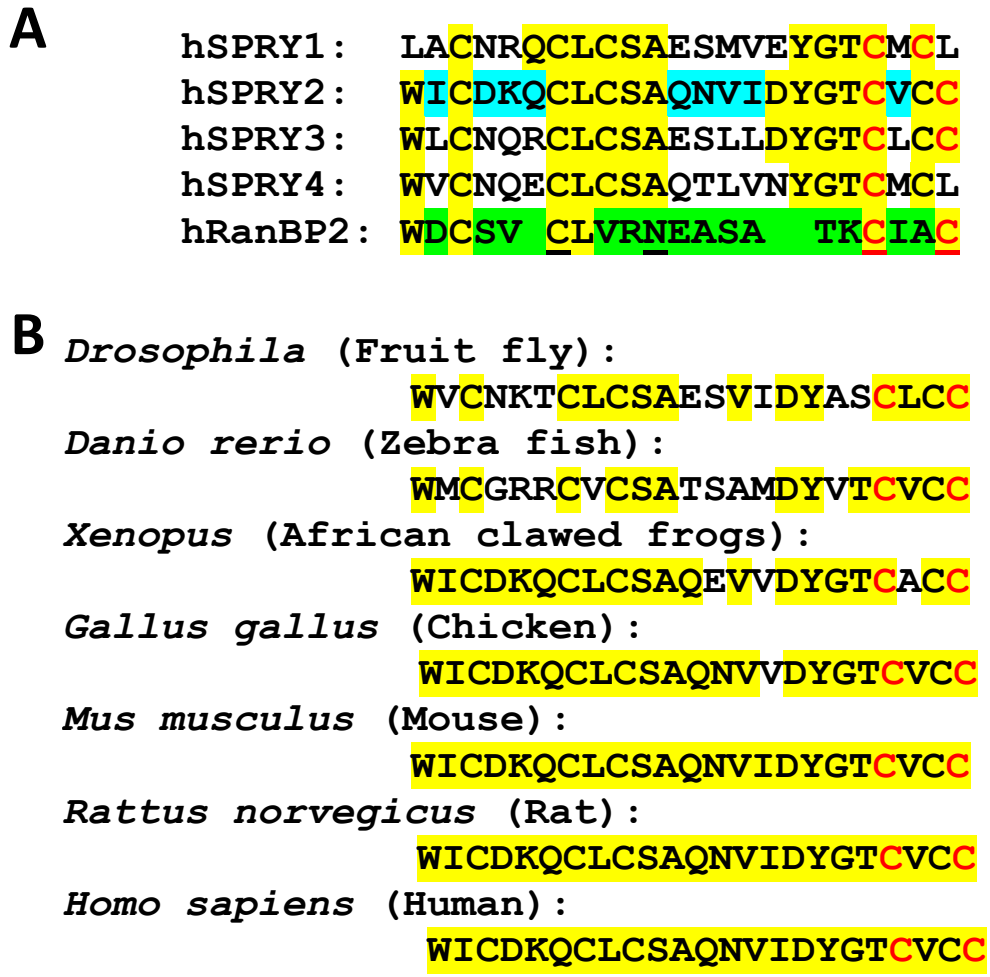

Figure 4.1. Amino acids 209-221 spanning the CRD (highlighted in yellow) of SPRY2 are conserved amongst SPRY isoforms (A) and among species (B), whilst also occuring within the RanBP2 sequence (highlighted in green). Cysteines 218 and 221 (highlighted in red) were selected for mutation in this study.

The SRC Homology 3 (SH3) domain.

Downstream of the CRD on SPRY2 on the C-terminal end is a proline-rich P*XX*P*X*R motif (termed the SH3 binding domain). Lao *et al*., (2006) suggested that the SH3 domain is exclusively responsible for silencing ERK phosphorylation through interaction of N-terminal GRB2 with the C-terminal SH3 domain of SPRY, which is achieved through preferential binding of PP2A over cCBL to the Y55 domain of SPRY2 (Lao *et al*., 2007). This indicates that exposure of the SH3 motif is required for SPRY2 to naturally function as an antagonist of growth factor signalling. However, other target proteins for the SH3 motif remain unidentified and their potential role in influencing SPRY2 function thus remains ambiguious.

Properties of human bronchial epithelial cells and their use as a model of the fetal lung.

SPRY2 expression has been poorly characterised in HBE. However, this study sheds some new light on its expression in HBE as shown in Chapter 3, Figure 3.3, which illustrated that SPRY2 is expressed in the HBE cell line despite its expression being much weaker relative levels expressed in the FDLE cells. The HBE cell line (16HBE14o-) used in this chapter were originally derived from immortalised bronchial surface epithelial cells from a 1-year-old transplant patient (Cozens *et al*., 1994) and were established in culture through transfection of a pSVori plasmid. Under culture conditions, the HBE cell line was found to retain morphological and functional features of the lung epithelium. For example, neighbouring cells develop tight junctions with one another to form a polarised ion transporting epithelial monolayer. Cl- transport across this epithelium occurs through the Cystic Fibrosis

Transmembrane Conductance Regulator (CFTR), which critically maintains fluid homeostasis in the postnatal lung (Larson *et al*., 2000). Interestingly, the HBE cell line exhibits high levels of CTFR protein and gene expression (Cozens *et al*., 1994), are capable of responding to FGF10 stimulation (Scott *et al*., 2010) and as shown in chapter 3, express SPRY2 albeit at approximately half the level of expression observed in FDLE (Figure 3.3). This evidence, coupled with the conserved morphological characteristics and functional ion transport gradients, provide the potential for the HBE cell line as a sutiable candidate to study aspects of fetal lung development.

The effect of modifying SPRY2 function on fetal lung development.

The common theme that stems from the literature with respect to modfications made to each of the protein domains on SPRY2 described above, is that they all influence SPRY2's function as an antagoniser of growth factor signalling and specifically as an inhibitor of ERK signalling, which is required for inducing growth of the airway in the fetal lung. However, little or nothing his known as to how similar adaptations to SPRY2 effect vascular growth of the fetal lung. Therefore, this chapter aims to examine the effects of modifying SPRY2 function on vascular signalling in response to SPRY2 overexpression and mutation of the functional Y55 residue, the CRD and the SH3-binding motif. The final part of this results chapter will examine the effects of SPRY2 knockdown by stable shRNA on HIF-1α transcriptional activity, kinase signalling and the gene expression of HIF-1α target genes including VEGF-A. In order to manipulate SPRY2 function *in vitro*, the HBE cell line was selected as a representative of the fetal lung in culture

Results

Overexpression of SPRY2^{WT} abolishes and SPRY2^{Y55F} induces HIF-1α promoter activity.

For vascular development to occur, HIF-1α activity must be induced. Therefore, HIF-1α activity was examined in HBE in response to overexpression of SPRY2^{WT} and constructs containing a null mutation in the Y55 tyrosine kinase phosphorylation domain (Y55F; SPRY2^{Y55F}) or the SH3 protein binding domain (P304A, P307A, P308A), where the proline residues have been subsituted for phenylalanines. Figure 4.2A shows the effects of transfecting these vectors in HBE has on HIF-1α activity. SPRY2^{WT} abolished HIF-1α activity with increasing overexpression with a signficant difference in activity observed at a concentration of 2.5μgDNA.well^{-1} relative to untransfected cells. HIF-1α activity did not change significantly with overexpression of SPRY2$^{P304A-P307A-P308A}$. However, HIF-1α activity was induced upon overxpression of SPRY2^{Y55F} and this induction was also statistically significant at 2.5μgDNA.well^{-1}. Figure 4.2B shows confirmation by western blot analysis of the overexpression of SPRY2 protein in HBE, upon transfection of all three vectors.

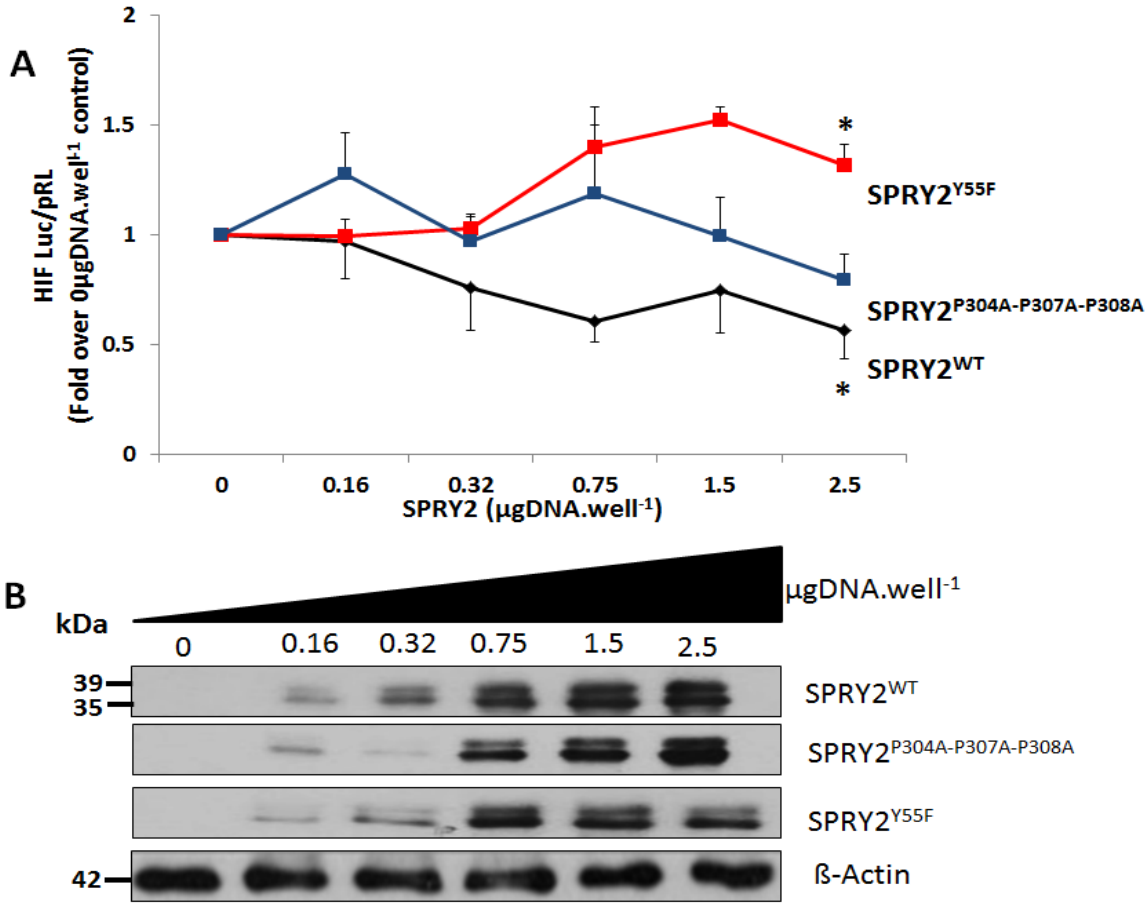

Figure 4.2. Overexpression of SPRY2^{WT} and Y55F/SH3 mutants and their effect on HIF-1α activtiy. All experiments were performed at fetal pO_2. A. Activity of HIF-1α is measured as the HIF-luc luminescent response divided by that of pRL. Values plotted are expressed as the fold change value relative to the endogenous response (SPRY2 0µgDNA.well^{-1}). Error bars are $\bar{x}$ ± SEM of the fold change; n = 6. Statistical analysis was carried out on the raw data where asterisks denote statistical significance (SPRY2^{WT}; $P < 0.05$; SPRY2^{Y55F} = 0.05; student's t-test) relative to the corresponding endogenous response (0µgDNA.well^{-1}). B. Blots are representative of 3 independent experiments. Actin was blotted as a control for protein loading and is representative of the overexpression of all three SPRY2 western blots shown here.

Overexpression of SPRY2$^{Y55F/P304A-P307A-P308A}$ does not alter MAPK, PI3K and mTORC1 signalling.

The result shown in Figure 4.2 established that HIF-1α activity was induced above the level evoked by hypoxia alone by overexpression of the SPRY2^{Y55F} mutant, whereas the SH3 mutant tended to abrogate the inhibitory effect of SPRY2^{WT}. HIF-1α activity is known to be regulated by ERK1/2, AKT and P70-S6K (Minet *et al*., 2000; Leung *et al*., 2011) and so the enodgenous activity of these kinases was assessed upon transfection of the SPRY2^{WT} vector and the Y55F and SH3 mutants, as seen in Figure 4.3. 2.5μgDNA.well^{-1} of each of the SPRY2 vectors was transiently transfected into HBE and the phosphorylation pattern of P70-S6K, AKT and ERK1/2 was assessed. When compared to the endogenous HBE response, mutation of the Y55 and SH3 domains of SPRY2 showed no significant change in the expression levels of of P70-S6K, AKT and ERK1/2.

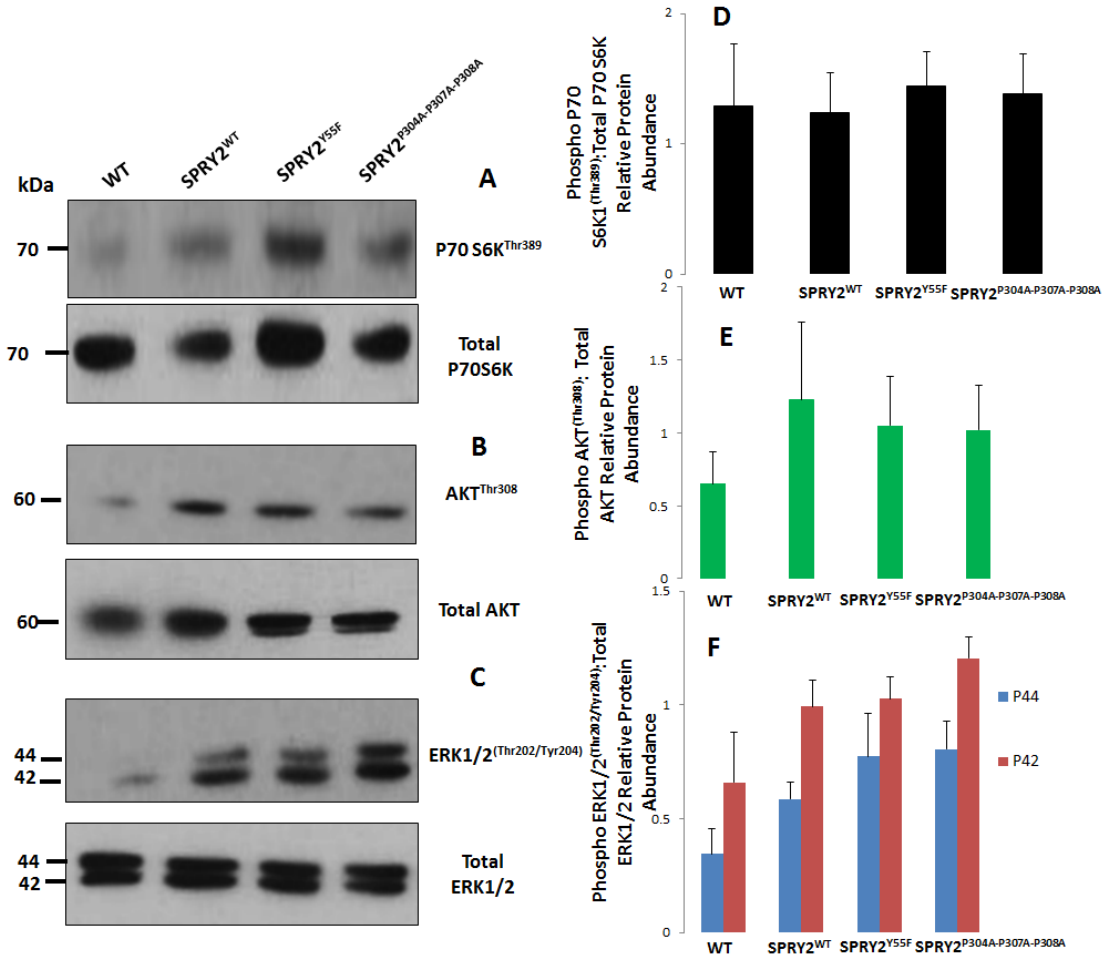

Figure 4.3. Relative protein kinase abundance upon overexpression ± mutation of SPRY2. Blots and densitometry are representative of 3 independent experiments. A. P70-S6K phosphorylation measured at the Thr^{389} residue. B. AKT phosphorylation measured at the threonine 308 (Thr^{308}) residue. C. p44/p42 (ERK1/2) phosphorylation measured at theronine 202 (Thr^{202}) and tyrosine 204 (Tyr^{204}) resdiues respectively. Densitometric analysis of P70-S6K (D), AKT (E) and ERK1/2 (F) relative protein abundance is shown where bars represent the ratio of phosphorylated protein abundacne over total protein abundance. Error bars are $\bar{x}$ ± SEM (n = 3).

Mutation of the CRD of SPRY2 abolishes HIF-1α activity.

WT-SPRY2 was subcloned from the pXJ40 vector into a pCMV-Dual vector to generate N-terminal FLAG and C-terminal MYC tagged SPRY2. Cysteines at postions 218 and 221 of the putative ZnF domain were mutated to alanines and each construct was then used to generate stably transformed HBE cell lines. The effects of HIF-1α activity in response to the expression of these three constructs (Figure 4.4) were examined in each cell line. HIF activity was significantly suppressed in each cell line relative to the untransformed cells and the magnitude of this effect was greatest for the C218A mutant ($P = 0.03$).

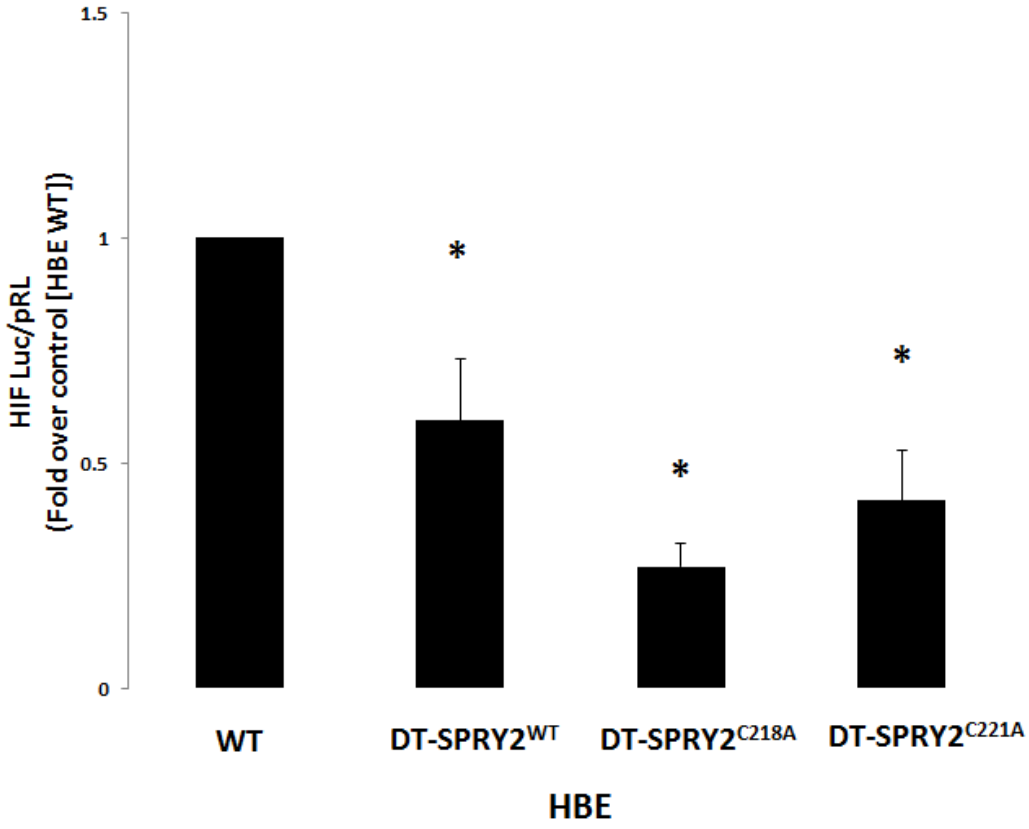

Figure 4.4. HIF-1α activity of the stable HBE-SPRY2 cell lines measured by luciferase reporter gene assay. Cells were maintained at 3% pO_2. HIF-1α activity is measured as the HIF–luc luminescent response over that of pRL. Values presented here represent fold change over the HBE WT response. Error bars are representative of this fold change and are $\bar{x}$ ± SEM; n = 4. Asterisks denote statistical significance ($P < 0.05$) when compared to the WT response and statistical analysis was carried out on the raw data (student's t-test).

HIF-1α protein stability and H3 phospho-acetylation are unaltered by SPRY2 overexpression and cysteine mutation.

In chapter 3, a potential role for SPRY2 in regulating VEGF-A gene expression was established. This potential was characterised by the observation that the loss of nSPRY2^{39kDa} correlated with an increase in phospho-acetylation of H3. To link this to vascular signalling , the protein stability of HIF-1α was examined in order to assess whether the changes observed in Figure 4.4. occurred as a result of cleavage and clearence of HIF-1α from the nucleus. Additionally, H3 phospho-acetylation was examined in these same cells to asses if the CRD of SPRY2 had an influence on histone modifications. Figure 4.5. shows protein abundance of HIF-1α, SPRY2 and S10 phosphorylation/K14 acetylation of H3 in each of the SPRY2 HBE cell lines. HIF-1α nuclear protein abundance did not change upon overexpression of DT-SPRY2^{WT} or both cysteine mutants (Figure 4.5A). nSPRY2 protein was present in all SPRY2 stable cell lines and was statistically significant relative to the amount of nSPRY2 protein in untransformed HBE cells (Figure 4.5B). However, there were no differences observed in H3 phospho-acetylation between each cell line.

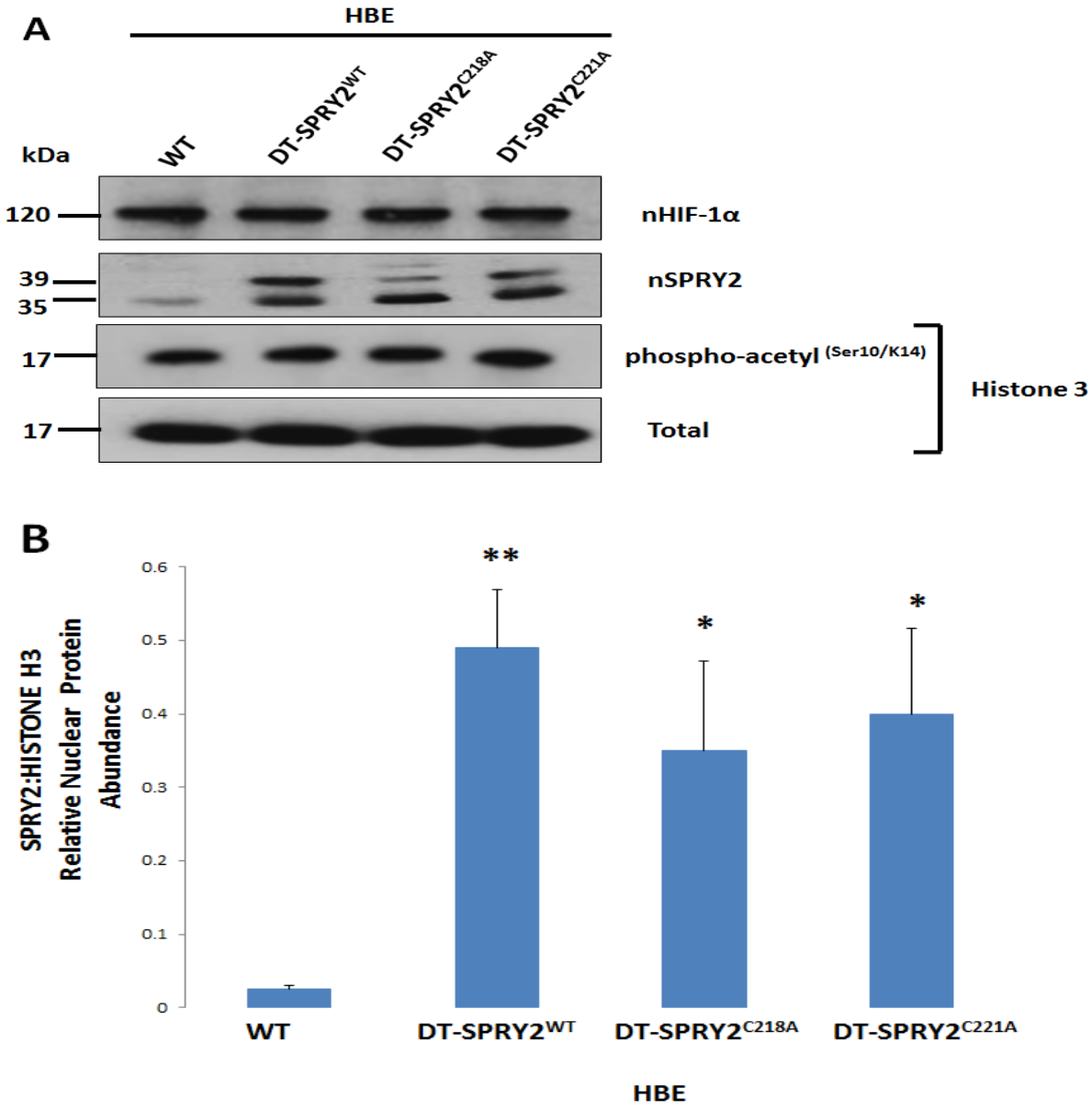

Figure 4.5. Nuclear HIF-1α and SPRY2 protein abundance and H3 phospho-acetylation in response to C218A and C221A mutation. Blots and densitometry are representative of 5 independent experiments. A. Total H3 was blotted as a control for protein loading and for validation of nuclear protein extraction. B. Denstiometric analysis of nSPRY2 protein abundance relative to H3 protein abundance. Error bars are $\bar{x}$ ± SEM of the raw data (n = 5). Asterisks indicate statistical significance relative to the WT response (DT-SPRY2^{WT}; $P < 0.01$; DT-SPRY2^{C218A} and DT-SPRY2^{C221A}; $P < 0.05$; student's t-test).

SPRY2 interaction with HIF-1α is abolished upon cysteine mutation.

In chapter 3, a weak interaction was observed between SPRY2 and the HRE of the rat VEGF-A promoter, while a strong association was established between SPRY2 and CBP/p300 binding at the GC-rich sites downstream on the promoter (Figure 3.10). This suggests that an interaction may exist between SPRY2 and the HIF-1α-CBP/p300 complex. To investigate this further, an IP was carried out in order to establish if an interaction existed between these proteins. In light of the observation that cysteine mutation suppressed HIF-1α transcriptional acitvity (Figure 4.4), it was hypothesised that cysteine mutation would suppress the putative interaction between SPRY2 and the HIF-1α-CBP/p300 complex. Figure 4.6 shows the outcome of a Co-IP whereby SPRY2 antibody was used to 'pull-down' both HIF-1α and CBP/p300 protein. The western blot shows that SPRY2 interacts with HIF-1α in both WT HBE and overexpressed DT-SPRY2^{WT} cell lines and this interaction is attenuated upon C218 and C221 mutation. Attempts at pulling down CBP/p300 with SPRY2 proved unsuccessful (data not shown).

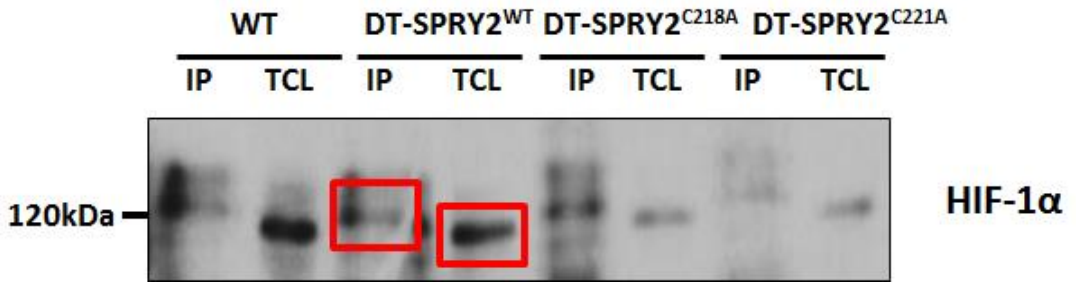

Figure 4.6. Co-IP showing SPRY2 interaction with HIF-1α is lost upon mutation of C218 and C221. Cells lysates were incubated with protein-A-sepharose beads conjugated with 1µg SPRY2 antibody and were probed for HIF-1α upon western blotting. Blot shown here is representative of 3 independent experiments. The band highlighted within the red box is HIF-1α protein. TCL denotes total cell lysate.

Mutation of SPRY2 at Cysteine 218 induces VEGF-A gene expression.

To further investigate the loss of HIF-1α activity upon cysteine mutation of SPRY2, qPCR assays were performed to examine if this loss of HIF activity correlated with a change in the expression of the primary HIF-1α target gene, VEGF-A. Figure 4.7. shows VEGF-A gene expression levels from each of the stable SPRY2 cell lines. Little or no change was observed between the HBE WT and DT-SPRY2^{WT} overexpression. A strong induction of VEGF-A gene expression was observed in the DT-SPRY2^{C218A} mutant relative to WT levels, which was found to be statistically significant ($P < 0.05$). However, DT-SPRY2^{C221A} did not induce VEGF-A gene expression.

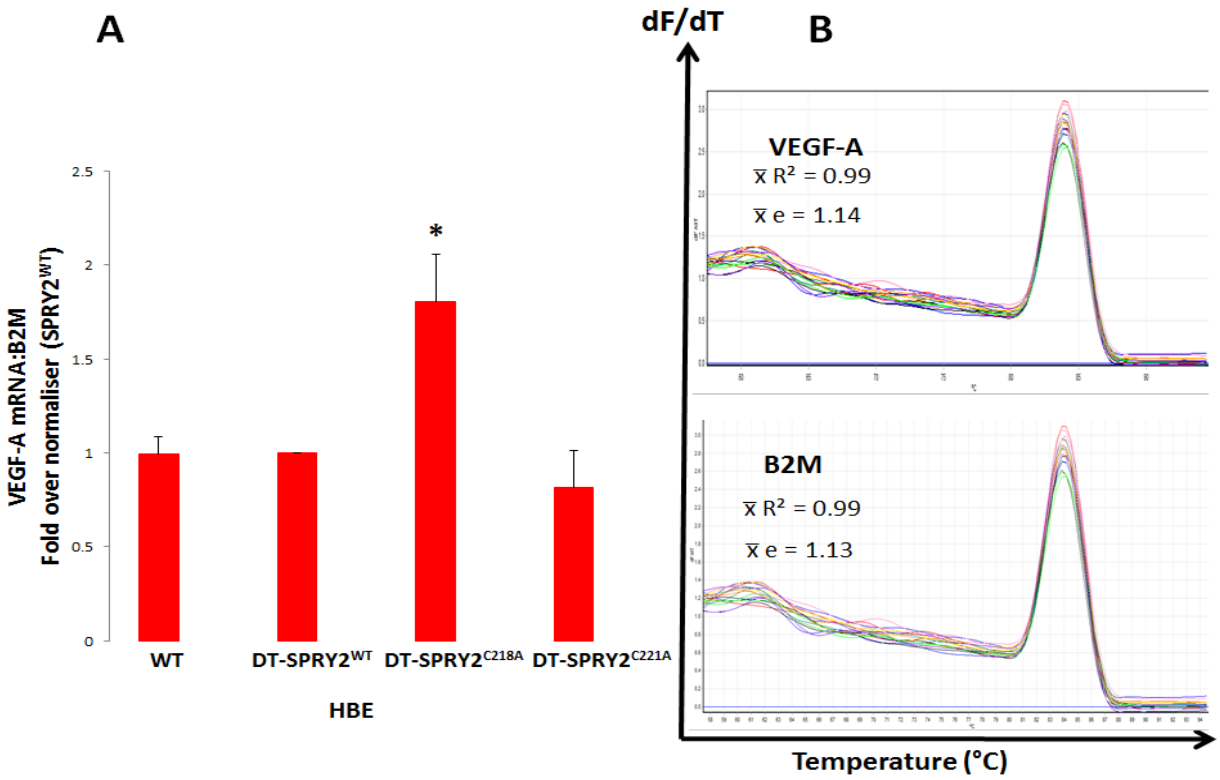

Figure 4.7. VEGF-A gene expression levels in response to overexpression of SPRY2^{WT} SPRY2^{C218A} and SPRY2^{C221A}. A. VEGF-A mRNA levels were measured over B2M mRNA levels and graph bars represent fold change over the DT-SPRY2^{WT} response. Error bars are $\bar{x}$ ± SEM of fold change (n = 4). Asterisks indicate statistical significance relative to HBE WT ($P < 0.05$) where statistical analysis was carried out on the raw data. B. Representative melt curves for both the VEGF-A and B2M demonstrate the fidelity of the qPCR reaction. Mean R^2 and efficiencies over 4 independent assays are provided.

Mutation of SPRY2 at C218 and C221 abolishes the ability of SPRY2 to bind to the HRE of the VEGF-A promoter.

Figure 4.6 established that SPRY2 interacts with HIF-1α, while Figure 3.10 also showed that SPRY2 binds to several DNA-binding domains of the VEGF-A promoter, where a weak interaction was observed at the HRE site. To link these observations with the loss of HIF-1α activity induced by cysteine mutation of SPRY2, ChIP assays were performed to assess if mutation at C218 and C221 had any effect on the affinity of SPRY2 to bind to this region of the VEGF-A promoter (Figure 4.8). SPRY2 was shown to bind strongly to the HRE upon overexpression (DT-SPRY2^{WT}) and this effect was attenuated with C218 mutation and abolished upon C221 mutation. The fidelity of this interaction was confirmed through the use of C-myc antibody in the ChIP assay (Figure 4.8B), as each of the DT-SPRY2 vectors harbour a C-terminal myc tag (Figure 4.7C).

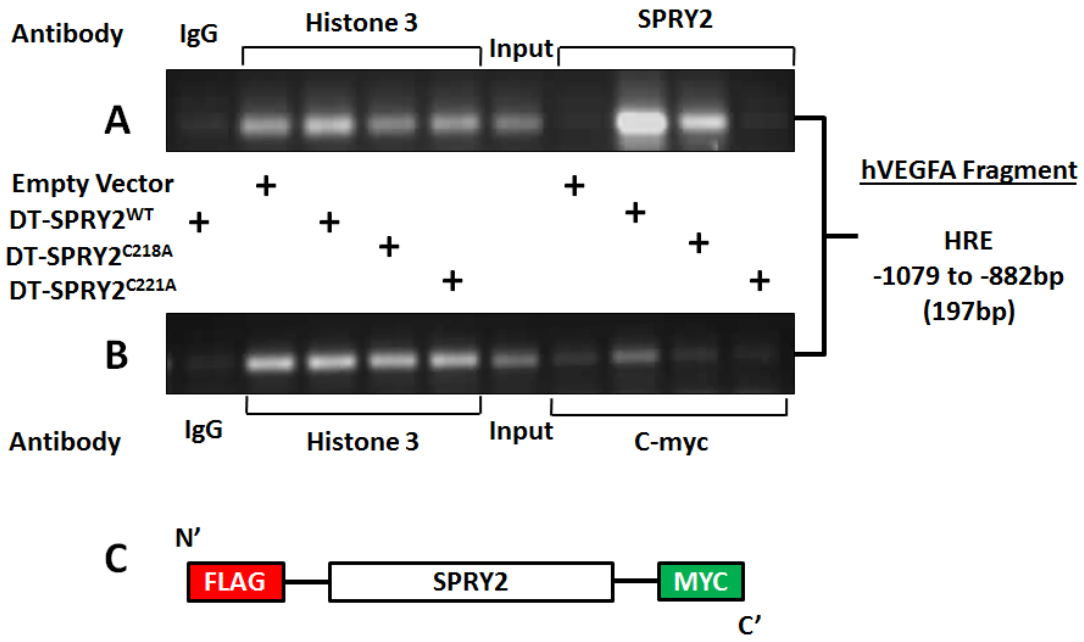

Figure 4.8. ChIP assays showing the effect of C218 and C221 mutation upon SPRY2 binding to the HRE of the VEGF-A promoter (A). Independent confirmation of this interaction is provided by the C-myc ChIP assay (B) as myc is fused to C-terminal SPRY2 in all three constructs (C). HBE cells were transiently transfected with 4µgDNA.well of each construct, where the empty vector transfected in was pCMV. H3 ChIP and the Input DNA were run as positive controls for the assay and the IgG ChIP was run as a negative control. qPCR reactions were run on 1% agarose gel and were stained with ethidium bromide. Molecular weight of bands observed is 197bp. Results are representative of 2 independent experiments.

Stable transfection of SPRY2 shRNA in HBE silences SPRY2 protein and gene expression.

To determine the effects of SPRY2 knockdown on HIF-1α activity and VEGF-A expression, HBE cells were stably transformed with either non-target (NT) or SPRY2 shRNA. Figure 4.9 shows confirmation of SPRY2 knockdown at the protein level in both cytosolic and nuclear fractions. Protein abundance of SPRY2 was found to be significantly lower in the SPRY2 shRNA HBE line, irrespective of pO_2. Further confirmation of SPRY2 knockdown is provided in Figure 4.10 where SPRY2 mRNA is significantly reduced in the SPRY2 shRNA stable cell line at both fetal and normoxic pO_2 where the extent of knockdown is approximately 60-70%.

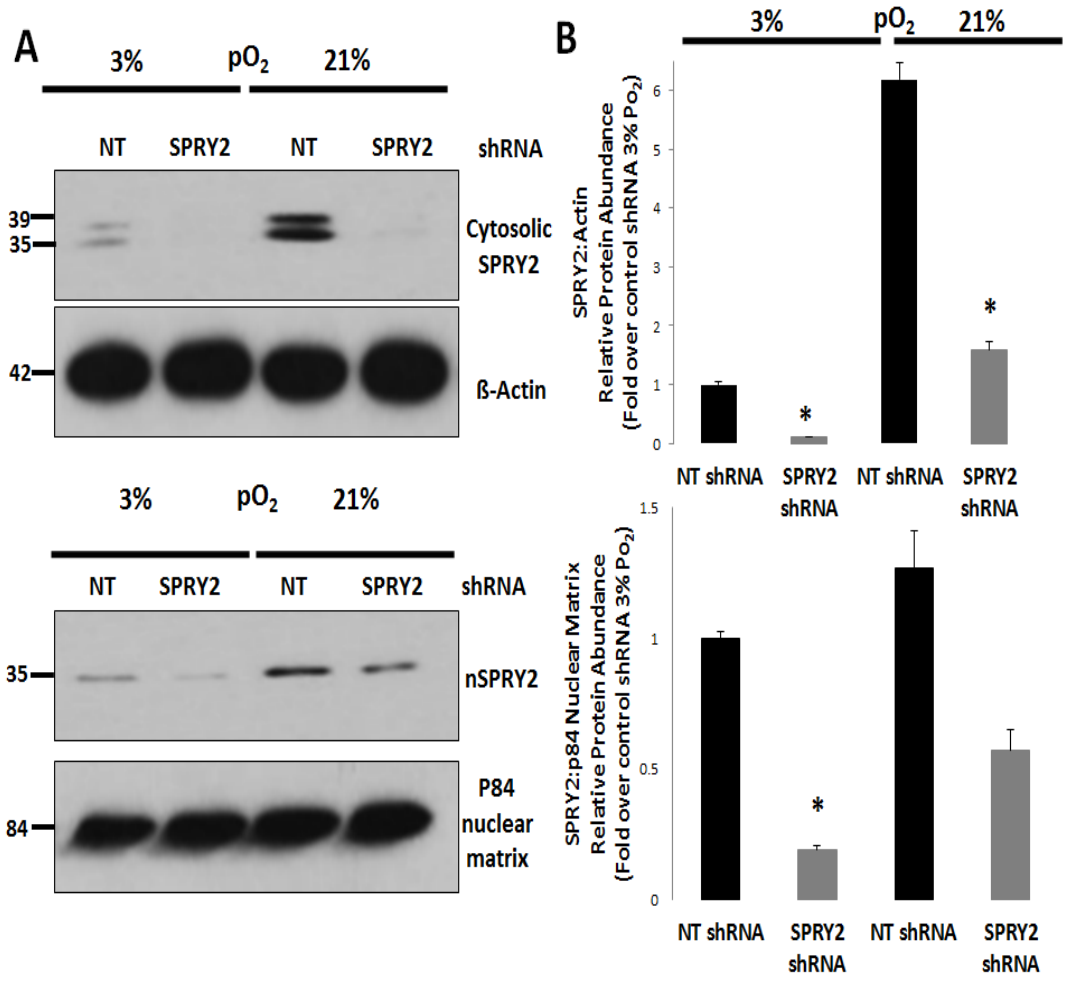

Figure 4.9. Western blot analysis confirming knockdown of SPRY2 protein with SPRY2 shRNA in HBE. Blots and densitometry are representative of 3 independent experiments where error bars are $\bar{x} \pm$ SEM. A. Upper panel: Cytosolic SPRY2 protein abundance. Lower panel: Nuclear SPRY2 protein abundance. In either case, ß-Actin and P84 nuclear matrix proteins served as respective loading controls. B. Densitometric analysis of the cytosolic and nuclear expression of SPRY2 was measured over ß-Actin and P84 respectively. Asterisks denote statistical significance ($P < 0.05$; $n = 3$) relative to the response observed in the control shRNA at the respective pO_2.

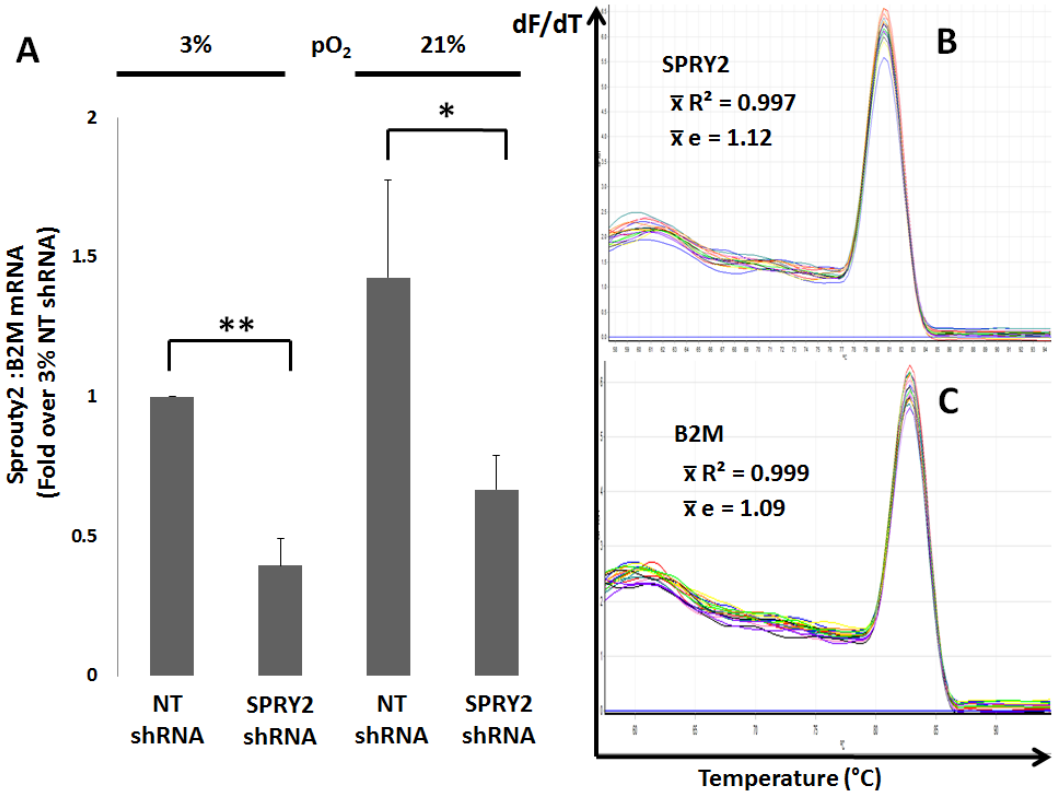

Figure 4.10. SPRY2:B2M mRNA in the control and SPRY2 shRNA HBE cell lines in response to both fetal and normoxic pO_2. A. SPRY2 mRNA was measured over B2M mRNA where the bars represent fold change in gene expression relative to the control shRNA at 3% pO_2. Error bars are $\bar{x}$ ± SEM of fold change (n = 4). Asterisks indicate statistical significance between SPRY2 and control shRNA at the respective pO_2. Statistical analysis was carried out on the raw data (* $P < 0.05$; ** $P < 0.01$; student's t-test). B. Melt curve representatives for both SPRY2 and B2M genes, provided with average efficiency and R^2 values (n = 4).

Knockdown of SPRY2 induces signalling of MAPK and mTORC1 in HBE.

Figures 4.2 demonstrated that mutation of the functional domains of SPRY2 significantly altered HIF-1α transcriptional activity and that this occurred without any significant change in kinase activity. This result was surprising given the central position occupied by SPRY2 in growth factor signalling responses and thus the effect of SPRY2 knockdown was investigated on these pathways in response to FGF10 stimulation. Figure 4.11 shows protein abundance levels of mTORC1 as measured by P70-S6K phosphorylation at Thr^{389}, in response to FGF10 stimulation in both control (Figure 4.11A) and SPRY2 shRNA (Figure 4.11B) HBE cell lines. In NT shRNA, the ratio of phosphorylation at Thr^{389} to total P70-S6K expression appeared to increase with increasing FGF10 stimulation whereas a decline in the expression of P70-S6K phosphorylation was observed with SPRY2 shRNA (Figure 4.11A, B, D). However, at endogenous levels, there was greater P70-S6K activity observed with SPRY2 shRNA relative to the control and this observation trended towards significance (Figure 4.11C).

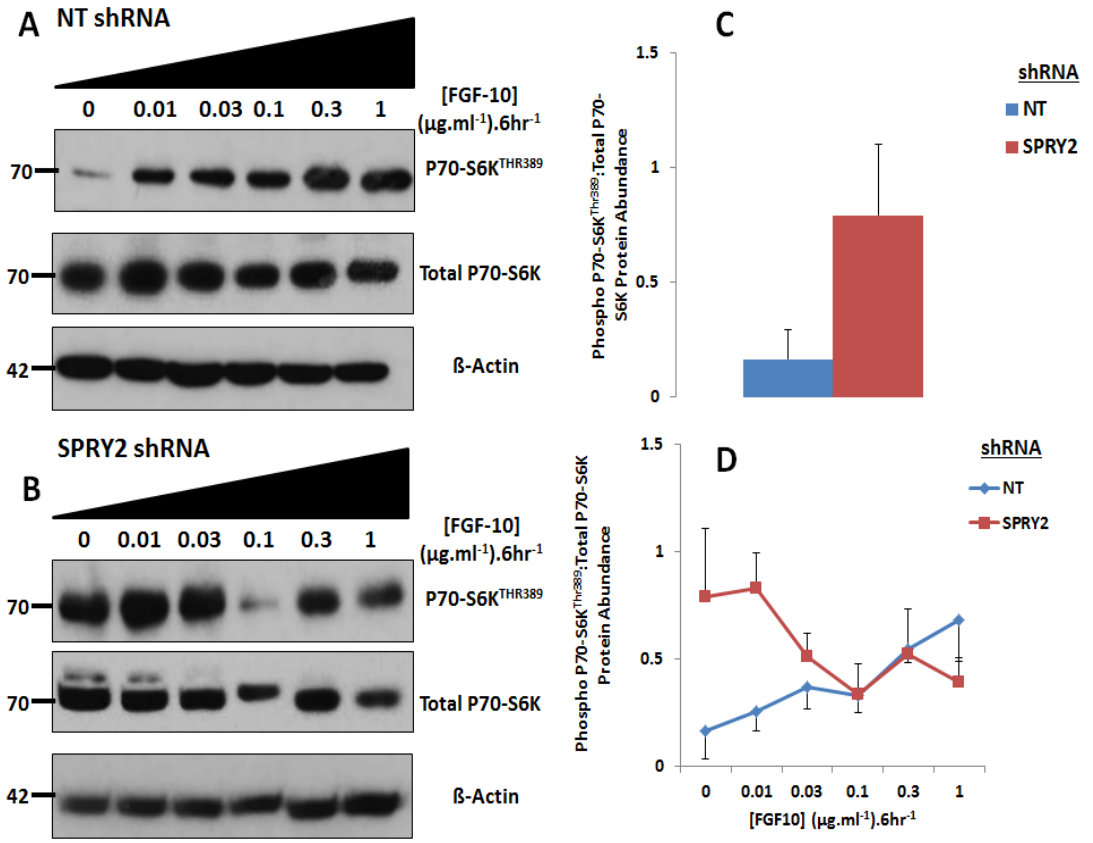

Figure 4.11. Phospho P70-S6K^{Thr389}: Total P70-S6K relative protein abundance in NT and SPRY2 shRNA HBE cell lines in response to increasing FGF10 concentration. Cells were cultured at fetal pO_2 and treated with FGF10 prior to whole cell lysis and subsequent western blot analysis. Actin was blotted as a loading control. Blots and densitometry are representative of 3 independent experiments where error bars are $\bar{x}$ ± SEM. A. P70-S6K^{Thr389} / Total P70-S6K in control shRNA. B. P70-S6K^{Thr389} / Total P70-S6K in SPRY2 shRNA. C. Densitometric analysis of endogenous P70-S6K activity in both shRNA cell lines where the induction in P70-S6K activity observed with SPRY2 shRNA trended towards significance (P = 0.0576; student's t-test). D. Densitometric analysis of P70-S6K activity in both shRNAs in response to increasing FGF10 concentration.

The effect of SPRY2 shRNA and FGF10 stimulation on PI3K activity, as measured by AKT Thr^{308} phosphorylation, is shown in Figure 4.12. Changes in AKT phosphorylation in response to FGF10 are associated with changes in the abundance of AKT protein and the direction of this response varied in magnitude from one assay to the next. As a result, the compiled data showed no significant effect of either FGF10 or SPRY2 knockdown on PI3K activity.

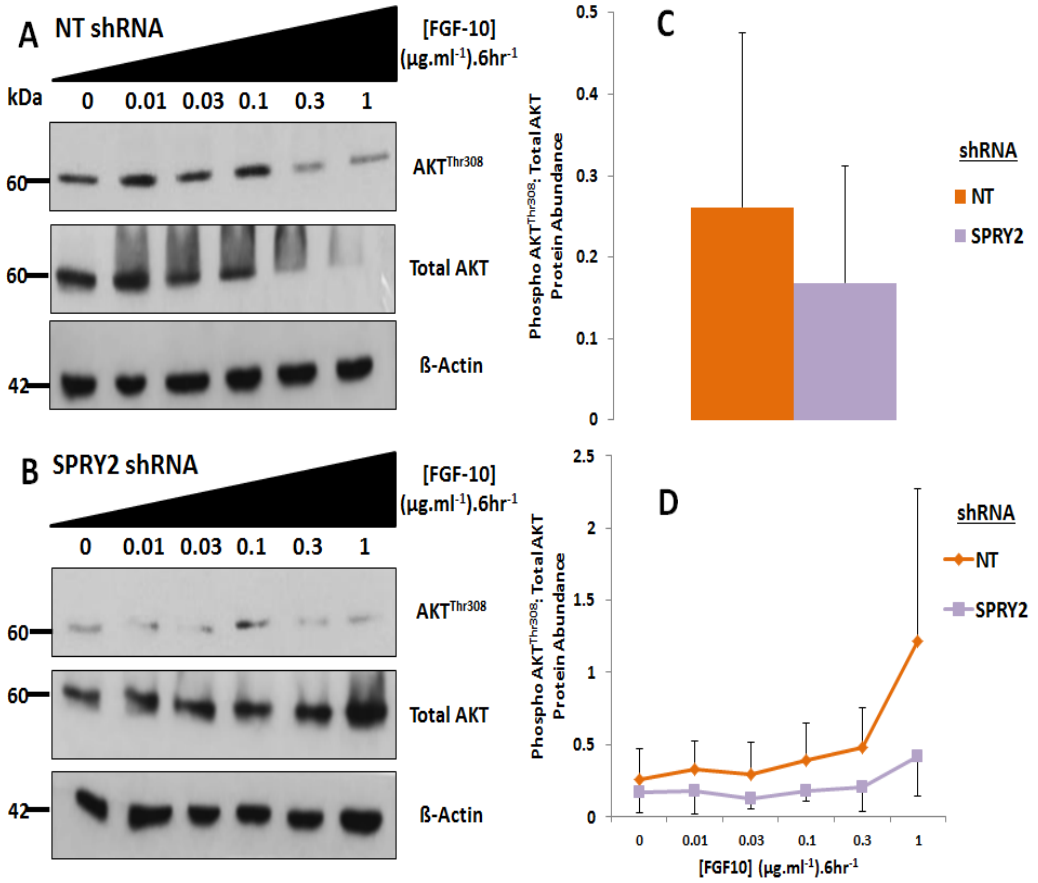

Figure 4.12. Phospho AKT^{Thr308}: Total AKT relative protein abundance in NT and SPRY2 shRNA HBE cell lines in response to increasing FGF10 concentration. Blots and densitometry are representative of 3 independent experiments where error bars are $\bar{x}$ ± SEM. A. AKT^{Thr308} / Total AKT in control shRNA. B. AKT^{Thr308} / Total AKT in SPRY2 shRNA. C. Densitometric analysis of endogenous AKT activity in both shRNA cell lines. D. Densitometric analysis of AKT activity in both shRNAs in response to increasing FGF10 concentration.

Figure 4.13 shows the effect of SPRY shRNA coupled with increasing FGF10 stimulation on the protein abundance of ERK1/2. ERK1/2 protein expression was measured at the p44 (Thr^{202}) and p42 phosphorylation residues (Tyr^{204}) in both NT and SPRY2 shRNA HBE cell lines (Figure 4.13A, B). Without FGF10 stimulation, ERK1 (p44) and ERK2 (p42) activity is induced upon SPRY2 knockdown by shRNA, relative to the NT shRNA (Figure 4.13C). Upon FGF10 stimulation, ERK1 and 2 activities increased in the NT shRNA with increasing FGF10 concentration. However, in the SPRY2 shRNA, ERK1 and 2 activities appear to increase specifically at 0.1$\mu g.ml^{-1}$ FGF10 before returning to levels observed in the endogenous response (Figure 4.13D, E).

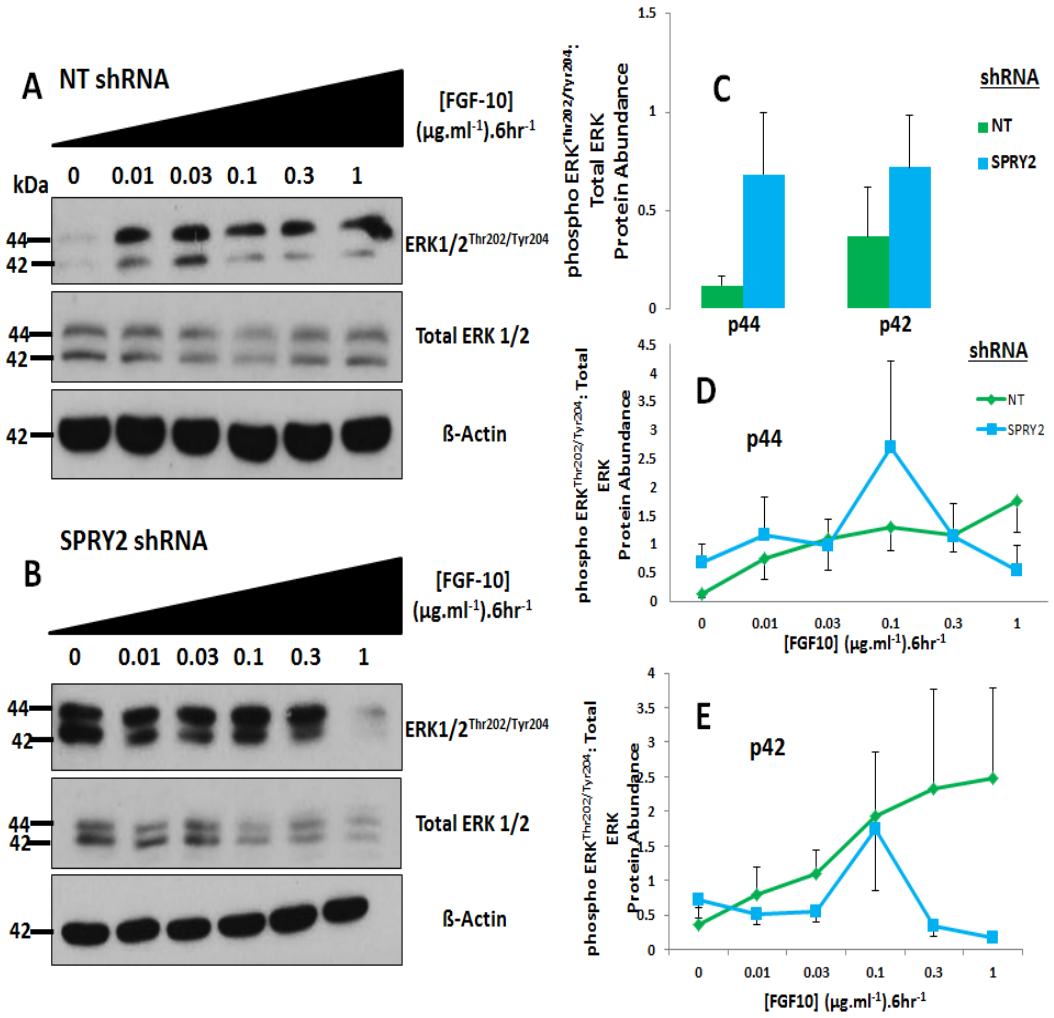

Figure 4.13. Phospho ERK1/2$^{Thr202/Tyr204}$: Total ERK1/2 relative protein abundance in NT and SPRY2 shRNA HBE cell lines in response to increasing FGF10 concentration. Blots and densitometry are representative of 4 independent experiments where error bars are x̄ ± SEM. A. ERK1/2$^{Thr202/Tyr204}$ / Total ERK1/2 in control shRNA. B. ERK1/2$^{Thr202/Tyr204}$ / Total ERK1/2 in SPRY2 shRNA. C. Densitometric analysis of endogenous ERK1/2 activity in both shRNA cell lines. D. Densitometric analysis of ERK1 (p44) activity in both shRNAs in response to increasing FGF10 concentration. E. Densitometric analysis of ERK2 (p42) activity in both shRNAs in response to increasing FGF10 concentration.

SPRY2 knockdown induces activity of HIF-1α at normoxic pO_2.

In the lung vasculature, activation of mTORC1 is required to induce the vascular activity of HIF-1α. SPRY2 knockdown gave rise to mTORC1 and ERK1/2 activity as shown in figures 4.11 and 4.13. Previous results from Scott *et al*., (2010), demonstrated that mTORC1 signalling induced HIF-1α activity. Therefore, the effect of SPRY2 knockdown on HIF transcriptional activity was measured and VEGF-A expression at fetal and normoxic pO_2. Figure 4.14 shows cytosolic and nuclear HIF-1α protein abundance in both NT and SPRY2 shRNA cell lines. In the cytosol, HIF-1α abundance was suppressed in hypoxia upon SPRY2 shRNA. However, upon incubation at normoxia, HIF-1α protein abundance was induced upon SPRY2 shRNA and this induction trended towards significance (P = 0.07; student's t-test). Additionally, nuclear HIF-1α protein abundance is also induced upon SPRY2 knockdown, where a marked change was observed in hypoxia, which also trended towards significance (P = 0.06; student's t-test). Only a relatively small induction of nuclear HIF-1α protein abundance was observed in normoxia.

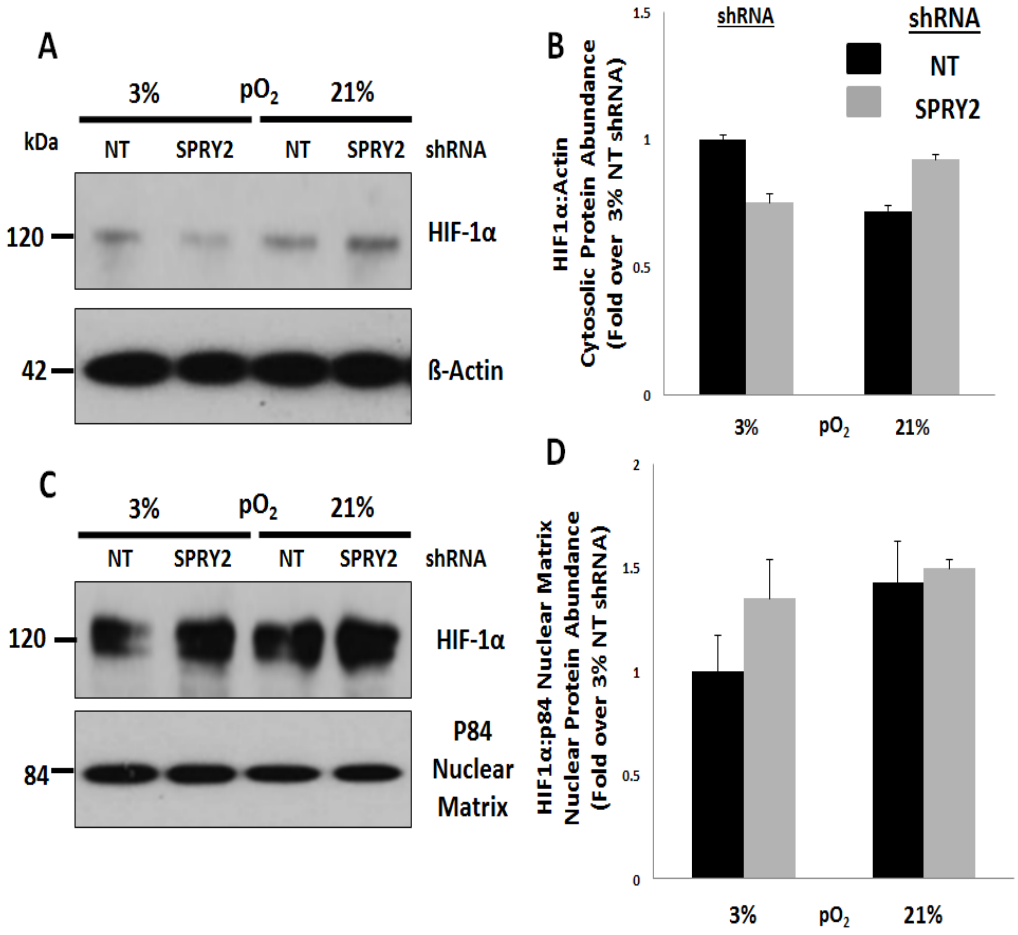

Figure 4.14. HIF-1α cytosolic and nuclear protein abundance in NT and SPRY2 shRNA stable cell lines. Cells were cultured in separate evenly seeded 6-well dishes for approximately 18 hours at both at both fetal and normoxic pO_2 prior to lysis and fractionation. Blots and densitometry shown represent 3 independent experiments where error bars are $\bar{x} \pm$ SEM of fold change. A. Cytosolic HIF-1α protein abundance with ß-Actin blotted as a control for protein loading. B. Densitometric analysis of cytosolic HIF-1α protein. C. Nuclear HIF-1α protein abundance. P84 nuclear matrix was run as a control for protein loading and validation of successful nuclear protein extraction. D. Densitometric analysis of nuclear HIF-1α protein.

Following on from the observation in Figure 4.14, the effect of SPRY2 knockdown on HIF-1α transcriptional activity was examined. Figure 4.15 shows endogenous HIF-1α activity in both NT and SPRY2 shRNA HBE cell lines at both fetal and normoxic pO_2 measured by luciferase reporter gene assay. At fetal pO_2, a small decrease in HIF-1α activity is observed with SPRY2 shRNA relative to the control response. At normoxic pO_2 there is a near 4-fold induction of HIF-1α activity with SPRY2 knockdown. However, this induction is not significant relative to its NT shRNA counterpart (P = 0.09; student's t-test).

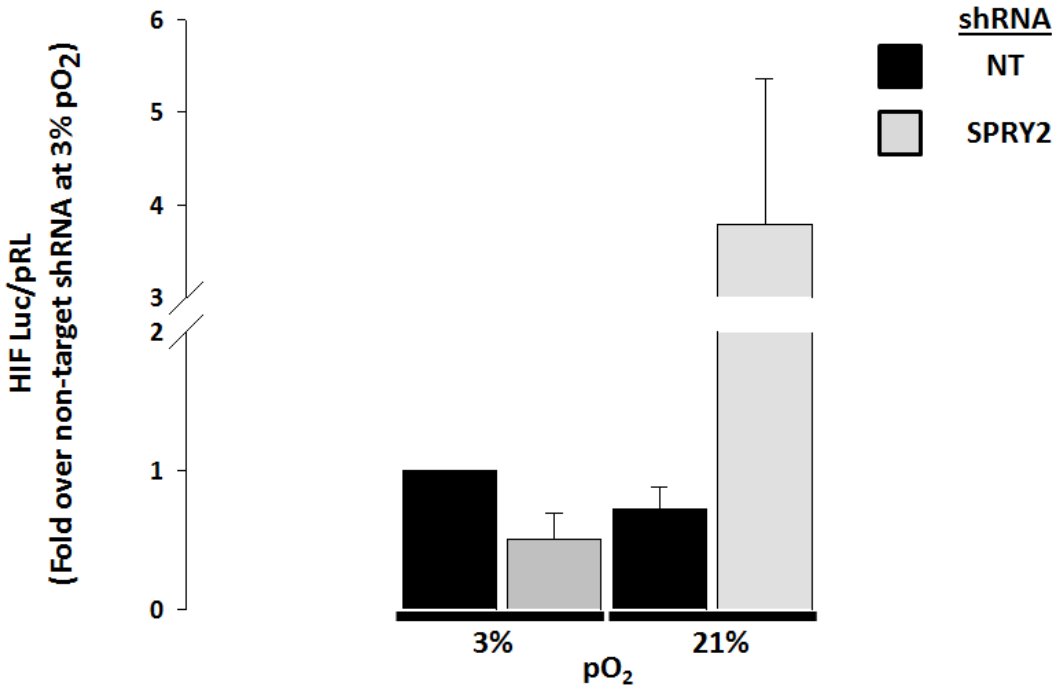

Figure 4.15. HIF-1α activity measured by luciferase reporter gene assay. Activity of HIF-1α is measured as the HIF-luc luminescent response divided by that of pRL. Values generated are expressed as fold change relative to the response observed in the control shRNA at 3% pO_2. Error bars are $\bar{x}$ ± SEM of the fold change (n = 5).

Loss of SPRY2 amplifies VEGF-A gene expression and alters CCND1 and BNIP3 expression.

The impact that SPRY2 knockdown has on HIF-1α led to further investigation as to whether SPRY2 influences expression of the primary gene product of HIF-1α, VEGF-A. Figure 4.16 shows the outcome of qPCR assays which show measurements of VEGF-A gene expression in both NT and SPRY2 shRNAs. At both fetal and normoxic pO_2, VEGF-A gene expression is induced in the SPRY2 shRNA relative to the response observed in its NT shRNA counterpart. This induction was shown to be statistically significant at both fetal and normoxic pO_2.

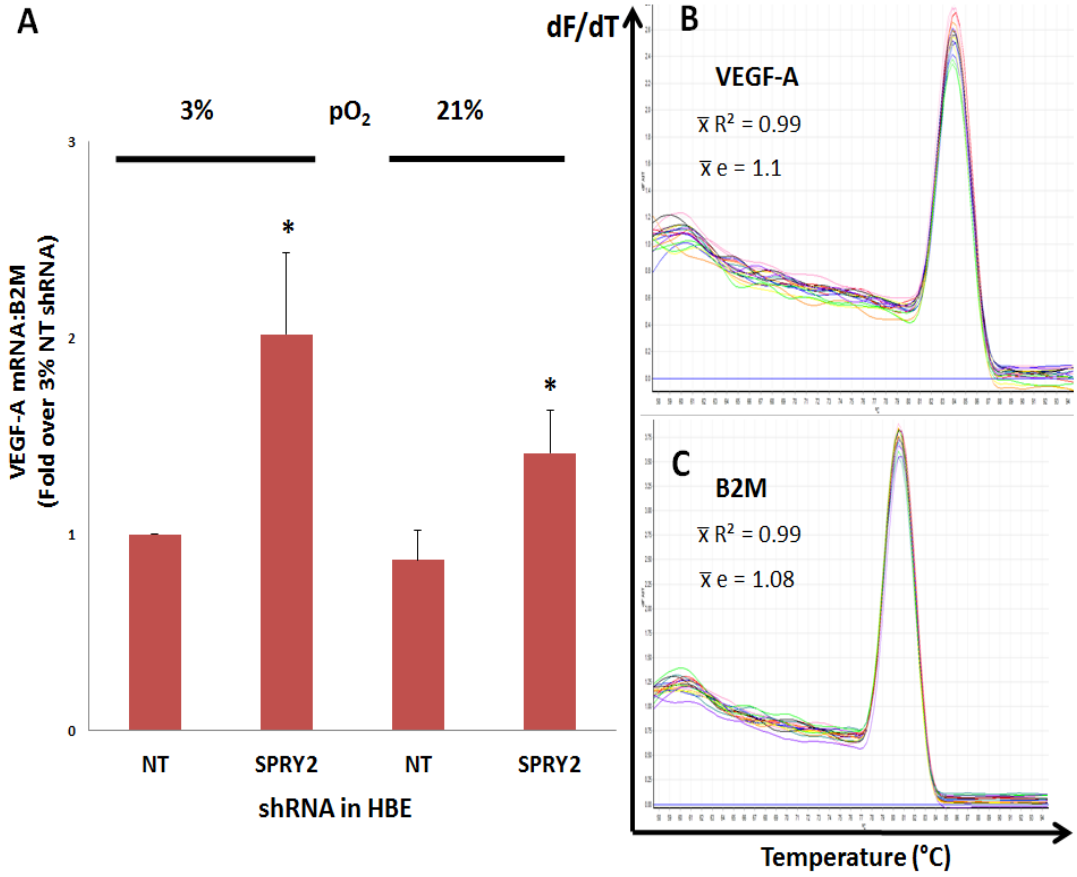

Figure 4.16. qPCR assay of VEGF-A gene expression in both NT and SPRY2 shRNA HBE cell lines. Graphs and melt curves are representative of 4 independent experiments. A. Values generated are VEGF-A mRNA measured over B2M mRNA and graph bars represent fold change relative to the NT 3% shRNA response. Error bars are $\bar{x}$ ± SEM of the fold change. Asterisks in the SPRY2 shRNA denote statistical significance relative to the NT shRNA response at the corresponding pO_2 and statistical analysis was carried out on the raw data ($P < 0.05$; student's t-test). Melt curve representatives for VEGF-A (B) and B2M (C) are shown with their corresponding average efficiency and R^2 values.

Having observed a significant role for SPRY2 in regulating VEGF-A gene expression, the influence of SPRY2 knockdown on the expression of other HIF target genes was investigated. The HIF target genes examined in this study were Cyclin D1 (CCND1) and BCL2/adenovirus E1B 19kDa Interacting Protein 3 (BNIP3). Figure 4.17 shows the effect that SPRY2 knockdown has upon CCND1 (4.16A) and BNIP3 (4.17B) gene expression at both fetal and normoxic pO_2. Regardless of pO_2, a strong suppression of CCND1 gene expression is observed in SPRY2 shRNA relative to the NT shRNA response. This effect is also observed with BNIP3 gene expression but only at normoxic pO_2, whereas BNIP3 expression is actually amplified with SPRY2 shRNA at fetal pO_2. Taking oxygen into account, CCND1 gene expression was found to be greater at normoxia relative to hypoxia and this trended towards significance in NT shRNA HBE ($P = 0.06$; student's t-test), while interestingly, HBE cells harbouring SPRY2 shRNA show a significant induction of BNIP3 gene expression in hypoxia relative to the normoxic response.

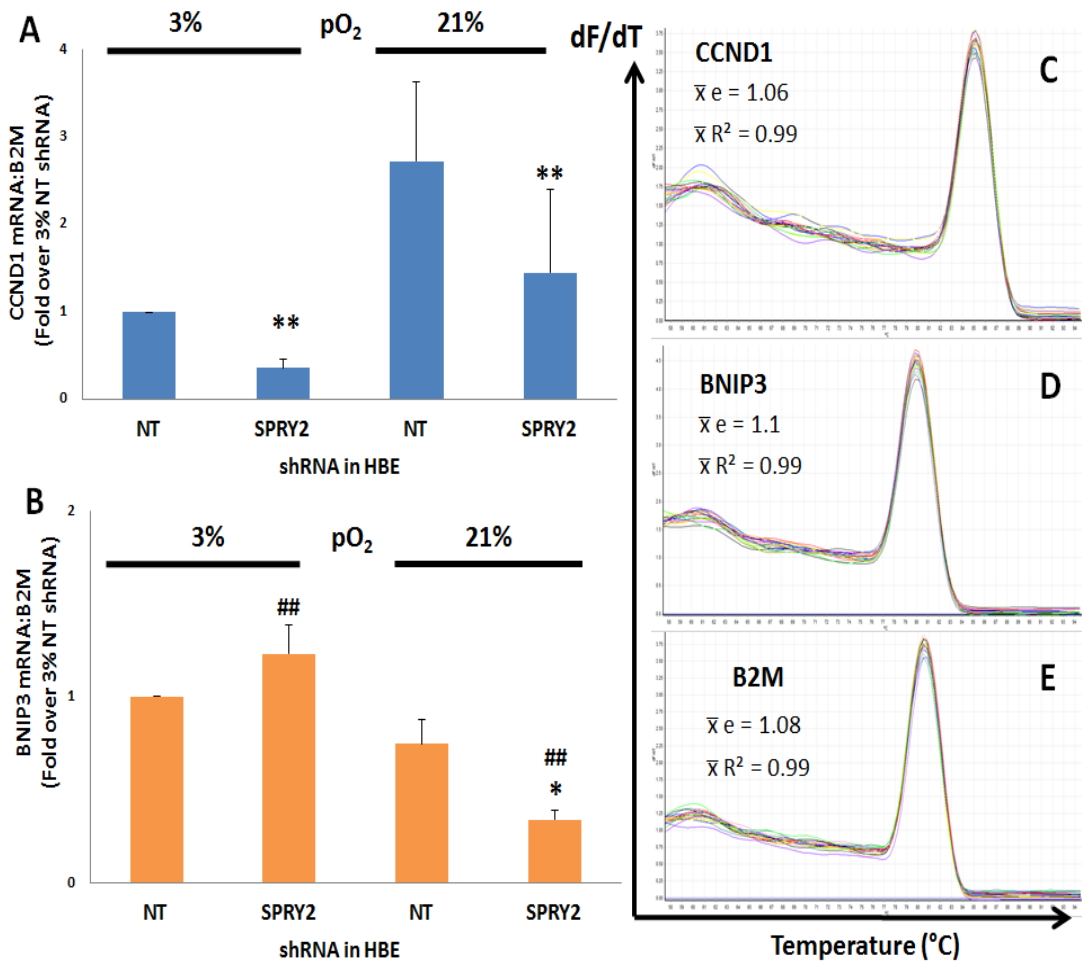

Figure 4.17. qPCR assay of CCND1 and BNIP3 gene expression in both control and SPRY2 shRNA HBE cell lines. Graphs and melt curves are representative of 4 independent experiments. Values generated are CCND1 (A) / BNIP3 (B) mRNA measured over B2M mRNA and graph bars represent fold change relative to the control 3% shRNA response. Error bars are x̄ ±SEM of the fold change. Asterisks in the SPRY2 shRNA denote statistical significance relative to the NT shRNA response at the corresponding pO_2 (* $P < 0.05$; ** $P < 0.01$; student's t-test). Hashtags denote statistical significance between SPRY2 shRNA at both O2 (## $P < 0.01$; student's t-test). Melt curve representatives for CCND1 (C), BNIP3 (D) and B2M (E) are shown with their corresponding average efficiency and R^2 values.

At normoxia, knockdown of SPRY2 shRNA promotes binding of the HIF-1α-CBP/p300 scaffold to the HIF response element on the hVEGF-A promoter.

To link the observations of SPRY2 shRNA-induced VEGF-A gene expression to that of HIF-1α activation, ChIP assays were performed to investigate if knockdown of SPRY2 influenced binding of HIF-1α to the VEGF-A promoter. Figure 4.18 shows the effect that knockdown of SPRY2 by shRNA has on the affinities of HIF-1α and its transcriptional co-activator CBP/p300 to bind to the HRE on the hVEGF-A promoter. At hypoxia, binding of the HIF-1α-CBP/p300 complex to the VEGF-A appeared to be unaltered by SPRY2 shRNA. However, at normoxia, a strong signal for both HIF-1α and CBP/p300 is observed in the SPRY2 shRNA cell line relative to the NT shRNA signal.

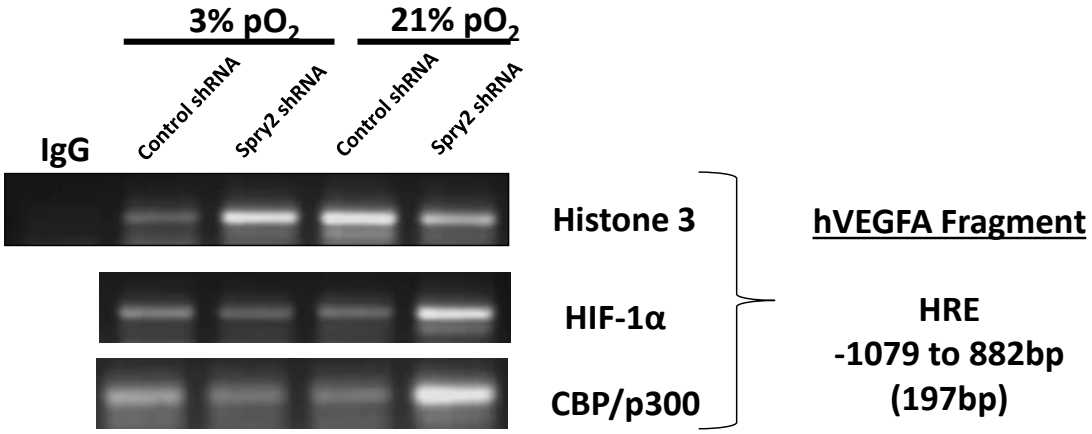

Figure 4.18. ChIP assay showing the interaction of HIF-1α and CBP/p300 with the HRE of the hVEGF-A promoter in both NT and SPRY2 shRNA HBE cells. IgG and H3 chipped DNA were run as negative and positive controls respectively in the qPCR reaction. qPCR reactions were run on 1% agarose gel and were stained with ethidium bromide. Molecular weight of bands observed is 197bp. Results shown are representative of 3 independent experiments.

Discussion

Prior to this study, SPRY2 function in the fetal lung had primarily been described in relation to airway growth, where it acts to antagonise the MAPK pathway through silencing of GRB2 (Casci *et al*., 1999; Tefft *et al*., 2002). However, the data presented in Figure 4.2 suggests a potential role for SPRY2 in directing vascular growth through regulation of HIF-1α activity. Figure 4.19 shows the anticipated configurations of SPRY2 in response to Y55 and SH3 domain mutation.

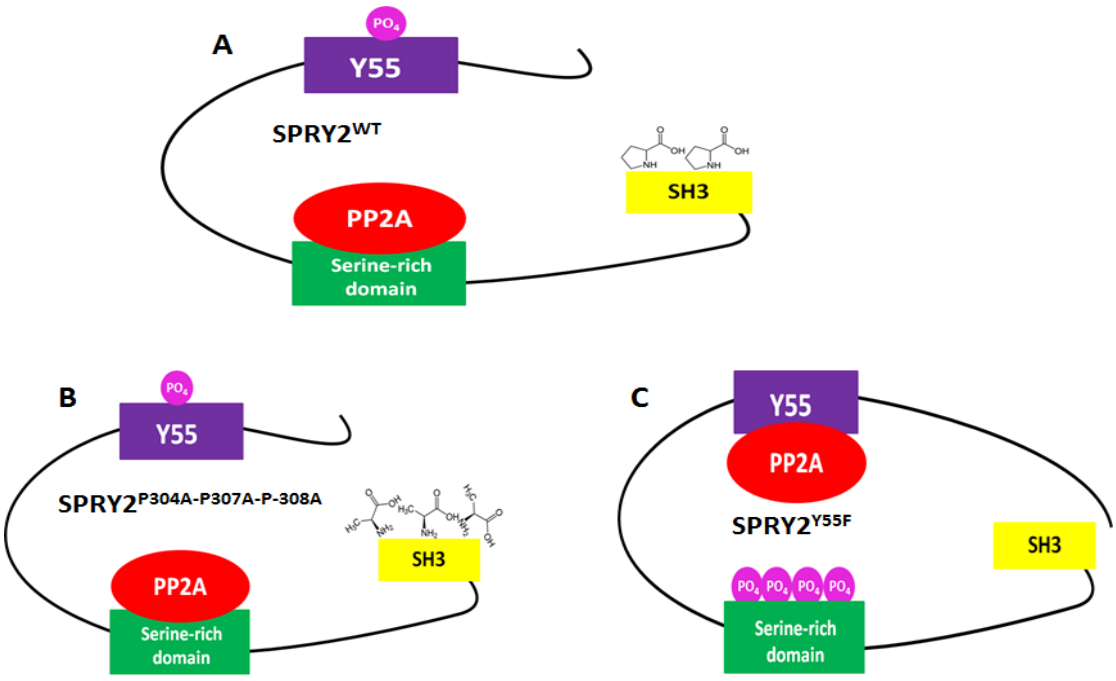

Figure 4.19. Schematic representation of SPRY2 protein structure upon overexpression (A), mutation of the SH3 domain (B) and mutation of the Y55 domain. A. SPRY2 activity is induced upon c-Src phosphorylation of the Y55 domain, which promotes putative interaction of proteins with the SH3 domain. B. While SPRY2 activity is induced, the potential for the SH3 domain to bind other proteins is lost upon mutation of this domain. C. Upon null mutation of the Y55 domain, it is assumed that the SPRY2 remains 'inactive', as c-Src cannot phosphorylate the Y55 domain.

Upon overexpression of SPRY2 (Figure 4.18A), it is assumed that Src-phosphorylation of Y55 occurs, which in turn promotes PP2A-induced dephosphorylation of the serine-rich domain. This consequently allows the SH3 domain to become exposed, whose proline-rich 'anchor' could potentially bind interacting partners of HIF-1α and present them to cCBL for subsequent degradation. Upon mutation of the SH3 binding domain of SPRY2 (Figure 4.18B), HIF-1α activity was initially induced at low levels of transient overexpression but this activity tended to decrease upon increased overexpression of the mutant. Under these circumstances, it is perceived that the potential for SPRY2 to sequester proteins for cCBL-targeted degradation is abolished, which would indicate that the SH3 domain specifically is not involved in regulating HIF-1α activity. Conversely, HIF-1α activity progressively increased upon transient overexpression of the Y55 mutant. This observation concurs with data published from our lab previously (Scott *et al*., 2010), where SPRY2^{Y55F} also produced a rise in HIF-1α activity and VEGF-A secretion. Under these circumstances, it is assumed that upon Y55 mutation, c-Src cannot phosphorylate Y55, the SH3 domain remains concealed and SPRY2 cannot interact with cCBL (Figure 4.18C). This observation suggests that HIF-1α activity is linked to SPRY2 through phosphorylation of its Y55 residue, which in turn promotes interaction of SPRY2 with cCBL, resulting in sequestration and subsequent degradation of HIF-1α interacting proteins, contributing to the loss of HIF-1α activity in the epithelium. One such interacting protein could be CBP/p300, which transcriptionally co-activates with HIF-1α in the nucleus (Land & Tee, 2007). However, attempts at establishing an interaction between CBP/p300 and SPRY2 by Co-IP in this study proved unsuccessful.

Overexpression of SPRY2^{WT} and the Y55/SH3 mutants did not alter P70-S6K, AKT and ERK1/2 phosphorylation relative to endogenous levels observed in WT HBE (Figure 4.3). This observation suggests that the changes in HIF activity induced by SPRY2 protein modification are not mediated by differences in kinase activity. As such, these modifications may directly alter stability of the HIF-1α protein itself. However, experiments have yet to be carried out in order to ascertain this. Furthermore, it should be noted that overexpression of SPRY2^{WT} produced a P70-S6K response near identical to that observed in WT HBE and surprisingly also showed an induction in the activity of AKT and ERK1/2 relative to the expression observed in WT HBE. This observation may have been caused by the HBE cells becoming too saturated with the amount of SPRY2^{WT} DNA transfected and as a result, the kinase activity observed may not be indicative of the true effect of overexpression and/or mutation of SPRY2 protein.

As discussed earlier in this chapter, the function of the CRD of SPRY2 is not well understood. One school of thought suggests that it could act as a membrane targeting sequence and so disruption of this process by mutating C218 or C221 could increase the overall availability of SPRY2 to interact and repress HIF-1α activity. It was hypothesised that this region is involved in DNA binding since the region spanning C218-C221 shares homology with the ZnF domain of RanBP2. Overexpression of the C218A and C221A mutants significantly repressed HIF-1α transcriptional activity (Figure 4.4), which was correlated by the abolishment of SPRY2 interaction with HIF-1α (Figure 4.6) and with the HRE of the VEGF-A promoter (Figure 4.8). This novel finding would suggest the CRD of SPRY2 is responsible for

regulating the degree at which SPRY2 interacts with the VEGF-A promoter and ensures the fidelity of HIF-driven VEGF-A expression. However, this idea is complicated by the observation that HIF protein stability did not change upon DT-SPRY2^{WT} overexpression or CRD mutation (Figure 4.5) and that C218A mutation induced VEGF-A gene expression (Figure 4.7). Taking into consideration the general consensus surrounding the function of the CRD of SPRY isoforms, where it is thought to facilitate membrane translocation of SPRY itself (Impagnatiello *et al*., 2001), it is possible that SPRY2 may interact with HIF-1α directly through binding at C218 and upon membrane translocation, HIF-1α activity could be silenced and thus down-regulate expression of the VEGF-A gene. However, this study does not take into account the ability of both cysteine mutants to induce membrane translocation of SPRY2 so this theory is speculative. The next step in this study would have been to test if SPRY2 palmitoylation is influenced by mutation of both of these cysteine residues. However, time and resources proved to be a limiting factor.

A clearer picture of the role of SPRY2 in vascular signalling emerged using shRNA knockdown of SPRY2; this was consistently observed at the level of protein and gene expression (Figures 4.9 and 4.10) and thus subsequent experiments were conducted in confidence that SPRY2 was expressed at low levels in these cells. At endogenous levels, mTORC1 activity as measured by P70-S6K phosphorylation at Thr^{389} increased in SPRY2 shRNA HBE (Figure 4.11) and this induction trended towards significance. Similarly, ERK1/2 phosphorylation was also induced in SPRY2 shRNA HBE (Figure 4.13). FGF10 dose-dependently induced mTORC1 and ERK1/2 activity in the NT shRNA cells. The former observation accords with Scott *et al*., (2010), which showed

that FGF10 stimulated HIF-1α vasculogenic activity via SPRY2. The ERK1/2 response observed is consistent with several reports that its activity in lung *in vitro* models is induced by FGF10 (Upadhyay *et al*., 2003; Ding *et al*., 2007). However, other studies have reported that attenuated FGF10 stimulation can suppress ERK1/2 phosphorylation (Mailleux *et al*., 2005; Scott *et al*., 2010). The decline in FGF10-induced P70-S6K and ERK1/2 phosphorylation observed in the data suggests that the absence of SPRY2 destabilises the proliferative signal of FGF10 to induce downstream signalling of ERK and mTORC1, which could pose complications for epithelial differentiation of the airway and the vasculature respectively. Furthermore, the data presented here also conflicts with the notion presented by Land (2011), who used evidence from Scott *et al*., (2010) to suggest that FGF10 signalling favours mTOR activity over that of ERK1/2, implying that SPRY2 directs partitioning of the FGF10 signal down either pathway. In that regard, the effect of SPRY2 shRNA coupled with FGF10 stimulation on PI3K activity was examined. As the PI3K pathway is distinct from the MAPK signalling cascade, it was postulated whether SPRY2 directed signalling of FGF10 to mTORC1 down through the PI3K pathway. AKT phosphorylation was low in SPRY2 shRNA HBE relative to NT shRNA levels and this was not recovered by FGF10 stimulation (Figure 4.12). This observation is in agreement with a study by Lito *et al*., (2009), who demonstrated that AKT phosphorylation decreased with down-regulation of SPRY2 and subsequently postulated that SPRY2 prevents DNA-damage induced apoptosis through part-regulation of AKT. This is further supplemented by evidence showing that SPRY2 overexpression results in induced AKT phosphorylation (de Alvaro *et al*., 2005; Sutterlüty *et al*., 2007). To account for the varying kinase response to FGF10

stimulation, more repeats of these experiments would be required. However, time and resources proved to be a limiting factor. In addition to this, both cell lines were seeded at different densities to account for the difference in growth rates between the two cell lines, with the aim of achieving similar levels of cell confluency. This may also have played a role in the varied responses observed in kinase activity. However, the endogenous responses observed were consistent across all experiments.

HIF-1α protein stability was unaffected by SPRY2 shRNA at both fetal and normoxic pO_2 (Figure 4.14). In hypoxia, endogenous HIF-1α activity was slightly lower with SPRY2 shRNA, supporting the view that SPRY2 may act to regulate HIF-1α activation rather than stability. However, VEGF-A gene expression was significantly induced (Figure 4.16), which would suggest that the hypoxic expression of VEGF-A may be induced independently of SPRY2-mediated HIF activation or that SPRY2 might have another function in the nucleus. Surprisingly, HIF-1α activity was vastly induced in SPRY2 shRNA HBE at normoxia (Figure 4.15) and subsequent analysis by qPCR showed that significant up-regulation of VEGF-A mRNA also occurred in the absence of SPRY2 at normoxia (Figure 4.16). HIF-1α can potentially be activated in tumours under normoxic conditions through genetic alterations in the oxygen-signalling pathway (So, 2012). For example, HIF-1α is stabilised in normoxia upon mutation of proline 564 and PHD activity is inhibited upon interaction with Tricarboxylic Acid (TCA) intermediates such as α-ketoglutarate, succinate (Fang *et al*., 2001) and fumarate (Isaacs *et al*., 2005)

Given that SPRY2 acts as tumour suppressor in many organs, including the lung, this novel observation suggests that SPRY2 may ensure activation of HIF-1α only occurs in hypoxia, as its loss correlates with amplified HIF-1α activity in normoxia. This finding conveniently correlates with data from the ChIP assays, which show that in normoxia, HIF-1α and its transcriptional co-activator, CBP/p300, bind strongly to the HRE of the hVEGF-A promoter (Figure 4.18) upon shRNA silencing of SPRY2 in HBE. This would mean that VEGF-A secretion from the epithelium is amplified in the absence of SPRY2 under normoxic conditions, further implying that the oxygen sensing component of HIF-1α, the PHD domain, may be regulated by SPRY2. This idea appears to be supported by the observation that SPRY2 favours interaction with PHD1-3 isoforms during normoxia (Anderson *et al*., 2011). Chen *et al*., (2010) demonstrated that both gene and protein levels of SPRY2 were decreased in response to hypoxia and this in agreement with the protein and mRNA data presented in Figure 4.9 and 4.10 respectively. This would suggest that SPRY2 has its greatest repressive effect at normoxia where it ensures that HIF-1α and its specific target gene, VEGF-A are both activated only in hypoxia.

Besides VEGF-A, SPRY2 appears to also play a role in the regulation of other HIF regulated genes. The data presented in Figure 4.17A shows that CCND1 gene expression was severely down-regulated in SPRY2 deprived HBE in both fetal and normoxic pO_2. CCND1 is an established target gene of HIF-2α (Raval *et al*., 2005), where it functions as a regulator of the G_1/S phase of the cell cycle and is known to form a complex with Cyclin-dependent Kinases (CDK). This complex induces phosphorylation of retinoblastoma protein (pRb) allowing its entry into the S phase

of the cell cycle (Vízkeleti *et al*., 2012). Overexpression of CCND1 disrupts the Rb pathway and is commonly observed in lung carcinomas and Non-small-cell Lung Cancers (NSCLC) and this expression is consistent with the emergence of epithelial tumours in many tissues (Betticher *et al*., 1997). Down-regulation of CCND1 has been shown to induce cell cycle arrest (Sun *et al*., 2008) and the data presented here appears to show that this correlates with silencing of SPRY2. This would suggest that SPRY2 may mediate CCND1 function on the cell cycle but presently there is no evidence that establishes a role for SPRY2 in mediating cell cycle progression. However, given the role of SPRY2 as a tumour suppressor, it is surprising that CCND1 gene expression is not up-regulated in the absence of SPRY2. Regardless of SPRY2 shRNA, CCND1 gene expression was found to be greater at normoxia relative to hypoxia and this trended towards significance in the NT shRNA response. This finding, coupled with the SPRY2 shRNA-induced activity of HIF-1α activity in normoxia, suggests that hyper-activation and overexpression of HIF-1α and CCND1 respectively, may promote tumour formation. Furthermore, this finding is supplemented by the fact that CCND1 expression is enhanced upon silencing of VHL (Bindra *et al*., 2002), where the hydroxylation of the HIF subunits occurs and its subsequent degradation is inhibited.

BNIP3 is a member of the Bcl-2 family of proteins and its expression is up-regulated in hypoxia (Regula *et al*., 2002). Upon induction, BNIP3 localises to the mitochondria where it where it triggers apoptosis of myocytes, neurons and epithelial cells (Jurasz *et al*., 2011). The consensus that BNIP3 expression is induced in response to hypoxia is supported by the data presented here, which shows that BNIP3 gene expression is

greater in hypoxia relative to normoxia regardless of SPRY2 knockdown (Figure 4.17B). However, the absence of SPRY2 further induced BNIP3 expression in hypoxia, whereas at normoxia, BNIP3 gene expression was significantly down-regulated upon SPRY2 knockdown relative to the control response. The loss of BNIP3 is consistent with the formation of tumours, where down-regulation of BNIP3 leads to the failure of tumour cells to apoptose, which clinically results in decreased patient survival (Burton & Gibson, 2009). Given the loss of BNIP3 is induced further by SPRY2 shRNA in normoxia; it would appear that SPRY2 may regulate BNIP3 activation through direct regulation of HIF-1α, thereby suppressing the activity of both HIF-1α and its target gene, BNIP3, at normoxia. However, this result is inconsistent with the hyper-activation of HIF-1α observed under these conditions as shown in Figure 4.15.

Conclusions

Based on the results presented in this chapter, it is possible that SPRY2 plays a role in regulating epithelial development of both the airway and the vasculature. In hypoxia, SPRY2 acts to repress HIF-1α transcriptional activity. Mutation of SPRY2 at the C-terminal SH3 domain relieves this repression, while mutation of SPRY2 at Y55 promotes HIF-1α activity, independent of kinase activity. This study sheds new light on the function of the CRD of SPRY2, whereby mutation of the CRD suppressed HIF-1α activity and abolished SPRY2 interaction with HIF-1α and the VEGF-A promoter, which appears to support the hypothesis that the CRD of SPRY2 acts as a DNA binding domain. The absence of SPRY2 in HBE induces ERK1/2 and mTORC1 activity and also the expression of hypoxia-regulated genes; VEGF-A and BNIP3, whilst at

same time, disrupting the FGF10/FGFR2b feedback loop. This chapter also presents an additional potential nuclear role for SPRY2 whereby it may mediate cell cycle progression through regulation of CCND1. Finally, the results also postulate that SPRY2 acts to repress the activation of HIF and its regulated gene products at normoxia. The results of this and the previous chapter and their implications on the airway and vascular development of the fetal lung will be discussed further in the general discussion.

Chapter 5 - General Discussion

Introduction

Prior to this study, the majority of research on SPRY2 in the developing lung epithelium has primarily focused on its role to antagonise signalling of the FGF10/FGFR2b axis, thereby suppressing the proliferative signal to ERK resulting in reduced airway branching morphogenesis. However, little is known regarding the intimate coordination between growth of the airway and vascular trees and as such little is reported of the role of SPRY2 in regulating the molecular mechanisms that orchestrate this co-ordination. This issue is addressed in this thesis, where the original aim was to establish a potential role for SPRY2 in co-ordinating both airway and vascular development of the epithelium.

Overexpression of SPRY2 inhibits airway and vascular growth of the fetal lung.

Overexpression of the SPRY isoforms has been consistently shown to inhibit growth-factor-induced cell growth and proliferation (Edwin *et al*., 2006). While much of the literature confines SPRY2 function to its role in inhibiting the growth-factor-mediated MAPK signalling cascade, the results presented in this thesis show that overexpression of both $SPRY2^{WT}$ and $DT\text{-}SPRY2^{WT}$ constructs in HBE represses vascular development via HIF-1α transcriptional activity. This observation suggests that SPRY2 is involved in negatively regulating HIF-1α activity, which is further supported by the evidence that knockdown of SPRY2 by shRNA had the opposite effect on HIF-1α activity.

Phosphorylation of SPRY2 at Y55 regulates basal HIF-1α activity.

The earliest experiments examining SPRY2 function established that its activation was linked to tyrosine phosphorylation, with particular emphasis placed on phosphorylation of the Y55 residue (Sasaki *et al.*, 2001; Fong *et al*., 2003). Subsequently, much of the research on SPRY2 function *in vitro* has focused on the manipulation this residue. This led to the creation of the Y55F mutant, which functions by forming heterodimers with endogenous SPRY2 and interferes with binding of SPRY2 to its targets in the MAPK pathway (Wietecha *et al*., 2011). Sutterlüty *et al*., (2007) confirmed this in lung cells by showing that overexpression of SPRY2^{Y55F} resulted in the failure of SPRY2 to inhibit ERK phosphorylation. In this thesis, SPRY2^{Y55F} overexpression significantly up-regulated endogenous HIF-1α activity and this observation occurred independently of FGF10 stimulation and kinase signalling activity. This indicates that endogenous SPRY2 acts to antagonise HIF-1α activity as it does with MAPK signalling. This is further supplemented by the observation that knockdown of SPRY2 by shRNA promoted both endogenous ERK1/2 and mTORC1 phosphorylation, thus linking the inhibitory function of SPRY2 to both airway and vascular signalling cues.

The SH3 domain of SPRY2: a docking station for G-proteins?

Further experimentation with modifying SPRY2 function led to the discovery of a proline-rich C-terminal domain; the *PXXPXR* motif, termed here the SH3-binding motif. Lao *et al*., (2006) made a series of point mutations within the *PXXPXR* motif of SPRY2 and subsequently demonstrated a reduction in the ability of SPRY2 to bind to

GRB2 within the MAPK pathway. This observation proved that the SH3 binding domain of GRB2 can bind to the proline-rich P*XXPX*R motif of SPRY2. The results in this thesis surprisingly did not show an increase in ERK1/2 phosphorylation upon SH3 mutation of SPRY2. However, HIF-1α activity was induced, suggesting that the SH3 domain may act in concert with the Y55 domain to repress HIF-1α activity. Given that the SH3 motif of SPRY2 can interact with GRB2, a G-protein consisting of a SH3-SH2-SH3 domain configuration, it is possible that this region of the SPRY2 protein can interact with other SH3-domain-containing proteins that are known to regulate mTORC1 expression, which is required for HIF-1α activation. Evidence to support this hypothesis is provided by Ying *et al*., (2010), who described that Ras-related C3 Botulinum Toxin Substrate 1 (RAC1), a known regulator of mTORC1 (Saci *et al*., 2011), is inhibited via SPRY2 interaction with the SH3 domain of ßPix; a membrane-targeting Guanine Nucleotide Exchange Factor (GEF) protein required for RAC1 activation. Furthermore, a recent publication from Kim *et al*., (2012), demonstrated that SH3 Domain-binding Protein 4 (SH3BP4) binds to the Recombination Activating Genes (RAG) GTPase complex through its SH3 domain resulting in the failure of this complex to become activated, which leads to a suppression of mTORC1 activity. The identification of SH3 binding sites on several GAP members such as RasGAP (Bos *et al*., 2007) and RAC1 provide further credence for their potential to interact with SPRY2. Therefore, it is possible that SPRY2 may act as a docking station for SH3 containing proteins, particularly G-proteins (considering GRB2 is a known binding partner). The SH3 binding domain then presents these proteins to cCBL, which is bound to the Y55 domain of SPRY2, where it functions to degrade and silence the activity of proteins bound to the SH3 binding motif.

Regulation of basal vascular signalling by SPRY2 occurs independently of the PI3K/AKT signalling cascade.

The results presented in this thesis show that endogenous AKT phosphorylation was unaffected upon modifications made to the SPRY2 protein. This would suggest that SPRY2 antagonises mTORC1 activation independently of PI3K activity. Several studies have indeed reported that S6K phosphorylation at Thr^{389} is PI3K-independent (Tamburini *et al*., 2009; Park *et al*., 2010). If this is the case, then something else must be driving the activation of mTORC1. A possible candidate for this could be Rheb; where its overexpression has been reported to induce mTOR signalling independently of PI3K activation (Goodman *et al*., 2010). This observation is reflected in data from Scott *et al*., (2010), who showed that mTORC1 activity was induced via S6K phosphorylation at Thr^{389} through co-expression of Rheb and HIF-1α in Human Epithelial Mesenchymal Lung Fibroblast Cells (HELMF). However, it is unclear if Rheb interacts with SPRY2 as it is not known to possess a SH3-binding domain. To complicate matters further, it has been established that amino acid-induced activity of mTORC1 can occur independently of Rheb, by means of RAG-GTPase catalysis (Kim *et al*., 2008).

Silencing SPRY2 disrupts the FGF10/FGFR2b/SPRY2 feedback mechanism.

The results in this thesis establish that knockdown of SPRY2 could pose implications on the co-ordinated development of the airway and the vasculature as both ERK1/2 and mTORC1 activities are induced at endogenous levels. The observation that AKT expression was repressed upon SPRY2 shRNA provides further evidence that

downstream regulation of mTORC1 by SPRY2 occurs independently of the PI3K/AKT signalling cascade. As alluded to in the results, SPRY2 shRNA appeared to also destabilise the FGF10 proliferative signal that promotes protein-kinase activity, which provides further evidence that SPRY2 is a vital component of the negative feedback mechanism that governs FGF10 stimulation. This suggests that disruption of the FGF10/FGFR2b/SPRY2 feedback mechanism could lead to unsustained proliferation of both airway and vascular signalling. Thus, it would appear that this feedback mechanism is dependent upon SPRY2 acting as 'molecular clock' where it is responsible for regulating the duration of the FGF10 signal, which would imply that SPRY2 is responsible for directing the bifurcation of the developing airway. This idea is discussed at length by Scott *et al*., (2010) who described the FGF10/FGFR2b/SPRY2 relationship as an 'airway branching periodicity regulator' which also factors in HIF-1α driven vasculogenesis. However, it is possible that this mechanism may extend to the nucleus where SPRY2 potentially facilitates the unwinding of DNA from its histone core in a time-dependent facet. It should be noted that FGF10 treatment on these cells was carried out at a dose-dependent rate so it may have been more informative to have carried out a time-course experiment to establish if SPRY2 expression was altered in a time-dependent manner upon FGF10 stimulation.

While this study is confined to examining the SPRY2-FGF10 feedback mechanism, SPRY2 activity is also linked in a feedback mechanism with other growth factor transmembrane complexes, such as the EGF receptor (EGFR). In a similar mechanistic activity to FGFs, EGFR dimerisation induces signalling of both the MAPK and PI3K/AKT pathways promoting cell growth and migration respectively. Their role

in lung development is to promote maturation of the ATII cells and the secretion of surfactant (Li *et al*., 2012). However, unlike FGF10, overexpression of SPRY2 has been reported to enhance EGFR signalling preventing its interacting with cCBL (Kim & Bar-Sagi, 2004). Therefore it may have been informative to also examine the effect of modifying SPRY2 function upon EGF signalling in the lung epithelium.

SPRY2 regulates both airway and vascular signalling.

Scott e*t al*., (2010) reasoned that SPRY2^{Y55F} permits Rheb-GTP driven activation of mTORC1 since the mutant is incapable of binding cCBL and direct targeted degradation of the TSC1/2 complex that is responsible for inhibiting mTORC1 signalling activity. However, the mechanism behind the interaction between SPRY2 and TSC1/2 is unknown. It is also unclear if there is a role for the SH3-binding motif of SPRY2 in regulating this process or if indeed the TSC1/2 complex interacts with this motif. Therefore, this thesis predicts a new mechanism by which mTORC1 activity is directly regulated by SPRY2, which deviates from that described by Scott *et al*., (2010) (Figure 5.1). The SH3 domain of a GAP (e.g. RAC1, RAG GTPase) that is known to constitutively activate mTORC1, binds to the C-terminal *PXXPXR* motif on SPRY2 where it is targeted for degradation by cCBL. This causes inhibition of mTORC1 activity resulting in the failure of HIF-1α to translocate to the nucleus and induce the expression of vascular genes. Conversely, putative interaction of TSC1/2 to the *PXXPXR* motif would promote uncoupling this complex allowing Rheb-GTP catalysis and the activation of mTORC1. While this new model is comprised of evidence from the results in this thesis and that of the literature, there is no experimental basis to establish the ability of the *PXXPXR* motif of SPRY2 to

specifically interact with GAP proteins bearing SH3 binding domains. It is also unknown if this motif selectively targets any SH3-domain-containing proteins or if indeed these proteins will compete with each other for binding to SPRY2. In order to prove this, a Co-IP assay could be setup to see if GAP proteins interact with SPRY2 and if any putative interaction is abolished by mutation of the *PXXPXR* motif of SPRY2.

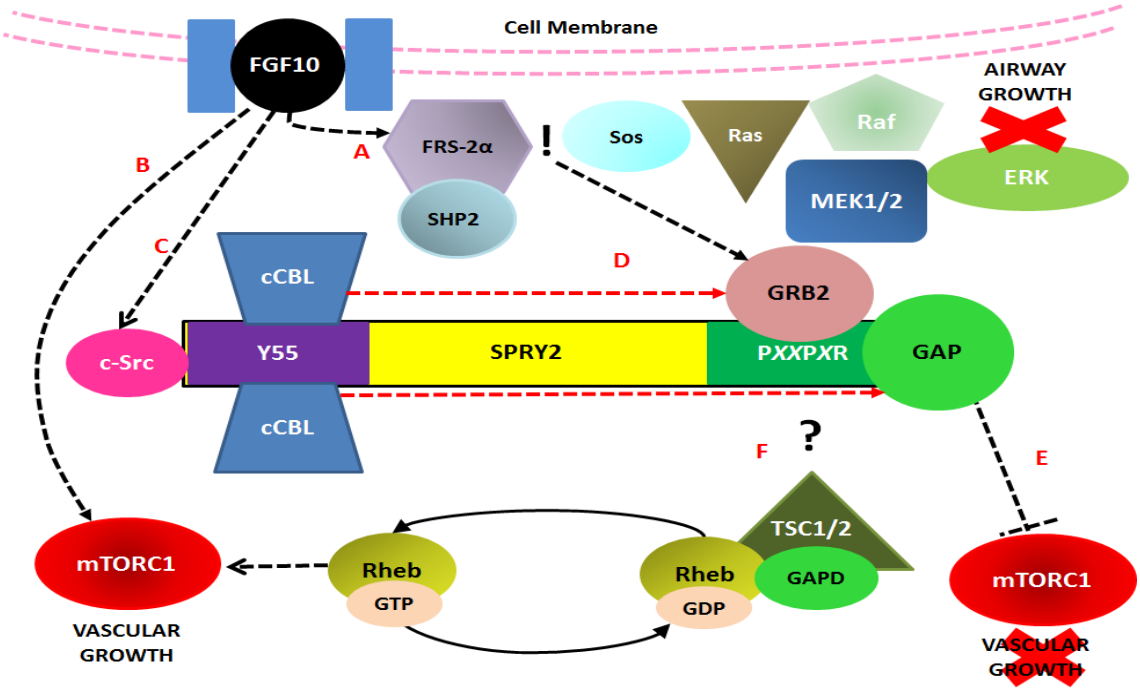

Figure 5.1. Model of SPRY2 regulating co-ordinated airway and vascular signalling of lung epithelium. A. FGF10 stimulates RTK signalling of the MAPK pathway at the cell membrane. B. FGF10 also stimulates activity of mTORC1 downstream, independently of PI3K/AKT activity. C. c-Src binds to the Y55 domain of SPRY2 upon FGF10 stimulation and phosphorylates SPRY2 permitting exposure of the cryptic C-terminal *PXXPXR* domain and the interaction of cCBL with SPRY2 at Y55. D. GRB2 is sequestered by the proline-rich *PXXPXR* motif of SPRY2 where it is subsequently degraded by cCBL (red dashed arrow). The net effect is a disruption of the MAPK signalling cascade and a failure of ERK to signal growth of the airway towards the FGF10 stimulus. E. Vascular signalling is inhibited through the interaction between SPRY2 and the SH3 binding sites of GAP proteins at the *PXXPXR* motif. These GAP proteins are subsequently silenced by cCBL interaction in a similar mechanism to that of GRB2 sequestration by SPRY2. F. Putative interaction between the TSC1/2 complex and the *PXXPXR* motif permits Rheb-GTPase driven mTORC1 activity as originally speculated by Scott *et al.*, (2010).

Could SPRY2 regulate the oxygen-sensing component of HIF-1α?

At normoxia, HIF-1α is targeted for destruction which occurs through O_2-dependent hydroxylation of proline residue by pVHL E3 ubiquitin ligase (Maxwell *et al*., 1999; Bruick & McKnight, 2001). Knowles *et al*., (2006) determined that a lack of hydroxylation of at least one of the prolyl residues was responsible for the expression of HIF-1α in normoxia. However, this induction in HIF-1α expression was caused through application the potent tumour promoter drug, Phorbol 12-myristate 13-acetate (PMA). The alternative approach in this study was to silence the known tumour suppressor gene SPRY2, which resulted in a hyper-activation of HIF-1α expression in normoxia and was complemented by the enhanced interaction between HIF-1α and CBP/p300 to the VEGF-A promoter. This suggests that SPRY2 may act upon the oxygen sensing capabilities of HIF1α under normoxic conditions. A possible explanation for this is that SPRY2 may interact with the pVHL E3 ubiquitin ligase in normoxia, upon which it permits pVHL to administer degradation of HIF-1α. Evidence to suggest this primarily stems from the fact that SPRY2 can interact with a number of other E3 ubiquitin ligases. While the interaction between SPRY2 and cCBL is well-defined, another E3 ubiquitin ligase known to interact with SPRY2 is Seven-in-Absentia Homolog 2 (SIAH2), where it acts to regulate SPRY2 protein stability and sustain MAPK activity independently of RTK-induced tyrosine phosphorylation of SPRY2 (Nadeau *et al*., 2007). Additionally, SIAH2 is also responsible for regulating the stability of the PHD1 and PHD3 domains of HIF-1α in hypoxia, whilst ensuring that HIF-1α transcriptional activity is prevented at normoxia (Nakayama *et al*., 2004; Qi *et al*., 2008). Given this dual function of SIAH2, it is possible that SPRY2 may act to

present SIAH2 with the PHD domains of HIF-1α, much like the mechanism whereby SPRY2 presents cCBL with its substrates in order to inhibit ERK and potentially mTORC1 activity. Anderson *et al*., (2011), established through Co-IP that SPRY2 preferentially interacts with pVHL in normoxia which provides further credence for a role for SPRY2 in regulating HIF-1α stability. Additionally, by mutating the proline residues on SPRY2, Anderson *et al*., (2011) showed that the interaction between SPRY2 and pVHL was severely diminished and SPRY2 protein had stabilised. This confirmed a mechanism whereby SPRY2 too is hydroxylated by PHDs and is subsequently destroyed by pVHL E3 ubiquitin ligase. This suggests that a potential feedback mechanism occurs between pVHL targeted degradation of HIF-1α and SPRY2. However, where exactly pVHL interacts with SPRY2 has not yet been established and it is also unclear if this process disrupts the potential for mTORC1 to interact with HIF-1α and induce its nuclear translocation. Given that this thesis has examined the role of the proline-rich SH3 motif of SPRY2, it could be possible to assess if pVHL would fail to interact with SPRY2 upon mutation of its SH3 binding motif. This would present an additional means whereby SPRY2 regulates HIF-1α activity, which is independent of mTORC1 activity but dependent on oxygen. In order to link both SIAH2 and pVHL function upon HIF-1α with their ability to interact with SPRY2, a model is presented in Figure 5.2. This model demonstrates a putative mechanism whereby SPRY2 presents either E3 ubiquitin ligase SIAH2 or pVHL with the PHD of HIF-1α, where it can direct degradation of this protein in normoxia.

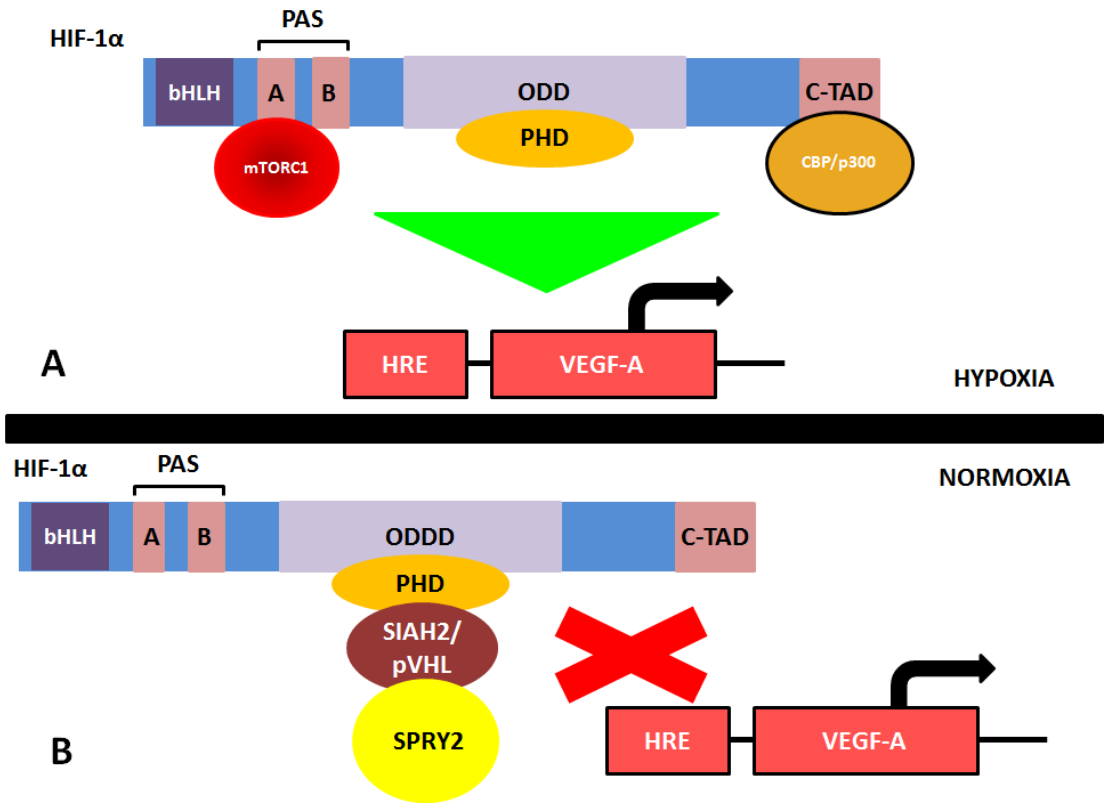

Figure 5.2. Model of SPRY2-mediated HIF-1α activity in hypoxia and normoxia. A. In hypoxia, mTORC1 binds to a TOS motif within the first PAS domain (Land & Tee, 2007) near the N-terminal bHLH domain. Upon nuclear translocation, CBP/p300 binds to the C-TAD of HIF-1α and induces transcriptional activity of VEGF-A. B. SPRY2 presents the SIAH2 or pVHL E3 ubiquitin ligase to target degradation of the PHD on HIF-1α and silence its activation, thus preventing transcriptional activation of VEGF-A.

The role of the CRD of SPRY2: does it regulate VEGF-A expression in a HIF-dependent manner?

The results presented in this thesis provide indication of a novel role for the CRD of SPRY2. Mutation of C218 and C221 suppressed HIF-1α activity and this was accompanied by the failure of both of these mutants to bind to the HRE of the VEGF-A promoter. This suggests that the CRD of SPRY2 plays an important role in regulating the extent at which SPRY2 functions to repress HIF-driven VEGF-A expression. In light of the ZnF binding homology with RanBP2, the putative ZnF domain of SPRY2 may be involved in recruiting HIF-1α away from the HRE of the VEGF-A promoter, thus preventing its transcriptional activation. If this is the case, then HIF-1α must directly interact with SPRY2. This is supported by the evidence in Figure 4.6, whereby SPRY2 was shown to interact with HIF-1α, which further suggests that a complex may exist between these two proteins. Furthermore, the results from this experiment showed that cysteine mutation abolished this interaction, which further supports the hypothesis that the CRD of SPRY2 is responsible for directing HIF-1α driven transcriptional activation of VEGF-A.

On the other hand, these hypotheses are complicated by the observation that HIF-1α protein abundance was unaltered across each cell line and mutation of C218A actually induced VEGF-A gene expression, which suggests that VEGF-A expression may occur via a HIF-independent mechanism. The VEGF-A promoter is comprised of a number of different of DNA-binding sites, which bind transcription factors that are responsible for up-regulating VEGF-A gene expression, independently of HIF. Two of these sites were examined on the hVEGF-A promoter in this study, the STAT3 and

GC-rich Sp1/3 transcription factor binding sites located further downstream. However, problems were encountered with the ChIP assay analysis in this study in trying to establish binding of SPRY2 and the mutants at these regions, so it is difficult to ascertain if SPRY2 may regulate VEGF-A in a HIF-independent manner.

STATS are a group of transcription factors that become phosphorylated upon RTK and/or cytokine activity, resulting in their subsequent translocation to the nucleus where they bind to promoters of genes and regulate their transcriptional activity (Yu & Jove, 2004). Interestingly, STAT phosphorylation can also be induced from the activity of non-RTKs such as Src kinase (Yu *et al*., 1995), which is also known to phosphorylate SPRY2. The STAT3 isoform has been shown to correlate with VEGF production in a variety of human cancers and previous ChIP assays by Niu *et al*., (2002), revealed that STAT3 binds to the VEGF promoter *in vivo* and thus directly regulates VEGF gene expression. This was confirmed by the observation that mutation of the STAT3 binding domain abolished VEGF gene expression. Further ChIP assays by Gray *et al*., (2005) showed that there is evidence to suggest that STAT3 and HIF-1α bind to the VEGF promoter simultaneously upon Src activity. They also demonstrated by Co-IP that both HIF-1α and STAT3 interact with each other, which led to the conclusion that it is possible that HIF-1α and STAT3 could form a complex on the VEGF promoter as the HRE and STAT3 binding sites are in close proximity. This observation draws interesting parallels with the results in this thesis as like STAT3, SPRY2 was shown to Co-IP with HIF-1α and bind to the VEGF-A promoter. Therefore it is possible that like STAT3, SPRY2 could complex with HIF-1α on the VEGF-A promoter and direct transcriptional regulation of the VEGF-A gene.

The next step to establish this would be to demonstrate by Co-IP if SPRY2 also interacts with STAT3.

Sp1 and its repressor Sp3 are also critical regulators of HIF-independent VEGF-A gene expression and function downstream near the transcriptional start site in GC-rich regions, which are highly susceptible to methylation. Milanini-Mongiat *et al*., (2002), showed that phosphorylation of Sp1 upon ERK activation promotes VEGF expression and mutation of the serine and threonine residues of Sp1 subsequently abrogated VEGF expression. Furthermore, Sp1 up-regulation of VEGF transcriptional activity is thought to occur downstream of PI3K activity in a HIF-independent manner (Choi *et al*., 2011). The interaction between SPRY2 and these DNA-binding sites suggests that SPRY2 regulation of VEGF-A gene expression may occur via both HIF-independent (through GC-rich domain binding) and/or HIF-dependent mechanisms (via complex formation with HIF-1α and STAT3).

Given the hypothesised role of the CRD in facilitating SPRY membrane localisation (Lim *et al*., 2000), an assay to measure protein palmitoylation such as that designed by Forrester *et al*., (2011), could've been conducted to assess whether mutation of SPRY2 at C218A/C221A affected the ability of SPRY2 to traffic to the cell membrane, as established by Impagnatiello *et al*., (2001). Given that SPRY2 translocates to the plasma membrane in response to FGF10 (Lim *et al*., 2000) this would suggest that mutation of the CRD would lead to a disruption of the SPRY2 inhibitory action upon both the MAPK and mTORC1 signalling pathways. To link CRD function of SPRY2 to that of the Y55 and *PXXPXR* motif, it may have been intuitive to conduct experiments

examining kinase activity which would've provided further insight if the CRD of SPRY2 affected both MAPK and mTORC1 signalling pathways.

The nuclear role of SPRY2: an epigenetic regulator of gene expression?

The major finding of this thesis was the novel discovery of SPRY2 protein in the nucleus in both cultured *ex vivo* FDLE and *in vitro* HBE. While nuclear localisation of SPRY2 has been reported only in mouse embryonic fibroblasts (Ahn *et al*., 2010) and neuronal cells (Aranda *et al*., 2008), its function in the nucleus remains unknown. Given that the results show a correlation between the FGF10-induced loss of full-length SPRY2 and the increase in H3 phospho-acetylation, a new role for FGF10 is described in this thesis whereby FGF10 induces unwinding of DNA from their histone core, which is catalysed by histone acetyltransferase activity, leading to increased gene expression. This occurs in the absence of full-length SPRY2, whose expression correlates with that of HDAC1 and 2. This would mean that SPRY2 could act to repress mitotic initiation and subsequent gene expression and this effect is relieved by dose-dependent FGF10 stimulation.

As FGF10 is known to induce the signalling pathways that govern airway and vascular development, it is assumed that FGF10 would induce the major vascular gene product, VEGF-A and the results in this thesis show a trend for this to be the case. Furthermore, SPRY2 was shown to interact with the VEGF-A promoter, particularly at regions spanning CpG methylation sites. As alluded to in the results, these CpG islands are in close proximity to the transcriptional start site and are susceptible to DNA methylation through interaction with methyl-CpG-binding proteins, which can

lead to gene silencing (Nan *et al*., 1997). An example of such a protein is Methyl CpG Binding Protein 2 ($MeCP_2$), which is expressed in lung tissue and has been shown to bind to and methylate CpG domains on the Peroxisome Proliferator-activated Receptor-gamma (PPAR-γ) promoter (Joss-Moore *et al*., 2011), a nuclear receptor that is expressed in airway epithelium and regulates both lung epithelial cell differentiation and gene expression (Wang *et al*., 2001). Considering that both DNA methylation and histone deacetylation interplay to silence gene expression and that deacetylation appears to correlate with SPRY2 expression (as shown in Figure 3.6), it is possible that SPRY2 acts to antagonise transcriptional activation through either or both of these processes in order to regulate the interaction of transcription factors (such as Sp1/3) with the GC-rich domain.

In order to collate these observations, a model is presented in Figure 5.3, postulating the mechanism behind FGF10-induced gene expression, which is antagonised by SPRY2 activity. However, this model does not take into account if SPRY2 regulates airway growth in a similar manner. A potential experiment to test this would to measure the expression of genes that are hallmarks of the MAPK pathway, such as Interleukin 1ß (IL-1ß), IL-6 and IL-8, which were shown to be sensitive to specific MAPK inhibitors (Hedges *et al*., 2000).

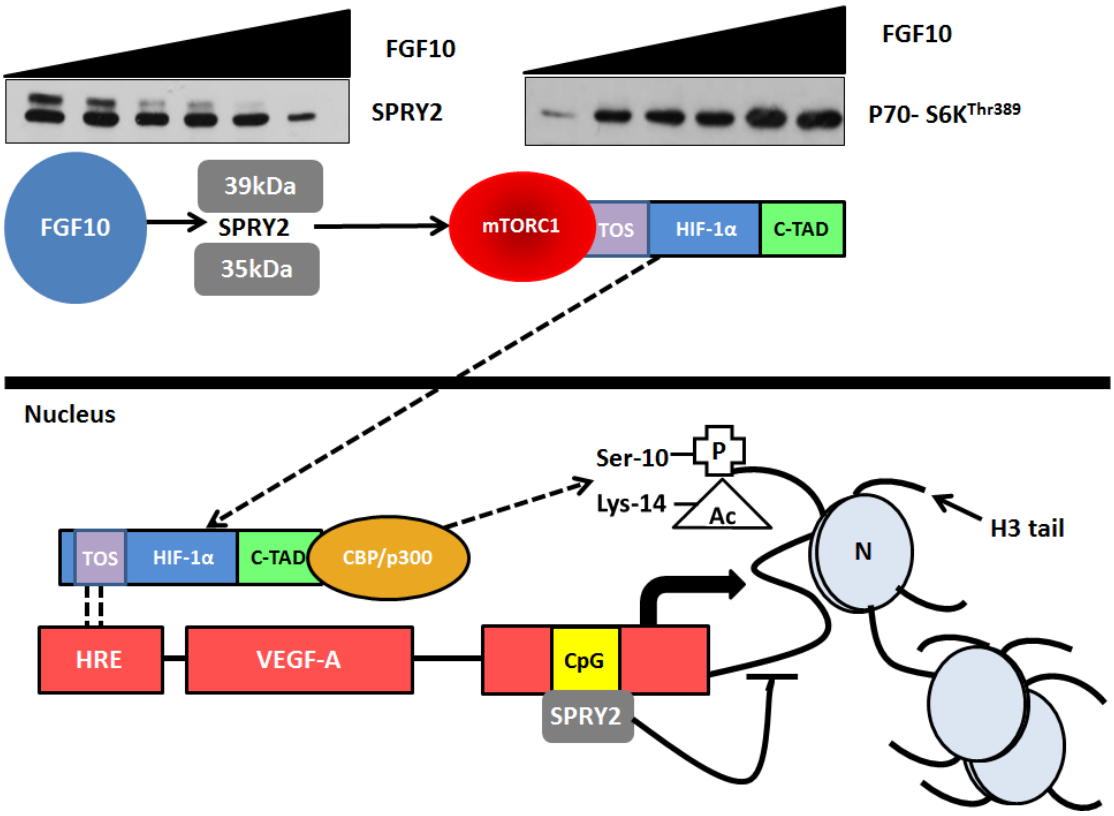

Figure 5.3. Proposed model of vascular gene expression induced FGF10 evoked 'cleavage' of SPRY2. The loss of full-length SPRY2 permits FGF10-induced activation of mTORC1 which binds to the TOS motif on HIF-1α signalling its translocation to the nucleus. In the nucleus, the histone acetyltransferase CBP/p300 binds to the C-TAD domain of HIF-1α and this complex binds to the HRE of the VEGF-A promoter. Simultaneously, CBP/p300 catalyses the phosphate and acetyl groups exposed on the Histone 3 tails, leading to unwinding of the VEGF-A DNA from its Histone core and thus increasing the potential for transcriptional activation and subsequent gene expression. Transcriptional activation is governed by SPRY2 interaction with the CpG island domain inducing methylation and silencing of the promoter thereby inhibiting VEGF-A gene expression.

The ideas presented in this thesis also suggest a more global role for SPRY2 as a key regulator of cell division. Evidence to support this hypothesis is provided by Tang *et al*., (2011), who showed that the loss of SPRY2 function resulted in the abnormal mitotic arrangement of the spindle fibres, which led to abnormalities in airway shape and also conveniently correlated with increased ERK1/2 activity, albeit through the use of mathematical models. The results presented in this thesis provide more insight into a potential role for SPRY2 in regulating mitotic cell cycle activity, where a loss of SPRY2 was shown to have an adverse effect on gene expression, particularly that of CCND1, whose expression was severely compromised upon SPRY2 knockdown in HBE. Complimenting this finding is a study by Mayer *et al*., (2010), who conducted northern blot experiments to show that SPRY2 RNA is expressed during the exit phase of the cell cycle. This publication also demonstrated SPRY2 expression declined in the G_1/S boundary of the cell cycle, which they attribute to cCBL interaction. However, this study fails to establish a potential function for SPRY2 in regulating the cell cycle. The results from this study appear to suggest that SPRY2 may act to direct cell-cycle progression by regulating the expression of CCND1. To further investigate this possibility, a microarray experiment could be used to identify if SPRY2 is indeed a regulator of the cell cycle, much like the one conducted by Whitfield *et al*., (2002), who isolated mitotic Human Cancer Cell Line Cells (HeLa) and manufactured cDNA microarrays to determine a library of cell-cycle regulated genes. However, the capacity to conduct such an experiment was unavailable.

SPRY2: the missing link that coordinates airway and vascular growth of the fetal lung.

The results in this thesis have presented an argument that SPRY2 acts an antagonist of growth-factor induced airway and vascular growth, coupled with the novel observation that SPRY2 is present in the nucleus where it potentially acts to repress gene expression. In order to link these two functions together and thus establish SPRY2 as a key regulator of co-ordinated lung airway and vascular development, a model has been constructed describing the mechanism behind co-ordinated airway and vascular growth of the fetal lung (Figure 5.4), which expands upon the integrated model of airway and vasculogenesis described by Scott *et al*., (2010).

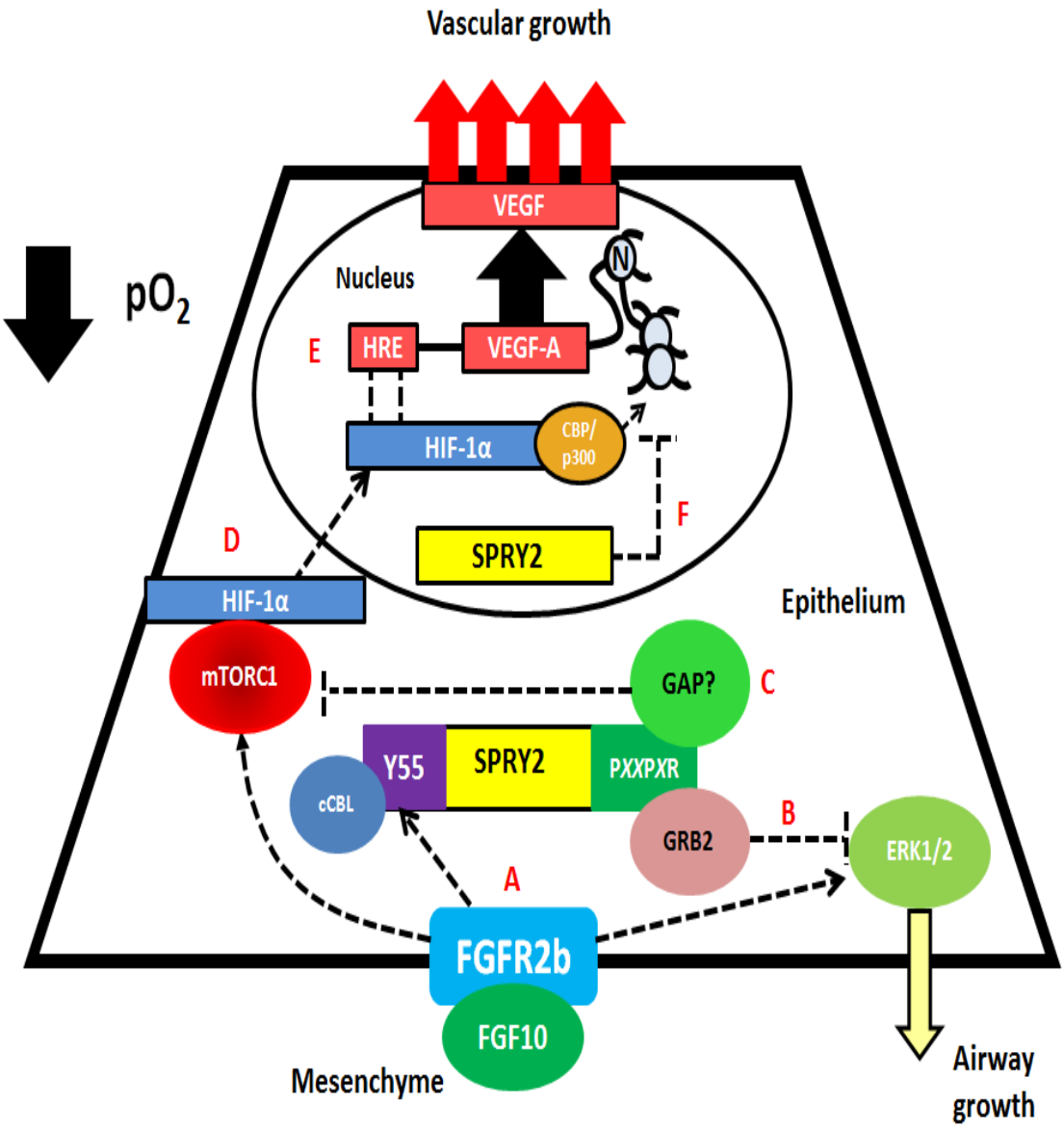

Figure 5.4. Model of co-ordinated airway and vascular growth regulated by SPRY2 in the fetal lung. A. FGF10 binds to its receptor FGFR2b at the leading edge of the airway tip where it signals downstream activation of ERK1/2 and mTORC1, whilst also inducing phosphorylation of SPRY2 at its Y55 domain. B. Phosphorylation of SPRY2 at Y55 exposes the C-terminal *PXXPXR* (SH3) motif where it recruits GRB2 from the MAPK signalling cascade. Subsequent silencing of GRB2 by cCBL results in the failure of ERK1/2 to become activated and airway growth is halted. C. Putative interaction between a GAP and the *PXXPXR* motif of SPRY2 leads to the inability of the GAP to activate mTORC1 in a PI3K-independent manner. D. In the event that mTORC1 is activated upon FGF10 stimulation, mTORC1 binds to HIF-1α and induces

its translocation to the nucleus. E. Upon nuclear translocation, HIF-1α promotes VEGF-A gene expression and subsequent vascular growth through interaction with its transcriptional co-activator, CBP/p300. F. SPRY2 acts to repress histone acetyltransferase activity through binding to 'CpG island' methylation sites on the VEGF-A promoter and subsequently silences transcriptional activation of the VEGF-A gene.

The clinical significance of SPRY2.

Lung cancer is the major cancer-related death worldwide and approximately 1.3 million people die annually from this disease (Lockwood et al., 2010). While SPRY2 is a known tumour suppressor for this cancer (Sutterlüty *et al*., 2007), it has also been extensively described to have a similar function in a number of other cancers, including that of the breast, liver and prostate (Gao *et al*., 2012; Lo *et al*., 2004; Wang *et al*., 2012b). How SPRY2 is down-regulated in cancer is unclear; however, it has been reported that in Human Heptaocellular Cell Carcinoma (HCC) and prostate cancer, SPRY2 is silenced epigenetically through promoter hypermethylation, where in HCC it triggers an increase in the FGF-induced MAPK-signalling (Lee *et al*., 2010). A diagnostic feature of human cancer is the disruption of the RTK signal transduction pathway. As a consequence, the majority of studies examining the role of SPRY2 as a tumour suppressor gene have focused on its ability to suppress RTK signalling. Shaw *et al*., (2007) reported on this by showing that mice bearing a V-Ki-ras2 Kirsten Rat Sarcoma Viral Oncogene Homolog (KRAS) mutation developed fewer tumours upon up-regulation of SPRY2. A subsequent study by Sutterlüty *et al*., (2007), further confirmed the tumour suppressor function of SPRY2 upon RTK signalling by examining SPRY2 expression in both KRAS WT and mutant NSCLC lines. The results

in this thesis demonstrate that the loss of SPRY2 results in unsustainable FGF10-induced MAPK activity thereby leading to possible unsustained development of the airway. However, Sutterlüty *et al*., 2007 also established that SPRY2 down-regulation in NSCLC could potentially interfere with another unidentified RAS-independent pathway.

Could this pathway be that of the vascular signalling pathway governed by SPRY2 independently of PI3K/AKT? The observations in this thesis showed that the loss of SPRY2 correlated with a marked increase in mTORC1 and VEGF-A activity in hypoxia. Under this presumption, the FGF10 proliferative signal is unsustainable through the loss of SPRY2 expression, which could lead to inflammation and hyper-vascularity of the developing lung. On the other hand, the results in this thesis report the novel observation that a loss of SPRY2 in normoxia drastically elevates HIF-1α transcriptional activity, possibly caused by the inability of pVHL to interact with SPRY2. The role of HIF-1α in normoxia is poorly characterised but it is thought to potentially play a role in tissue homeostasis (Stroka *et al*., 2001). However, HIF can be activated in cancer which has been reported to be caused by inactivation of tumour suppressor genes (Talks *et al*., 2000) and overexpression of HIF-1α has been observed in many cancers (Ke & Costa, 2006). Given that SPRY2 is a known tumour suppressor gene and how it has been manipulated in the HBE cell line, it is possible that silencing of the SPRY2 gene promotes unsustained HIF-1α transcriptional activity, which disrupts tissue homeostasis leading to increased potential for tumourigenesis. The evidence from the results presented in this study and that of

the literature provide further indication that SPRY2 may be a novel therapeutic target for treating lung diseases such as asthma and cystic fibrosis.

Experimental limitations of this study.

To date, studies of SPRY2 function have been confined to *in vitro* cell models through the use of transient or stably transfected cell lines (Gao *et al*., 2012). For the purposes of this study, there are a number of ethical issues that are raised regarding the use of a fetal *in vivo* model so the closest representation of such a model was represented *ex vivo* by the primary cultured FDLE isolated from E19 rat lungs and through the use of the HBE immortalised cell line. The effects of FGF10 and SPRY2 on HAT/HDAC activity in FDLE were further examined by carrying out HAT/HDAC assays. However, the results were not informative but with improvements made to this procedure, then it is possible that an effect could be determined. It should be noted that some of the variation observed in the data could be attributed to the varying growth rates of each cell line, which made it difficult to establish similar cell confluence. It should also be mentioned that in instances where the data did not infer statistical significance, the ideas which follow on from said data were driven by the trends observed.

Main Conclusions

The original aim of this thesis was to establish a potential role for SPRY2 in co-ordinating airway and vascular growth of the fetal lung. The main findings from this project provide evidence that SPRY2 does indeed play a role in both facets of growth while shedding some light on several possible mechanisms through which this co-ordinated development is achieved. FGF10 stimulation induces Y55 phosphorylation and C-terminal activity of the SH3 domain of SPRY2, which is required to suppress both airway (which is known) and vascular signalling cues via the MAPK and mTORC1 respectively. SPRY2 is present in the nucleus of both fetal and adult lung epithelium where it acts to repress HAT activity, regulate cell-cycle progression (specifically CCND1 expression) and bind to methylation sites of the VEGF-A promoter thus regulating the expression of vascular genes. This thesis also provides a novel function for the CRD of SPRY2, whereby this region plays a role in regulating HIF-driven VEGF-A transcription. Furthermore, SPRY2 appears to facilitate HIF-1α degradation at normoxia thereby further implicating its role as a tumour suppressor. Therefore, the results presented in this thesis appear to be in agreement with the original hypothesis, which stated that: 'SPRY2 acts as the "missing link" that governs co-ordinated development of the airway and vascular trees in the fetal lung' where it acts as a link between its role as a negative feedback regulator of FGF10-induced airway outgrowth and its role in regulating FGF10-induced transcriptional activation of the VEGF-A gene.

Future direction

While the work in this thesis presents several novel functions for SPRY2 in facilitating co-ordinated lung development, a number of ambiguities persist. One such ambiguity surrounding SPRY2 function is its translocation to the cell membrane, possibly upon cys-palmitoylation, which is influenced by growth factor stimulation or through modifications made to its CRD. A recent unpublished observation from our lab has determined that SPRY2 is indeed palmitoylated in FDLE and the ability of the full-length form of SPRY2 to become palmitoylated is governed by FGF10 stimulation. At the time of writing, an experiment had been conducted to assess if mutations made at C218 and C221 of SPRY2 led to the failure of SPRY2 to palmitoylated to the cell membrane. Preliminary results have revealed that C221 mutation abolishes SPRY2 palmitoylation to the cell membrane. These experiments may answer the 'unanswered questions' queried by Guy *et al*., (2009) surrounding the true function of the CRD of SPRY2.

It is also important to consider that this regulatory function of SPRY2 is not just confined to the developing lung and that its expression extends to several organ systems. This is highlighted by recent unpublished work from our lab, which has established populations of SPRY2 and SPRY4 in the nuclei of SHS5Y neurons, a cell line extensively used in research of Alzheimer's disease. Not only were SPRY2/4 strongly nuclear in these cells, further IHC analysis determined that they are both involved in cell division, thus providing further evidence that SPRY may epigenetically regulate the development of these cells. Clearly, more work is required here but it is

possible that the role of SPRY2 in the developing lung established in this thesis may translate to other organ morphogenetic/developmental systems. As stated earlier in this discussion, the loss of SPRY2 correlates with the rise in cancer in a number of organs and tissues which highlights the need for further work to establish SPRY2 as a potential therapeutic agent.

References

ACARREGUI, M. J., GOSS, K. L. & SNYDER, J. M. (1997). Localization of vascular endothelial growth factor (VEGF), VEGF receptors and endothelial cell markers in human fetal lung *in vitro*. *Pediatric Research*. **41**: 40-40.

ACARREGUI, M. J., PENISTEN, S. T., GOSS, K. L., RAMIREZ, K. & SNYDER, J. M. (1999). Vascular endothelial growth factor gene expression in human fetal lung in vitro. *Am J. Respir Cell Mol Biol*. **20(1)**: 14-23.

ACOSTA, J. M., THÉBAUD, B., CASTILLO, C., MAILLEUX, A., TEFFT, D., WUENSCHELL, C., ANDERSON, K. D., BOURBON, J., THEIRY, J-P., BELLUSCI, S. & WARBURTON, D. (2001). Novel mechanisms in murine nitrofen-induced pulmonary hypoplasia: FGF-10 rescue in culture. *Am. J. Physiol. Lung Cell Mol. Physiol.* **281**: L250-L257.

AHLBRECHT, K., SEAY, U., SCHMITZ, J., HABERBERGER, R. V., KRAUS, R. M., HEROLD, S., BREIER, G., KEITH, B., SIMON, C., WHITSETT, J. A., GRIMMINGER, F., SEEGER, W. & VOSWINCKEL, R. (2008). Impact of the epithelial HIF 2 alpha system on lung development. *FASEB J.* **22** (Meeting abstract supplement). 930.2.

AHN, J-H., EUM, K-H. & LEE. M. (2010). Spry2 does not directly modulate Raf-1 kinase activity in v-Ha-ras-transformed NIH 3T3 fibroblasts. *BMB reports*. **43(3)**: 205-11.

ALBER, L. L., MANSOUR, S. L. & SUN, X. (2009). Conditional gene inactivation reveals roles for Fgf10 and Fgfr2 in establishing a normal pattern of epithelial branching in the mouse lung. *Dev Dyn*. **238(8)**: 1999-2013.

ALPHONSE, R. S., VADIVEL, A., COLTAN, L., EATON, F., BARR, A. J., DYCK, J. R. & THÉBAUD, B. (2011). Activation of Akt protects alveoli from neonatal oxygen-induced lung injury. *Am J Respir Cell Mol Biol*. **44(2)**: 146-54.

ANDERSON, K., NORDQUIST, K. A., GAO, X., HICKS, K. C., ZHAI, B., GYGI, S. P. & PATEL, T. B. (2011). Regulation of cellular levels of Sprouty2 protein by prolyl hydroxylase domain and von Hippel-Lindau proteins. *J. Biol Chem*. **286(49)**: 42027-36.

ARANDA, S., ALVAREZ, M., TURRÓ, LAGUNA, A. & DE LA LUNA, S. (2008). Sprouty2-mediated inhibition of fibroblast growth factor signaling is modulated by the protein kinase DYRK1A. *Mol Cell Biol*. **28(19)**: 5899-5911.

BAINES, D. L., RAMMINGER, S. J., COLLETT, A., HADDAD, J. J., BEST, O. G., LAND, S. C., OLVER, R. E. & WILSON, S. M. (2001). Oxygen-evoked Na^+ transport in rat fetal distal lung epithelial cells. *J. Physiol*. **532(Pt 1)**: 105-13.

BAZER, F. W., KIM, J., KA, H., JOHNSON, G. A., WU, G. & SONG, G. (2012). Select nutrients in the uterine lumen of sheep and pigs affect conceptus development. *Journal of Reproduction and Development*. **58(2)**: 180-188.

BELLSUCI, S., FURUTA, Y., RUSH, M., HENDERSON, R., WINNIER, G. & HOGAN, B. L. M. (1997). Involvement of Sonic hedgehog (SHH) in mouse embryonic lung growth and morphogenesis. *Development*. **124**: 53-63. (b)

BELLUSCI, S., GRINDLEY, J., EMOTO, H., ITOH, N. & HOGAN, B. L. M. (1997). Fibroblast Growth Factor 10 (FGF10) and branching morphogenesis in the embryonic mouse lung. *Development* **124**: 4867-4878. (a)

BERTHIAUME, Y., VOISIN, G. & DAGENAIS, A. (2006). The alveolar type I cells: the new knight of the alveolus? *The Journal of Physiology*. **572**: 609-610.

BETTICHER, D. C., HEIGHWAY, J., THATCHER, N. & HASELTON P. S. (1997). Abnormal expression of CCND1 and RB1 in resection margin epithelia of lung cancer patients. *Br J Cancer*. **75(12)**: 1761-8.

BINDRA, R. S., VASSELLI, J. R., STEARMAN, R., LINEHAN, W. M. & KLAUSNER, R. D. (2002). VHL-mediated hypoxia regulation of cyclin D1 in renal carcinoma cells. *Cancer Res*. **62(11)**: 3014-9.

BIRD, A. (2002). DNA methylation patterns and epigenetic memory. *Genes & Development*. **16**: 6-21.

BISHOP, A. E. (2004). Pulmonary epithelial stem cells. *Cell Prolif.* **37**: 89-96.

BOS, J. L., REHMANN, H. & WITTINGHOFER, A. (2007). GEFs and GAPs: critical elements in the control of small G proteins. *Cell*. **129(5)**: 865-877.

BRADFORD, M. M. (1976). A rapid and sensitive method for the quantitation of microgram quantities of protein utilizing the principle of protein-dye binding. *Anal Biochem*. **7(72)**: 248-54.

BRAGG, A. D., MOSES, H. L. & SERRA, R. (2001). Signaling to the epithelium is not sufficient to mediate all of the effects of transforming growth factor beta and bone morphogenetic protein 4 on murine embryonic lung development. *Mech Dev*. **109(1)**: 13-26.

BROWN, K. R., ENGLAND, K. M., GOSS, K. L., SNYDER, J. M. & ACARREGUI, M. J. (2001). VEGF induces airway epithelial cell proliferation in human fetal lung in vitro. *Am J Physiol Lung Cell Mol Physiol*. **281(4)**: L1001-10.

BRUICK, R. K. (2000). Expression of the gene encoding the proapoptotic Nip3 protein is induced by hypoxia. *Proc Natl Acad Sci USA*. **97(16)**: 9092-9087.

BRUICK, R. K. & MCKNIGHT, S. L. (2001). A conserved family of prolyl-4-hydroxylases that modify HIF. *Science*. **294(5545)**: 1337-1340.

BUCHER, U. & REID L. M. (1961). Development of intrasegmental bronchial tree: the pattern of branching and development of cartilage at various stages of intra-uterine life. *Thorax*. **16**: 207-18.

BURRI, P. H. & MOSCHOPULOS, M. (1992). Structural analysis of fetal rat lung development. *Anat Rec*. **234**: 399-418.

BURTON, T. R. & GIBSON, S. B. (2009). The role of Bcl-2 family member BNIP3 in cell death and disease: NIPping at the heels of cell death. *Cell Death Differ.* **16(4)**: 515-523.

CABRITA, M. A. & CHRISTOFORI, G. (2008). Sprouty proteins, masterminds of receptor tyrosine kinase signaling. *Angiogenesis*. **11**: 53-62.

CABRITA, M. A., JAGGI, F., WIDJAJA, S. P. & CHRISTOFORI, G. (2006). A functional interaction between Sprouty proteins and Caveolin-1. *Journal of Biological Chemistry*. **281**: 29201-29212.

CARDOSO, W. V. & LÜ, J. (2006). Regulation of early lung morphogenesis: questions, facts and controversies. *Development*. **133**: 1611-1624.

CASCI, T., VINÓS, J. & FREEMAN, M. (1999). Sprouty, an intracellular inhibitor of Ras signaling. *Cell* **96**: 655-665.

CASTELLANO E. & DOWNWARD, J. (2011). RAS interaction with PI3K: more than just another effector pathway. *Genes & Cancer*. **2(3)**: 261-273.

CHANDRAMOULI, S., YU, C. Y., YUSOFF, P., LAO, D-H., LEONG, H. F., MIZUNO, K. & GUY, G. R. (2008). Tesk1 interacts with Spry2 to abrogate its inhibition of ERK phosphorylation downstream of tyrosine kinase signaling. *Journal of Biological Chemistry*. **283**: 1679-1691.

CHANG, M. M-J., SHIH, L. & WU, R. (2008). The Pulmonary Epithelium: Cell Types and Functions. *John Wiley & Sons, Ltd*. **Chapter 1:** 1-26.

CHARAN, N. B., THOMPSON, W. H. & CARVALHO, P. (2007). Functional anatomy of bronchial veins. *Pulmonary pharmacology & therapeutics*. **20(2)**: 100-103.

CHARAN, N. B., TURK, M. G. & DHAND, R. (1984). Gross and subgross anatomy of bronchial circulation in sheep. *J. Appl. Physiol: Respirat. Environ. Exercise Physiol*. **57**: 658-684.

CHEN, J., CHEN, Z., CHINTAGARI, N. R., BHASKARAN, M., JIN, N., NARASARAJU, T. & LIU, L. (2006). Alveolar type I cells protect rat lung epithelium from oxidative injury. *Physiology*. **572**: 625-638.

CHEN, H., KLUZ, T., ZHANG, R. & COSTA, M. (2010). Hypoxia and nickel inhibit histone demethylase JMJD1A and repress Spry2 expression in human bronchial epithelial BEAS-2B cells. *Carcinogenesis*. **31(12)**: 2136-2144.

CHITRA, E., LIN, Y-W., DAVAMANI, F., HSIAO, K-N., SIA, C., HSIEH, S-Y., WEI, O. L., CHEN, J-H. & CHOW, Y-H. (2010). Functional interaction between *Env* oncogene from Jaagsiekte sheep retrovirus and tumour suppressor Sprouty2. *Retrovirology*. **7**: 62.

CHOI, S. B., PARK, J. B., SONG, T-J. & CHOI, S. Y. (2011). Molecular mechanism of HIF-1-independent VEGF expression in a hepatocellular carcinoma cell line. *International Journal of Molecular Medicine*. **28**: 449-454.

CHUANG, P-T. & MCMAHON, A. P. (2003) Branching morphogenesis of the lung: new molecular insights into an old problem. **13(2)**: 86-91.

CLAYTON, A. L. & MAHADEVAN, L. C. (2003). MAP kinase-mediated phosphoacetylation of histone H3 and inducible gene regulation. *FEBS Lett*. **546**: 51-58.

COMPERNOLLE, V., BRUSSELMANS, K., ACKER, T., HOET, P., TJWA, M., BECK, H., PLAISANCE, S., DOR, Y., KESHET, E., LUPU, F., NEMERY, B., DEWERCHIN, M., VAN VELDHOVEN, P., PLATE, K., MOONS, L., COLLEN, D. & CARMELIET, P. (2002). Loss of HIF-2α and inhibition of VEGF impair fetal lung maturation, whereas treatment with VEGF prevents fatal respiratory distress in premature mice. *Nature Medicine*. **8**: 702-710.

COZENS, A. L., YEZZI, M. J., KUNZELMANN, K., OHRUI, T., CHIN, L., ENG, K., FINKBEINER, W. E., WIDDICOMBE, J. H. & GRUENERT, D. C. (1994). CFTR expression and chloride secretion in polarized immortal human bronchial epithelial cells. *Am J Respir Cell Mol Biol*. **10(1)**: 38-47.

CREWS, S. T. (1998). Control of cell-lineage-specific development and transcription by bHLH-PAS proteins. *Genes Dev.* **12**: 607-620.

CUTZ, E. (1982). Neuroendocrine cells of the lung. An overview of morphologic characteristics and development. *Exp. Lung. Res.* **3**: 185-208.

DE ALVARO, C., MARTINEZ, N., ROJAS, J. M. & LORENZO, M. (2005). Sprouty-2 overexpression in C2C12 cells confers myogenic differentiation in the presence of FGF2. *Mol Biol Cell*. **16**: 4454-61.

DEMELLO, D. E., SWAYER, D., GALVIN, N. & REID L. M. (1997). Early fetal development of lung vasculature. *American Journal of Cell and Molecular Biology* **16**: 568-81.

DE MOERLOOZE, L., SPENCER-DENE, B., REVEST, J.-M., HAJIHOSSEINI, M., ROSEWELL, I. & DICKSON, C. (2000). An important role for the IIIb isoform of fibroblast growth factor receptor 2 (FGFR2) in mesenchymal-epithelial signalling during mouse organogenesis. *Development*. **127**: 483-492.

DEL MORAL, P. M., DE LANGHE, S. P., SALA, F. G., VELTMAAT, J. M., TEFFT, D., WANG, K., WARBURTON, D. & BELLUSCI, S. (2006). Differential role of FGF9 on epithelium and mesenchyme in mouse embryonic lung. *Developmental Biology* **293**: 77-89.

DEMAYO, F., MINOO, P., PLOPPER, C. G., SCHUGER, L., SHANNON, J. & TORDAY, J. S. (2002). Mesenchymal-epithelial interactions in lung development and repair: are modelling and remodelling the same process? *Am J Physiol Lung Cell Mol Physiol*. **283(3)**: L510-7.

DEUTSCH, G. H. & PINAR, H. (2002). Prenatal Lung Development. *Chronic obstructive lung diseases* **Chapter 2**: 7-14.

DING, W., SHI, W., BELLUSCI, S., GROFFEN, J., HEISTERKAMP, N., MINOO, P. & WARBURTON, D. (2007). Sprouty2 downregulation plays a pivotal role in mediating crosstalk between TGF-ß1 signaling and EGF as well as FGF receptor tyrosine kinase-ERK pathways in mesenchymal cells. *J. Cell. Physiol.* **212**: 796-806.

DOBBS, L. G. (1990). Isolation and culture of alveolar type II cells. *AJP-Lung Physiol*. **258 no. 4**. L134-L147.

EDWIN, F., SINGH, R., ENDERSBY, R., BAKER, S. J. & PATEL, T. B. (2006). The tumour suppressor PTEN is necessary for human Sprouty2-mediated inhibition of cell proliferation. *J. Biol. Chem.* **281(8)**: 4816-4822.

EDWIN, F., ANDERSON, K., YING, C. & PATEL, T. B. (2009). Intermolecular interactions of Sprouty proteins and their implications in development and disease. *Mol. Pharmacol.* **76(4)**: 679-691.

ESWARAKUMAR, V. P., LAX, I. & SCHLESSINGER, J. (2005). Cellular signaling by fibroblast growth receptors. *Cytokine & Growth Factor Reviews*. **16(2)**: 139-149.

EVANS, M. J., CABRAL, L. J., STEPHENS, R. J. & FREEMAN, G. (1975). Transformation of alveolar type 2 cells to type 1 cells following exposure to NO_2. *Experimental and Molecular Pathology*. **22(1):** 142-150.

EUBANK, T. D., RODA, J. M., LIU, H., O'NEIL, T. & MARSH, C. B. (2011). Opposing roles for HIF-1α and HIF-2α in the regulation of angiogenesis by mononuclear phagocytes. *Blood*. **117**: 323-332.

FANG, Y., WHITE, S. B., ZHAO, Q. & LEE, F. S. (2001). HIF-1α binding to VHL is regulated by stimulus-sensitive proline hydroxylation. *Proc. Natl. Acad. Sci. U. S. A.* **98(17)**: 9630-9635.

FERRARA, N., GERBER, H-P. & LECOUTER, J. (2003). The biology of VEGF and its receptors. *Nature Medicine*. **9**: 669-676.

FINNEY, B. A., DEL MORAL, P. M., WILKINSON, W. J., CAYZAC, S., COLE, M., WARBURTON, D., KEMP, P. J. & RICCARDI, D. (2008). Regulation of mouse lung development by the extracellular calcium-sensing receptor, CaR. *The Journal of Physiology* **586**: 6007-6019.

FONG, C. W., LEONG, H. F., WONG, E. S., LIM, J. YUSOFF, P. & GUY. G. R. (2003). Tyrosine phosphorylation of Sprouty2 enhances its interaction with c-Cbl and is crucial for its function. *Journal of Biological Chemistry*. **278**: 33456-33464.

FORRESTER, M. T., HESS, D. T., THOMPSON, J. W., HULTMAN, R., MOSELEY, M. A., STAMLER, J. S. & CASEY, P. J. (2011). Site-specific analysis of protein S-acylation by resin assisted capture. *J. Lipid Res*. **52(2)**: 393-8.

FRIAS, M., THOREEN, C., JAFFE, J., SCHRODER, W., SCULLEY, T., CARR, S. & SABATINI, D. (2006). mSin1 is necessary for Akt/PKB phosphorylation, and its isoforms define three distinct mTORC2s. *Curr Biol*. **16(18)**: 1865-1870.

FRITZSCHE, S., KENZELMANN, M., HOFFMANN, M. J., MÜLLER, M., ENGERS, R., GRÖNE, H-J. & SCHULZ, W. A. (2006). Concomitant down-regulation of SPRY1 and SPRY2 in prostate carcinoma. *Endocrine-Related Cancer*. **13**: 839-849.

GAMSJAEGER, R., LIEW, C. K., LOUGHLIN, F. E., CROSSLEY, M. & MACKAY, J. P. (2007). Sticky fingers: zinc-fingers as protein-recognition motifs. *Trends in Biochemical Sciences*. **32(2)**: 63-70.

GAO, M, PATEL, R., AHMAD, I., FLEMING, J., EDWARDS, J., MCCRACKEN, SAHADEVAN, K., SEYWRIGHT, M., NORMAN, J., SANSOM, O. & LEUNG, H. Y. (2012). SPRY2 loss enhances ErbB trafficking and PI3K/AKT signalling to drive human and mouse prostate carcinogenesis. *EMBO Mol Med.* **4(8)**: 776-790.

GAO, Y. & RAJ, J. U. (2010). Regulation of the pulmonary circulation in the fetus and newborn. *Physiol Rev*. **90(4)**: 1291-1335.

GEBB, S. A. & SHANNON, J. M. (2000). Tissue interactions mediate early events in pulmonary vasculogenesis. *Dev Dyn*. **217(2)**: 159-69.

GEBB. S. A. & TORDAY, J. (2008). Lung Devlopment. *Chronic Obstructive Lung Disease*. **Chapter 2**: 9-16.

GLENNY, R. W. (2010). Emergence of matched airway and vascular trees from fractal rules. *J Appl Physiol*. **110**: 1119-1129.

GLIENKE, J., FENTEN, G., SEEMANN, M., STURZ, A. & THEIRAUCH, K-H. (2000). Human SPRY2 inhibits FGF2 signalling by a secreted factor. *Mechanisms of Development* **96**: 91-99.

GONCHAROVA, E. A., AMMIT, A. J., IRANI, C., CARROLL, R. G., ESZTERHAS, A. J., PANETTIERI, R. A. & KRYMSKAYA, V. P. (2002). PI3K is required for proliferation and migration of human pulmonary vascular smooth muscle cells. *Am. J. Physiol. Lung Cell Mol. Physiol.* **283**: L354-363.

GOODMAN, C. A., MIU, M. H., FREY, J. W., MABREY, D. M., LINCOLN, H. C., GE. Y., CHEN. J. & HORNBERGER, T. A. (2010). A phosphatidylinositol-3-kinase/protein kinase B-independent activation of mammalian target of rapamycin signaling is sufficient to induce skeletal muscle hypertrophy. *Mol. Biol. Cell*. **21(18)**: 3258-3268.

GRAY, H. (1918). Anatomy of the human body. *Philadelphia: Lea & Febiger, 1918; Bartleby.com 2000*. **Chapter 1**: 1100.

GRAY, M. J., ZHANG, J., ELLIS, L. M., SEMENZA, G. L., EVANS, D. B., WATOWICH, S. S. & GALLICK, G. E. (2005). HIF-1alpha, STAT3, CBP/p300 and Ref-1/APE are components of a transcriptional complex that regulates Src-dependent hypoxia-induced expression of VEGF in pancreatic and prostate carcinomas. *Oncogene*. **24(19)**: 3110-20.

GROENMAN, F., RUTTER, M., CANIGGIA, I., TIBBOEL, D. & POST, M. (2007). Hypoxia-inducible factors in the first trimester human lung. *J. Histochem. Cytochem.* **55(4)**: 355-363.

GUY, G. R., JACKSON, R. A., YUSOFF, P. & CHOW, S. Y. (2009). Sprouty proteins: modified modulators, matchmakers or missing links? *J Endorcrinol*. **203**: 191-202.

HACOHEN., N, KRAMER, S., SUTHERLAND, D., HIROMI, Y. & KRASNOW, M. A. (1998). *Sprouty* encodes a novel antagonist of FGF signalling that patterns apical branching of the *Drosophila* airways. *Cell* **92**: 253-263.

HADARI, Y. R., KOUHARA, H., LAX, I. & SCHLESSINGER, J. (1998). Binding of Shp2 tyrosine phosphatase to FRS2 is essential for fibroblast growth factor-induced PC12 cell differentiation. *Mol Cell Biol*. **18**: 3966-3973.

HALL, A. B., JURA, N., DASILVA, J., JANG, Y. J., GONG, D. & BAR-SAGI, D. (2003). hSpry2 is targeted to the ubiquitin-dependent proteasome pathway by c-Cbl. *Current Biology*. **13**: 308-314.

HALL, S. M., HISLOP A. A. & HAWORTH S. G. (2002). Origin, differentiation and maturation of human pulmonary veins. *American Journal of Cell and Molecular Biology* **26**: 333-340.

HAN, R. N. N. & STEWART, D. J. (2006). Defective lung vascular development in endothelial nitric oxide synthase-deficient mice. *Trends in Cardiovascular Medicine* **16**: 29-34.

HANS, F. & DIMITROV, S. (2001). Histone H3 phosphorylation and cell division. *Oncogene*. **20**: 3021-3027.

HARA, S., HAMADA, J., KOBAYASHI, C., KONDO, Y. & IMURA, N. (2001). Expression and characterization of Hypoxia-Inducible Factor (HIF)-3α in human kidney: Suppression of HIF-mediated gene expression by HIF-3α. *Biochemical and Biophysical Research Communications*. **287**: 808-813.

HAUSOTT, B., VALLANT, N., SCHLICK, B., AUER, M., NIMMERVOLL, B., OBERMAIR, G. J., SCHWARZER, C., DAI, F., BRAND-SABERI, B. & KLIMASCHEWSKI, L. (2012). Sprouty2 and -4 regulate axon outgrowth by hippocampal neurons. *Hippocampus*. **22(3)**: 434-41.

HAY, N. & SONENBERG, N. (2004). Upstream and downstream of mTOR. *Genes & Dev*, **18**: 1926-1945.

HEDGES, J. C., SINGER, C. A., GERTHOFFER, W. T. (2000). Mitogen-activated protein kinases regulate cytokine gene expression in human airway myocytes. *Am J Respir Cell Mol Biol*. **23**: 86-94.

HERMANS, C. & BERNARD, A. (1999). Lung epithelium-specific proteins. Characteristics and potential applications as markers. *Am. J. Respir. Crit. Care Med.* **159(2)**: 646-678.

HISLOP, A. A. (2002). Airway and blood vessel interaction during lung development. *Journal of Anatomy* **201(4)**: 325-334.

HISLOP, A. A. (2005). Developmental biology of the pulmonary circulation. *Paediatr Respir Rev* **6**: 35-43.

HISLOP, A. A., WIGGLESWORTH, J. S. & DESAI, R. (1986). Alveolar development in the human fetus and infant. *Early Human Development* **13**: 1-11.

HOGAN, B. L. (1999) Morphogenesis. *Cell*. **96**: 225-233.

HOLMES, K., ROBERTS, O. L., THOMAS, A. M. & CROSS, M. J. (2007). Vascular endothelial growth factor receptor-2: Structure, function, intracellular signalling and therapeutic inhibition. *Cellular Signalling*. **19** (10): 2003-12.

HOLMQUIST-MENGELBIER, L., FREDLUND, E., LÖFSTEDT. T., NOGUERA, R., NAVARRO, S., NILSSON, H., PIETRAS, A., VALLON-CHRISTERSSON, J., BORG, A., GRADIN, K., POELLINGER, L. & PÅHLMAN, S. (2006). Recruitment of HIF-1α and HIF-2α to common target genes is differentially regulated in neuroblastoma: HIF-2α promotes an aggressive phenotype. *Cancer Cell*. **10(5)**: 413-423.

HUANG, J. & MANNING, B. D. (2009). A complex interplay between Akt, TSC2 and the two mTOR complexes. *Biochem. Soc. Trans.* **37(Pt 1)**: 217-222.

IMPAGNATIELLO, M-A., WEITZER, S., GANNON, G., COMPAGNI, A., COTTON, M. & CHRISTOFORI, G. (2001). Mammalian Sprouty-1 and -2 are membrane-anchored phosphoprotein inhibitors of growth factor signaling in endothelial cells. *J Cell Biol*. **152(5)**: 1087-1098.

ISAACS, J. S., JUNG, Y. J., MOLE, R., LEE, S., TORRES-CABALA, C., CHUNG, Y. L., MERINO, M., TREPEL, J., ZBAR, B., TORO, J., RATCLIFFE, P. J., LINEHAN, W. M. & NECKERS, L. (2005). HIF overexpression correlates with biallelic loss of fumarate hydratase in renal cancer: novel role of fumarate in regulation of HIF stability. *Cancer Cell*. **8**: 143-153.

JASSAL, D., HAN R. N., CANIGGIA, I., POST, M. & TANSWELL, A. K. (1991). Growth of distal fetal rat lung epithelial cells in a defined serum-free medium. *In Vitro Cell Dev Biol*. **27A(8)**: 625-32.

JESUDASON, E. C., KESHET, E. & WARBURTON, D. (2010). Entrained pulmonary clocks: epithelium and vasculature keeping pace. *Am. J. Physiol. Lung Cell Mol. Physiol.* **299**: L453-L454.

JONES, R. C. & CAPEN, D. E. (2011). Pulmonary vascular development. *Textbook of Pulmonary Vascular Disease*. **Chapter 3**: 25-60.

JOSS-MOORE, L. A., WANG, Y., OGATA, E. M., SAINZ, A. J., YU, X., CALLAWAY, C. W., MCKNIGHT, R. A., ALBERTINE, K. H. & LANE, R. H. (2011). IUGR differentially alters MeCP2 expression and H3K9Me3 of the PPARγ gene in male and female rat lungs during alveolarization. *Birth Defects Res. A. Clin. Mol. Teratol*. **91(8)**: 672-681.

JURASZ, P., YURKOVA, N., KIRSHENBAUM, L. & STEWART, D. J. (2011). VEGF masks BNIP3-mediated apoptosis of hypoxic endothelial cells. *Angiogenesis*. **14(2)**: 199-207.

KE, Q. & COSTA, M. (2006). Hypoxia-Inducible Factor-1 (HIF-1). *Molecular Pharmacology*. **70(5):** 1469-1480.

KEMP, P. J. & OLVER, R. E. (1996). G protein regulation of alveolar ion channels: implications for lung fluid transport. *Exp Physiol*. **81**: 493-504.

KIM, E., GORAKSHA-HICKS, P., LI, L., NEUFIELD, T. P. & GUAN, K. L. (2008). Regulation of TORC1 by Rag GTPases in nutrient response. *Nat. Cell. Biol.* **10(8)**: 935-945.

KIM, H. J. & BAR-SAGI, D. (2004). Modulation of signalling by Sprouty: a developing story. *Nat Rev Mol Cell Biol*. **5**: 441-450.

KIM, Y-M., STONE, M., HWANG, T. H., KIM, Y-G., DUNLEVY, J. R., GRIFFIN, T. & KIM D-H. (2012). SH3BP4 is a negative regulator of amino acid-Rag GTPase mTORC1 signaling. *Molecular Cell*. **46(29)**: 833-846.

KLUG, A. & SCHWABE, J. W. (1995). Protein motifs 5: Zinc fingers. *The FASEB Journal*. **9(8)**: 597-604.

KOTCH, L. E., IYER, N. V., LAUGHNER, E. & SEMENZA, G. L. (1999). Defective vascularization of HIF-1-null embryos is not associated with VEGF deficiency but with mesenchymal cell death. *Dev. Biol.* **209**: 254-267.

KNOWLES, H. J., MOLE, D. R., RATCLIFFE, P. J. & HARRIS, A. L. (2006). Normoxic stabilization of hypoxia-inducible factor-1α by modulation of the labile iron pool in differentiating U937 macrophages: effect of natural resistance-associated macrophage protein 1. *Cancer Res*. **66**: 2600.

KRISHNA, S. S., MAJUMDAR, I. & GRISHIN, N. V. (2003). Survey and summary: Structural classification of zinc fingers. *Nucleic Acids Research*. **31(2)**: 532-550.

LAND, S. C. (2011). Vascular growth in the fetal lung. *Vasculogenesis and Angiogensis: from Embryonic Development to Regenerative Medicine*. **Chapter 3**: 49-72.

LAND, S. C. & COLLETT, A. (2001). Detection of Cl- flux in the apical microenvironment of cultured foetal distal lung epithelial cells. *J. Exp. Biol.* **204(Pt 4)**: 785-95.

LAND, S. C. & TEE, A. R. (2007). Hypoxia-inducible Factor 1α is regulated by the Mammalian Target of Rapamycin (mTOR) via an mTOR signaling motif. *The Journal of Biological Chemistry*. **282(28)**: pp. 20534-20543.

LAO, D-H., CHANDRAMOULI, S., YUSOFF, P., FONG, C. W., SAW, T. Y., TAI, L. P., YU, C. Y., LEONG, H. F. & GUY, G. R. (2006). An SH3-binding sequence on the C-terminus of Sprouty2 is necessary for the inhibition of the Ras/ERK pathway downstream of fibroblast growth factor receptor stimulation. *Journal of Biological Chemistry*. **281**: 29993-30000.

LAO, D-H., YUSOFF, P., CHANDRAMOULI, S., PHILP, R. J., FONG, C. W., JACKSON, R. A., SAW, T. Y., YU, C. Y. & GUY, G. R. (2007). Direct binding of PP2A to Sprouty2 and phosphorylation changes are a prerequisite for ERK inhibition downstream of fibroblast growth factor receptor stimulation. *The Journal of Biological Chemistry*. **282, NO. 12:** pp. 9117-9126.

LARSON, J. E., DELCARPIO, J. B., FARBERMAN, M. M., MORROW, S. L. & COHEN, J. C. (2000). CFTR modulates lung secretory cell proliferation and differentiation. *AJP Lung Physiol*. **279(2)**: L333-341.

LAWSON, G. W., VAN WINKLE, L. S., TOSKALA, E., SENIOR, R. M., PARKS, W. C. & PLOPPER, C. G. (2002). Mouse strain modulates the role of the ciliated cell in acute tracheobronchial airway injury-distal airways. *Am J Pathol*. **160**: 315-327.

LEBECHE, D., MALPEL, S. & CARDOSO, W. V. (1999). Fibroblast growth factor interactions in the developing lung. *Mechanisms of Development*. **86**: 125-136.

LEE, S. A., LADU, S., EVERT, M., DOMBROWSKI, F., DE MURTAS, V., CHEN, X. & CALVISI, D. F. (2010). Synergistic role of sprouty2 inactivation and c-Met up-regulation in mouse and human hepatocarcinogensis. *Hepatology*. **52(2)**: 506-517.

LEUNG, K-W., NG, H-M., TANG, M. K. S., WONG, C. C. K., WONG, R. N. S. & WONG, A. S. T. (2011). Ginsenoside-Rg1 mediates a hypoxia-independent upregulation of hypoxia-inducible factor 1α to promote angiogenesis. *Angiogenesis*. **14(4)**: 515-522.

LEVY, M., MAUREY, C., CHAILLEY-HEU, B., MARTINOVIC, J., JAUBERT, F. & ISRAL-BIET, D. (2004). Developmental changes in endothelial vasoactive and angiogenic factors in the human perinatal lung. *Pediatr. Res.* **57**: 248-253.

LI H. J., LIU, Y., HAO, H. S., DU, W. H., ZHAO, X. M., WANG, D., QIN, T., MA, Y. J. & ZHU, H. B. (2012). Relationship of epidermal growth factor receptor in lung development. *Yi Chuan*. **34(1)**: 27-32.

LI, X., BRUNTON, V. G., BURGAR, H. R., WHELDON, L. M. & HEATH, J. K. (2004). FRS2-dependent SRC activation is required for fibroblast growth factor reprector-induced phosphorylation of Sprouty and suppression of ERK activity. *J Cell Science*. **117**: 6007-6017.

LIM, J., WONG, E. S., ONG, S. H., YUSOFF, P., LOW, B. C., GUY, G. R. (2000). Sprouty proteins are targeted to membrane ruffles upon growth factor receptor tyrosine kinase activation. Identification of a novel translocation domain. *J. Biol. Chem*. **275**: 32837-32845.

LIM, J., YUSOFF, P., WONG, E. S., CHANDRAMOULI, S., LAO, D. H., FONG, C. W. & GUY, G. R. (2002). The cysteine-rich sprouty translocation domain targets mitogen-

activated protein kinase inhibitory proteins to phosphatodyl 4, 5, -biphosphate in plasma membranes. *Molecular and Cellular Biology*. **22**: 7953-7966.
LITO, P., METS, B. D., APPLEDORN, D. M., MAHER, V. M. & MCCORMICK, J. J. (2009). Sprouty 2 regulates DNA damage-induced apoptosis in Ras-transformed human fibroblasts. *The Journal of Biological Chemistry*. **284(2)**: pp. 848-854.

LO, T. L. YUSOFF, P., FONG, C. W., GUO, K., MCCAW, B. J., PHILLIPS, W. A., YANG, H., WONG, E. S., LEONG, H. F., ZENG, Q., PUTTI, T. C. & GUY, G. R. (2004). The ras/mitogen-activated protein kinase pathway inhibitor and likely tumour suppressor proteins, sprouty 1 and sprouty 2 are deregulated in breast cancer. *Cancer Res*. **64(17)**: 6127-36.

LO, W-S., TRIEVEL, R. C., ROJAS, J. R., DUGGAN, L., HSU, J-Y., ALLIS, C. D., MARMORSTEIN, R. & BERGER, S. L. (2000). Phosphorylation of serine 10 in Histone H3 is functionally linked in vitro and in vivo to Gcn5-mediated acetylation at lysine 14. *Molecular Cell*. **5**: 917-926.

LOCKWOOD, W. W., CHARI, R., COE, B. P., THU, K. L., GARNIS, C., MALLOFF, C. A., CAMPBELL, J., WILLIAMS, A. C., HWANG, D., ZHU, C-Q., BUYS, T. P. H., YEE, J., ENGLISH, J. C., MACAULAY, C., TSAO, M-S., GAZDAR, A. F., MINNA, J. D., LAM, S. & LAM, W. L. (2010). Integrative genome analyses identify BRF2 as a novel lineage-specific oncogene in lung squamous cell carcinoma. *PLoS Medicine*. **7(7)**: 1-14 (e1000315).

LOPICCOLO, J., BLUMENTHAL, G. M., BERNSTEIN, W. B. & DENNIS, P. A. (2008). Targeting the PI3K/Akt/mTOR pathway: effective combinations and clinical considerations. *Drug Resist Updat.* **11(1-2)**: 32-50.

MAHADEVAN, L. C., WILLIS, A. C. & BARRATT, M. J. (1991). Rapid histone H3 phosphorylation in response to growth factors, phorbol esters, okadaic acid, and protein synthesis inhibitors. *Cell*. **65**: 775-783.

MAILLEUX, A. A., TEFFT, D., NDIAYE, D., ITOH, N., THIERY, J. P., WARBURTON, D. & BELLUSCI, S. (2001). Evidence that SPROUTY2 functions as an inhibitor of mouse embryonic lung growth and morphogenesis. *Mechanisms of Development*. **102**: 81-94.

MAILLEUX, A. A., KELLY, R., VELTMAAT, J. M., DE LANGHE, S. P., ZAFFRAN, S., THIERY, J. P. & BELLUSCI, S. (2005). FGF10 expression identifies parabronchial smooth muscle cell progenitors and is required for their entry into the smooth muscle cell lineage. *Development*. **132**: 2157-2166.

MANNING, B. D. & CANTLEY, L. C. (2007). AKT/PKB signaling: navigating downstream. *Cell*. **129(7)**: 1261-74.

MASON, J. M., MORRISON, D. J., BASSIT, B., DIMRI, M., BAND, H., LICHT, J. D. & GROSS, I. (2004). Tyrosine phosphorylation of Sprouty proteins regulates their ability to inhibit growth factor signaling: a dual feedback loop. *Mol Biol Cell*. **15(5)**: 2176-2188.

MATALON, S. & O'BRODOVICH, H. (1999). Sodium channels in alveolar epithelial cells: molecular characterization, biophysical properties and physiological significance. *Annual Review of Physiology*. **61**: 627-661.

MAXWELL, P. H., WIESENER, M. S., CHANG, G. W., CLIFFORD, S. C., VAUX, E. C., COCKMAN, M. E., WYKOFF, C. C., PUGH, C. W., MAHER, E. R. & RATCLIFFE, P. J. (1999). The tumour suppressor protein VHL targets hypoxia-inducible factors for oxygen-dependent proteolysis. *Nature*. **399(6733)**: 271-275.

MAYER, C-E., HAIGL, B., JANTSCHER, F., SIEGWART, G., GRUSCH, M., BERGER, W. & SUTTERLÜTY, H. (2010). Bimodal expression of Sprouty2 during the cell cyle is mediated by phase-specific Ras/MAPK and c-Cbl activities. *Cellular and Molecular Life Sciences*. **67(19)**: 3299-3311.

MCMURTY, I. F. (2002). Introduction: pre- and postnatal lung development, maturation, and plasticity. *Am J Physiol Lung Cell Mol Physiol*. **282**: L341-L344.

MEDINA, G. N., EHRLICH, L. S., CHEN, M. H., KHAN, M. B., POWELL, M. D. & CARTER, C. A. (2011). Sprouty2 binds ESCRT-II factor Eap20 and facilitates HIV-1 gag release. *J. Virol*. **85(14)**: 7353-7362.

MENSHYKAU, D., KRAEMER, C. & IBER, D. (2012). Branch mode selection during early lung development. *PLoS Comput. Biol*. **8(2)**: e1002377.

METZGER, R. J. & KRASNOW, M. A. (1999). Genetic control of branching morphogenesis. *Science*. **284**: 1635-1639.

METZGER, R. J., KLEIN, O. D., MARTIN, G. R. & KRASNOW, M. A. (2008). The branching programme of mouse lung development. *Nature*. **453**: 745-750.

MILANINI-MONGIAT, J., POUYSSÉGUR, J., PAGÈS, G. (2002). Identification of two Sp1 phosphorylation sites for p42/p44 mitogen-activated protein kinases: their implication in vascular endothelial growth factor gene transcription. *J. Biol. Chem.* **277**: 20631-20639.

MILLER, J., MCLACHLAN, A. D. & KLUG, A. (1985). Repetitive zinc-binding domains in the protein transcription factor IIIA from *Xenopus* oocytes. *The EMBO Journal*. **4(6)**: 1609-1614.

MILLER, L. A., WERT, S. E. & WHITSETT, J. A. (2001). Immunolocalization of sonic hedgehog (Shh) in developing mouse lung. *J. Histochem Cytochem*. **49(12)**: 1593-604.

MILLER, K. M., TJEERTES, J. V., COATES, J., LEGUBE, G., POLO, S. E., BRITTON, S. & JACKSON, S. P. (2010). Human HDAC1 and HDAC2 function in the DNA-damage response to promote DNA nonhomologous end-joining. *Nature Structural & Molecular Biology*. **17**: 1144-1151.

MINET, E., ARNOUHLD, T., MICHEL G., ROLAND I., MOTTET, D., RAES, M., REMACLE, J. & MICHIELS, C. (2000). ERK activation upon hypoxia: involvement in HIF-1 activation. *FEBS Lett*. **18; 468(1)**: 53-58.

MINOWADA, G. & MILLER, Y. E. (2009). Overexpression of Sprouty2 in mouse lung epithelium inhibits urethane-induced tumourigenesis. *Am. J. Respir. Cell Mol. Biol*. **40(1)**: 31-37.

NADEAU, R. J., TOHER, J. L., YANG, X., KOVALENKO, D. & FRIESEL, R. (2007). Regulation of Sprouty2 stability by mammalian Seven-in-Absentia homolog 2. *J. Cell. Biochem*. **100(1)**: 151-160.

NAKAYAMA, K, FREW, I. J., HAGENSEN, M., SKALS, M., HABELHAH, H., BHOUMIK, A., KADOYA, T., ERDJUMENT-BROMAGE, H., TEMPST, P., FRAPPELL, P. B., BOWTELL, D. D. & RONAI, Z. (2004). Siah2 regulates stability of prolyl-hydroxylases, controls HIF1alpha abundance, and modulates physiological responses to hypoxia. *Cell*. **117(7)**: 941-952.

NAN, X., CAMPOY, F. & BIRD, A. (1997). MeCP2 is a transcriptional repressor with abundant binding sites in genomic chromatin. *Cell*. **88(4)**: 471-481.

NIU, G., WRIGHT, K. L., HUANG, M., SONG, L., HAURA, E., TURKSON, J., ZHANG, S., WANG, T., SINIBALDI, D., COPPOLA, D., HELLER, R., ELLIS, L. M., KARRAS, J., BROMBERG, J., PARDOLL, D., JOVE, R. & YU, H. (2002). Constitutive Stat3 activity up-regulates VEGF expression and tumour angiogenesis. *Oncogene*. **21(13)**: 2000-2008.

NONAMI, A., TAKETOMI, T., KIMURA, A., SAEKI, K., TAKAKI, H., SANADA, T., TANIGUCHI, K., HARADA, M. & YOSHIMURA, A. (2005). The Sprouty-related protein, Spred-1, localizes in a lipid raft/caveola and inhibits ERK activation in collaboration with caveolin-1. *Genes to Cells*. **10**: 887-895.

NOWAK, S. J. & CORCES, V. G. (2004). Phosphorylation of histone H3: a balancing act between chromosome condensation and transcriptional activation. *TRENDS in Genetics*. **20(4)**: 214-220.

OLVER, R. E. & STRANG, L. B. (1974). Ion fluxes across the pulmonary epithelium and the secretion of lung liquid in the foetal lamb. *J. Physiol*. **270 (5638)**: 603-604.

ORNITZ, D. M. & ITOH, N. (2001). Fibroblast growth factors. *Genome Biology* **2**: 3005.1-3005.12.

PAGÈS, G. & POUYSSÉGER, J. (2005). Transcriptional regulation of the Vascular Endothelial Growth Factor gene – a concert of activating factors. *Cardiovasc Res*. **65(3)**: 564-73.

PARK, S., CHAPUIS, N., TAMBURINI, J., BARDET, V., CORNILLET-LEFEBVRE, P., WILLEMS, L., GREEN, A., MAYEUX, P., LACOMBE, C. & BOUSCARY, D. (2010). Role of the PI3K/AKT and mTOR signaling pathways in acute myeloid leukemia. *Haematologica*. **95(5)**: 819-828.

PEPICELLI, C. V., LEWIS, P. M. & MCMAHON, A. P. (1998). Sonic hedgehog regulates branching morphogenesis in the mammalian lung. *Curr Biol*. **24;8(19)**: 1083-6.

PFAFFL, M. W. (2001). A new mathematical model for relative quantification in real-time RT-PCR. *Nucl. Acids Res*. **29 (9)**: e45.

PRIGNET, C. & DIMITROV, S. (2003). Phosphorylation of serine 10 in histone H3, what for? *J. Cell Sci.* **116**: 3677-3685.

PULLEN, N. & THOMAS, G. (1997). The modular phosphorylation and activation of $p70^{S6K}$. *FEBS Letters*. **410(1)**: 78-82.

QI, J., NAKAYAMA, K., GAITONDE, S., GOYDOS, J. S., KRAJEWSKI, S., EROSHKIN, A., BAR-SAGI, D., BOWTELL, D. & RONAI, Z. (2008). The ubiquitin ligase Siah2 regulates tumourigenesis and metastasis by HIF-dependent and –independent pathways. *Proc. Natl. Acad. Sci. U S A.* **105(43)**: 16713-16718.

QIU, W., ZHUANG, S., VON LINTIG, F. C., BOSS, G. R. & PILZ, R. B. (2000). Cell type-specific regulation of B-Raf kinase by cAMP and 14-3-3 proteins. *Journal of Biological Chemistry*. **275**: 31921-31929.

RAJATAPITI, P., DE ROOIJ, J. D., BEURSKENS, L. W., KEIJZER, R., TIBBOEL, D., ROTTIER, R. J. & DE KRIJGER, R. R. (2010). Effect of oxygen on the expression of hypoxia-inducible factors in human fetal lung explants. *Neonatology*. **97(4)**: 346-54.

RAK, J., MITSUHASHI, Y., SHEEHAN, C., TAMIR, A., VILORIA-PETIT, A., FILMUS, J., MANSOUR, S. J., AHN, N. G. & KERBEL R. S. (2000). Oncogenes and tumour angiogenesis: differential modes of vascular endothelial growth factor up-regulation in ras-transformed epithelial cells and fibroblasts. *Cancer Res*. **60(2)**: 490-498.

RANKIN, E. B., RHA, J., UNGER, T. L., WU, C. H., SHUTT, H. P., JOHNSON, R. S., SIMON, M. C., KEITH, B. & HAASE, V. H. (2008). Hypoxia-inducible factor (HIF)-2 regulates vascular tumourigenesis in mice. *Oncogene*. **27(40)**: 5354-5358.

RANNELS, S. R. & RANNELS, D. E. (1989) The type II pneumocyte as a model of lung cell interaction with the extracellular matrix. *J. Mol Cell Cardiol.* **21**: 151-159.

RASMUSSEN, R. (2001). Quantification on the LightCycler. *Rapid Cycle Real-time PCR, Methods and Applications*. **Springer Press, Heidelberg**: 21-34.

RAVAL, R. R., LAU, K. W., TRAN, M. G. B., SOWTER, H., MANDRIOTA, S. J., LI, J-L., PUGH, C. W., MAXWELL, P. H., HARRIS, A. L. & RATCLIFFE, P. J. (2005). Contrasting properties of hypoxia-inducible factor (HIF-1) and HIF-2 in von hippel-lindau-associated renal cell carcinoma. *Molecular & Cell Biology*. **25(13)**; 5675-5686.

RAWLINS, E. L., OKUBO, T., XUE, Y., BRASS, D. M., AUTEN, R. L., HASEGAWA, H., WANG, F. & HOGAN, B. L. (2009). The role of Scgb1a1+ Clara cells in the long-term maintenance and repair of lung airway, but not alveolar, epithelium. *Cell Stem Cell*. **4(6)**: 525-534.

REGULA, K. M., ENS, K., KIRSHENBAUM, L. A. (2002). Inducible expression of BNIP3 provokes mitochondrial defects and hypoxia-mediated cell death of ventricular myocytes. *Circ Res*. **91**: 226-231.

REMESAL, A., PEDRAZ, C., SAN FELICIANO, L. & LUDEÑA, D. (2009). Pulmonary expression of vascular endothelial growth factor (VEGF) and alveolar septation in a newborn rat model exposed to acute hypoxia and recovered under conditions of air or hyperoxia. *Histol. Histopathol.* **24(3)**: 325-330.

ROCK, J. R. & HOGAN, B. L. M. (2011). Epithelial progenitor cells in lung development, maintenance, repair, and disease. *Annu. Rev. Cell Dev. Biol*. **27**: 493-512.

ROHMANN, E., BRUNNER, H. G., KAYSERILI, H., UYGUNER, O., NÜRNBERG, G., LEW, E. D., DOBBIE, A., ESWARAKUMAR, V. P., UZUMCU, A., ULUBIL-EMEROGLU, M., LEROY, J. G., LI, Y., BECKER, C., LEHNERDT, K., CREMERS, C. W., YÜKSEL-APAK, M., NÜRNBERG, P., KUBISCH, C., SCHLESSINGER, J., VAN BOKHOVEN, H. & WOLLNIK, B. (2006). Mutations in different compounds of FGF signaling in LADD syndrome. *Nat. Genet.* **38(4)**: 414-417.

SACI, A., CANTLEY, L. C. & CARPENTER, C. L. (2011). Rac1 regulates the activity of mTORC1 and mTORC2 and controls cellular size. *Mol. Cell*. **42(1)**: 50-61.

SALAUN, C., GREAVES, J. & CHAMBERLAIN, L. H. (2010). The intracellular dynamic of protein palmitoylation. *Journal of Cell Biology*. **191(7)**: 1229.

SARBASSOV, D., ALI, S., KIM, D., GUERTIN, D., LATEK, R., ERDJUMENT-BROMAGE, H., TEMPST, P. & SABATINI, D. (2004). Rictor, a novel binding partner of mTOR, defines a rapamycin-insensitive and raptor-independent pathway that regulates the cytoskeleton. *Curr Biol*. **14(14)**: 1296-1302.

SASAKI, A., TAKETOMI, T., WAKIOKA, T., KATO, R. & YOSHIMURA, A. (2001). Identification of a dominant negative mutant of Sprouty that potentiates fibroblast

growth factor – but not epidermal growth factor-induced ERK activation. *Journal of Biological Chemistry*. **276**: 36804-36808.

SATOH, T., TORII, S., NAKAYAMA, K. & NISHIDA, E. (2010). CrkL is a novel target of Sprouty2 in fibroblast growth factor signaling. *Genes to Cells* **15**: 161-168.

SCHRAUFNAGEL, D. E. (2010). Lung lymphatic anatomy and correlates. *Pathophysiology*. **17(4)**: 337-343.

SCOTT, C. L., WALKER, D. J., CWIKLINSKI, E., TAIT, C., TEE A. R. & LAND, S. C. (2010). Control of HIF-1α and vascular signalling in fetal lung involves cross talk between mTORC1 and the FGF-10/FGFR2b/Spry2 airway branching periodicity clock. *Am J Physiol Lung Cell Mol Physiol* **229**: L455-L471.

SEMENZA, G. L. & WANG G. L. (1992). A nuclear factor induced by hypoxia via de novo protein synthesis binds to the human erythropoietin gene enhancer at a site required for transcriptional activation. *Mol Cell Biol*. **12**: 5447-5454.

SENGER, D. R., GALLI, S. J., DVORAK, A. M., PERRUZZI, C. A, HARVEY, V. S. & DVORAK, H. F. (1983). Tumour cells secrete a vascular permeability factor that promotes accumulation of ascites fluid. *Science*. **219**: 983-985.

SHAN, L., ASTER, J. C., SKLAR, J. & SUNDAY, M. E. (2007). Notch-1 regulates pulmonary neuroendocrine cell differentiation in cell lines and in transgenic mice. *Am J Physiol Lung Cell Mol Physiol*. **292(2):** L500-9.

SHAW, A. T., MEISSNER, A., DOWDLE, J. A. CROWLEY, D., MAGENDANTZ, M., OUYANG, C., PARISI, T., RAJAGOPAL, J., BLANK, L. J., BRONSON, R. T., STONE, J. R., TUVESON, D. A., JAENISCH, R. & JACKS, T. (2007). Sprouty-2 regulates oncogenic K-ras in lung development and tumourigenesis. *Genes & Dev*. **21**: 694-707.

SHIMODA, L. A. & SEMENZA, G. L. (2011). HIF and the Lung. Role of hypoxia-inducible factors in pulmonary development and disease. *Am. J. Respir. Crit. Care Med*. **183**: 152-156.

SKURK, C., MAATZ, H., ROCNIK, E., BIALIK, A., FORCE, T. & WALSH, K. (2005). Glycogen-synthase kinase3β/β-catenin axis promotes angiogenesis through activation of vascular endothelial growth factor signaling in endothelial cells. *Circ Res*. **96**: 308-318.

SMITH, T. G., ROBBINS, P. A. & RATCLIFFE, P. J. (2008). The human side of hypoxia-inducible factor. *J. Haematol*. **141(3):** 325-334.

STEGGERDA, S. M. & PASCHAL, B. M. (2002). Regulation of nuclear import and export by the GTPase Ran. *Int. Rev. Cyol*. **217**: 41-91.

STROKA, D. M., BURKHARDT, T., DESBAILLETS, I., WENGER, R. H., NEIL, D. A. H., BAUER, C., GASSMANN, M. & CANDINAS, D. (2001). HIF-1 is expressed in normoxic tissue and displays an organ-specific regulation under systemic hypoxia. *The FASEB Journal*. **15(13)**: 2445-2453.

SUN, F., FU, H., LIU, Q., TIE, Y., ZHU, J., XING, R., SUN, Z. & ZHENG, X. (2008). Downregulation of CCND1 and CDK6 by miR-34a induces cell cycle arrest. *FEBS Lett*. **582(10)**: 1564-8.

SUNDAY, M. (1996). Pulmonary neuroendocrine cells and lung development. *Endocrine Pathology*. **7:** 173-201.

SUTHERLAND, D., SAMAKOVLIS, C. & KRASNOW, M. A. (1996). *branchless* encodes a *Drosophila* FGF homolog that controls tracheal cell migration and the pattern of branching. *Cell* **87**: 1091-1101.

SUTTERLÜTY, H., MAYER C. E., SETINEK, U., ATTEMS, J., OVTCHAROV, S., MIKULA, M., MIKULITS, W., MICKSCHE, M. & BERGER, W. (2007). Down-regulation of Sprouty2 in non-small cell lung cancer contributes to tumour malignancy via extracellular signal-regulated kinase pathway-dependent and independent mechanisms. *Mol Cancer Res*. **5(5)**: 509-20.

TALKS, K. L., TURLEY, H., GATTER, K. C., MAXWELL, P. H., PUGH, C. W., RATCLIFFE, P. J. & HARRIS, A. L. (2000). The expression and distribution of the hypoxia-inducible factors HIF-1α and HIF-2α in normal human tissues, cancers and tumour-associated macrophages. *Am. J. Pathol.* **157(2)**: 411-421.

TAMBURINI, J., GREEN, A. S., BARDET, V., CHAPUIS, N., PARK, S., WILLEMS, L., UZUNOV, M., IFRAH, N., DREYFUS, F., LACOMBE, C., MAYEUX, P. & BOUSCARY, D. (2009). Protein synthesis is resistant to rapamycin and constitutes a promising therapeutic target in acute myeloid leukemia. *Blood*. **114(8)**: 1618-1627.

TANG, N., MARSHALL, W. F., MCMAHON, M., METZGER, R. J. & MARTIN, G. R. (2011). Control of mitotic spindle angle by the RAS-regulated ERK1/2 pathway determines lung tube shape. *Science*. **333(6040)**: 342-345.

TANIGUCHI, C. M., EMANUELLI, B. & KAHN C. R. (2006). Critical nodes in signalling pathways: insights into insulin action. *Nat. Rev. Mol. Cell Biol*. **7**: 85-96.

TEFFT, J. D., LEE, M., SMITH, S., CROWE, D. L., BELLUSCI, S. & WARBURTON, D. (2002). mSprouty2 inhibits FGF10-activated MAP kinase by differentially binding to upstream target proteins. *Am. J. Physiol. Lung Cell Mol. Physiol.* **283(4)**: L700-706.

TEN HAVE-OPBROEK, A. A. W. (1991). Lung development in the mouse embryo. *Exp Lung Res*. **17**: 111-30.

UNBEKANDT, M., DEL MORAL, P-M., SALA, F. G., BELLUSCI, S., WARBURTON, D. & FLEURY, V. (2008). Tracheal occlusion increases the rate of epithelial branching of embryonic mouse lung via the FGF-10-FGFR2b-Sprouty2 pathway. *Mechanisms of Development*. **125**: 314-324.

UPADHYAY, D., CORREA-MEYER, E., SZNAJDER, J. I. & KAMP, D. W. (2003). FGF-10 prevents mechanical stretch-induced alveolar epithelial cell DNA damage via MAPK activation. *AJP – Lung Physiol*. **284(2)**: L350-L359.

VAILHÉ B., VITTET, D. & FEIGE, J-J. (2001). *In vitro* models of vasculogenesis and angiosgenesis. *Laboratory Investigation*. **81**: 439-452.

VAN TUYL, M., LIU, J., WANG, J., KULISZEWSKI, M., TIBBOEL, D. & POST, M. (2005). Role of oxygen and vascular development in epithelial branching morphogenesis of the developing mouse lung. *Am. J. Physiol. Lung Cell Mol. Physiol*. **288**; L167-L178.

VILLANUEVA, A., CHIANG, D. Y., NEWELL, P., PEIX, J., THUNG, S., ALSINET, C., TOVAR, V., ROAYAIE, S., MINGUEZ, B., SOLE, M., BATTISTON, C., VAN LAARHOVEN, S., FIEL, M. I., DI FEO, A., HOSHIDA, Y., YEA, S., TOFFANIN, S., RAMOS, A., MARTIGNETTI, J. A., MAZZAFERRO, V., BRUIX, J., WAXMAN, S., SCHWARTZ, M., MEYERSON, M., FRIEDMAN, S. L. & LLOVET, J. M. (2008). Pivotal role of mTOR signaling in hepatocellular carcinoma. *Gastroenterology*. **135(6)**: 1972-198411.

VÍZKELETI, L., ECSEDI, S., RÁKOSY, Z., OROSZ, A., LÁZÁR, V., EMRI, G., KOROKANI, V., KISS, T., ÁDÁNY, R. & BALÁZS, M. (2012). The role of CCND1 alterations during the progression of cutaneous malignant melanoma. *Tumour Biology*. **33(6)**: 2189-2199.

VOELKEL, N. F., VANDIVIER, R. W. & TUDER, R. M. (2006). Vascular endothelial growth factor in the lung. *AJP – Lung Physiol*. **Vol. 290 no. 2**. L209-L221.

WALTENBERGER, J, CLAESSON-WELSH, L., SIEGBAHNM A., SHIBUYA, M. & HELDIN, C-H. (1994). Different signal transduction properties of KDR and Flt1, two receptors for vascular endothelial growth factor. *The Journal of Biological Chemistry*. **Vol. 269, no. 43**. pp. 26988-26995.

WANG, A. C. C., DAI, X., LUU, B. & CONRAD, D. J. (2001). Peroxisome proliferator-activated receptor-γ regulates airway epithelial cell activation. *Am. J. Respir. Cell Mol. Biol.* **24(6)**: 688-693.

WANG, C., DELOGU, S., HO, C., LEE, S. A., GUI, B., JIANG, L., LADU, S., CIGLIANO, A., DOMBROWSKI, F., EVERT, M., CALVISI, D. F., CHEN, X. (2012). Inactivation of Spry2 accelerates AKT-driven hepatocarcinogenesis via activation of MAPK and PKM2 pathways. *J. Hepatol*. **57(3)**: 577-83. (b)

WANG, Y., KALLGREN, S. P., REDDY, B. D., KUNTZ, K., López-Maury, L., Thompson, J., Watt, S., Ma, C., Hou, H., Shi, Y., Yates III, J. R., Bähler, J., O'Connell, M. J. & Jia, S.

(2012). Histone H3 lysine 14 acetylation is required for activation of a DNA damage checkpoint in fission yeast. *Journal of Biological Chemistry*. **287**: 4386-4393. (a)

WARBURTON, D., BELLUSCI, S., DEL MORAL, P-M., KAARTINEN, V., LEE, M., TEFFT, D. & SHI, W. (2003). Growth factor signaling in lung morphogenetic centers: automaticity, stereotypy and symmetry. *Respiratory Research*. **4**: 5.

WEAVER, M., YINGLING, J. M. DUNN, N. R., BELLUSCI, S. & HOGAN (1999). Bmp signaling regulates proximal-distal differentiation of endoderm in mouse lung development. *Development*. **126**: 4005-4015.
WEAVER, M., DUNN, N. R. & HOGAN, B. L. M. (2000) Bmp4 and Fgf10 play opposing roles during lung bud morphogenesis. *Development*. **127**: 2695-2704.

WEIBEL, E. R. (2009). What makes a good lung? *Swiss Med Weekly*. **139(27-28)**: 375-386.

WEIBEL, E. R. & GOMEZ, D. M. (1962). Architecture of the human lung. *Science*. **137**: 577-85.

WEINSTEIN, M., XU, X., OHYAMA, K. & DENG, C. X. (1998). FGFR-3 and FGFR-4 function cooperatively to direct alveogenesis in the murine lung. *Development*. **125**: 3615-3623.

WENGER, R . H. (2002). Cellular adaptation to hypoxia: O_2-sensing protein hydroxylases, hypoxia-inducible transcription factors, and O_2-regulated gene expression. *The FASEB Journal*. **16(10)**: 1151-1162.

WHITFIELD, M. L., SHERLOCK, G., SALDANHA, A. J., MURRAY, J. L., BALL, C. A., ALEXANDER, K. E., MATESE, J. C., PEROU, C. M., HURT, M. M., BROWN, P. O. & BOTSTEIN, D. (2002). Identification of genes periodically expressed in human cell cycle and their expression in humans. *Mol. Cell. Biol.* **13(6)**: 1977-2000.

WHITSETT, J. A., WERT, S. E. & WEAVER, T. E. (2010). Alveolar surfactant homeostasis and the pathogenesis of pulmonary disease. *Annu Rev Med*. **61**: 105-19.

WIDDICOMBE, J. H. (2002). Regulation of the depth and composition of airway surface liquid. *J. Anat*. **201**: 313-318.

WIESENER, M. S., JURGENSEN, J. S., ROSENBERGER, C., SCHOLZE, C. K., HORSTRUP, J. H., WARNECKE, C., MANDRIOTA, S., BECHMANN, I., FREI, U. A., PUGH, C. W., RATCLIFFE, P. J., BACHMANN, S., MAXWELL, P. H. & ECKARDT, K. U. (2003). Widespread hypoxia-inducible expression of HIF-2alpha in distinct cell populations of different organs. *FASEB J*. **17**:271-273.

WIETECHA, M. S., CHEN, L., RANZER, M. J., ANDERSON, K., YING, C., PATEL, T. B. & DIPIETRO, L. A. (2011). Sprouty2 downregulates angiogenesis during mouse skin wound healing. *AJP – Heart*. **300(2)**: H459-H467.

WILLIAMS, M. C. (2003). Alveolar type I cells: molecular phenotype and development. *Annu Rev Physiol*. **65**: 669-6695.

WILTING, R. H., YANOVER, E., HEIDEMAN, M. R., JACOBS, H., HORNER, J., VAN DER TORRE, J., DEPINHO, R. A. & DANNENBERG, J-H. (2010). Overlapping functions of Hdac1 and Hdac2 in cell cycle regulation and haematopoiesis. *The EMBO Journal*. **29**: 2586-2597.

WONG, W. T., AGRÓN, E., COLEMAN, H. R., REED, G. F., CSAKY, K., PETERSON, J., GLENN, G., LINEHAN, W. M., ALBERT, P. & CHEW, E. Y. (2007). Genotype-Phenotype correlation in von-Hippel-Lindau disease with retinal angiomatosis. *Ophthalmic Molecular Genetics*. **125(2)**: 239-245.

YAMASAKI, M., MIYAKE, A., TAGASHIRA, S. & ITOH, N. (1996). Structure and expression of the rat mRNA encoding a novel member of the fibroblast growth factor family. *J. Biol. Chem*. **271**: 15918-15921.

YING, C., ANDERSON, K. M. & PATEL, T. B. (2010). SH3 domain of ßPix interacts with Sprouty2. *FASEB J.* **24**; 962.12.

YU, C. L., MEYER, D. J., CAMPBELL, G. S., LARNER, A. A. C., CARTER-SU, C., SCHWARTZ, J. & JOVE, R. (1995). Enhanced DNA-binding activity of a Stat3-related protein in cells transformed by the Src oncoprotein. *Science* **269**: 81-3.

YU, H. & JOVE, R. (2004). The STATs of cancer-new molecular targets come of age. *Nat. Rev. Cancer.* **4**: 97-105.

ZENG, X., WERT, S. E., FEDERICI, R., PETERS, K. G. & WHITSETT, J. A. (1998). VEGF enhances pulmonary vasculogenesis and disrupts lung morphogenesis *in vivo*. *Dev Dyn*. **211(3):** 215-27.

ZIELLO, J. E., JOVIN, I. S. & HUANG, Y. (2007). Hypoxia-inducible factor (HIF)-1 regulatory pathway and its potential for therapeutic intervention in malignancy and ischemia. *Yale Journal of Biology and Medicine*. **80(2)**: 51-60.

Web References

Morrisey, E. (2012). Signaling and epigenetic mechanisms regulating lung development and regeneration. Powerpoint presentation. Available from: http://videos.med.wisc.edu/files/Morrisey_01_18_12.pdf {Accessed 4.1.2013}.

Resp!Rare, Centre de reference des maladies respiratoires rares, 2012. Available from:

http://basenat.u707.jussieu.fr/site_respirare/index.php?option=com_content&view=article&id=59&Itemid=30&lang=en&limitstart=1{Accessed 6.4.2012).